BUILDING SCIENCE SERIES 34

Strength of Masonry Walls Under Compressive and Transverse Loads

U.S.
ARTMENT
OF
MMERCE
National
Bureau
of
Standards

The Building Science Series

The Building Science Series disseminates technical information developed at the National Bureau of Standards on building materials, components, systems and whole structures. The Series presents research results, test methods and performance criteria related to the structural and environmental functions and the durability and safety characteristics of building elements and systems.

These publications, similar in style and content to the NBS Building Materials and Structures Reports (1938–59), are directed toward the manufacturing, design, construction and research segments of the building industry, standards organizations and officials responsible for building codes.

The material for this Series originates principally in the Building Research Division of the NBS Institute for Applied Technology. The publications are divided into three general groups: Building Systems and Processes; Health, Safety and Comfort; and Structures and Materials. Listed below are other publications in the category of—

Structures and Materials

- Interrelations Between Cement and Concrete Properties: Part 1, Materials and Techniques, Water Requirements and Trace Elements. (C13.29/2:2) 35 cents
- Weather Resistance of Porcelain Enamels: Effect of Exposure Site and Other Variables After Seven Years. (C13.29/2:4) 20 cents
- Interrelations Between Cement and Concrete Properties: Part 2, Sulfate Expansion, Heat of Hydration, and Autoclave Expansion. (C13.29/2:5) 35 cents
- Some Properties of the Calcium Aluminoferrite Hydrates. (C13.29/2:6) 20 cents
- Organic Coatings, Properties, Selection, and Use. (C13.29/2:7) $2.50
- Interrelations Between Cement and Concrete Properties: Part 3, Compressive Strengths of Portland Cement Test Mortars and Steam-Cured Mortars. (C13.29/2:8) 55 cents
- Thermal-Shock Resistance for Built-Up Membranes (C13.29/2:9) 20 cents
- Shrinkage and Creep in Prestressed Concrete. (C13.29/2:13) 15 cents
- Experimental Determination of Eccentricity of Floor Loads Applied to a Bearing Wall. (C13.29/2:14) 15 cents
- Interrelations Between Cement and Concrete Properties: Part 4, Shrinkage of Hardened Portland Cement Pastes. (C13.29/2:15) 75 cents
- Causes of Variation in Chemical Analyses and Physical Tests of Portland Cement. (C13.29/2:17) 40 cents
- A Study of the Variables Involved in the Saturating of Roofing Felts. (C13.29/2:19) 30 cents
- Proceedings of a Seminar on the Durability of Insulating Glass. (C13.29/2:20) 75 cents
- Hail Resistance of Roofing Products. (C13.29/2:23) 25 cents
- Natural Weathering of Mineral Stabilized Asphalt Coatings on Organic Felt. (C13.29/2:24) 30 cents
- Structural Performance Test of a Building System. (C13.29/2:25) $1.25
- Exploratory Studies of Early Strength Development in Portland Cement Pastes and Mortars. (C13.29/2:28) 25 cents
- 1964 Exposure Test of Porcelain Enamels on Aluminum—Three Year Inspection. (C13.29/2.29) 25 cents
- Flexural Behavior of Prestressed Concrete Composite Tee—Beams (C13.29/2:31) 25 cents
- Compressive Strength of Slender Concrete Masonry Walls (C13.29/2:33) 40 cents

Send orders (use Superintendent of Documents Catalog Nos.) with remittance to: Superintendent of Documents, U.S. Government Printing Office, Washington, D.C. 20402. Remittance from foreign countries should include an additional one-fourth of the purchase price for postage.

[See mailing list announcement on last page.]

UNITED STATES DEPARTMENT OF COMMERCE • Maurice H. Stans, *Secretary*

NATIONAL BUREAU OF STANDARDS • Lewis M. Branscomb, *Director*

Strength of Masonry Walls

Under Compressive and Transverse Loads

F. Y. Yokel, R. G. Mathey, and R. D. Dikkers

Building Research Division
Institute for Applied Technology
National Bureau of Standards
Washington, D.C. 20234

Building Science Series 34

Nat. Bur. Stand. (U.S.), Bldg. Sci. Ser. 34, 74 pages (Mar. 1971)
CODEN: BSSNB

Issued March 1971

For sale by the Superintendent of Documents, U.S. Government Printing Office
Washington, D.C. 20402 (Order by SD Catalog No. C 13.29/2:34). Price 70 cents

Library of Congress Catalog Card Number: 77–608986

Contents

List of Symbols

A Area of net section
a Flexural compressive strength coefficient
af'_m Flexural compressive strength of masonry
b Width of wall
C_m Moment correction coefficient (section 7.3)
c Distance from centroid to outer fiber
E Modulus of elasticity
E_i Initial tangent modulus of elasticity
e Eccentricity relative to centroid of uncracked section
e_k Distance from centroid to edge of kern
F_a Allowable axial compressive stress
f_a Computed axial compressive stress
F_m Allowable flexural compressive stress
f_m Computed flexural compressive stress
f'_m Compressive strength of masonry determined from axial prism tests
f'_t Tensile strength of masonry determined from modulus of rupture tests
g Moment coefficient in the approximate evaluation for M_e (section 7.2.2.2)
h Unsupported height of wall
I Moment of inertia of section
I_n Moment of inertia of section based on uncracked net section
k Reduction coefficient to account for end fixity
kh Unsupported height of wall reduced for end fixity
M Moment
M_c Cracking moment (section 7.2.2.1)
M'_c Maximum cracking moment (section 7.2.2.1)
M_e Maximum moment capacity, computed using linear stress gradients (section 7.2.2.1)
M_{end} Maximum transverse end moment resulting from fixity at wall supports
M_{et} Total maximum moment capacity of cavity wall (section 8.4.4.3)
M_k Moment developed by P_k, applied at the edge of the kern
M_0 Maximum moment caused by transverse load under pin ended conditions
M'_0 Maximum moment in the direction of the transverse loads caused by these loads under given conditions of end fixity
M_t Maximum moment considering tensile strength with zero vertical load (section 7.2.2.1)
m Stiffness ratio in composite section (section 7.2.2.3)
P Applied vertical compressive load; also denotes resultant force on wall section
P' Resultant compressive force acting on wall section
P_{all} Allowable axial load
P_c Vertical load capacity when load is applied at the minimum eccentricity at which section cracking occurs (section 7.2.2.1)
P_{cr} Critical load for stability induced compression failure computed on the basis of a modified EI, accounting for section cracking and reduced stiffness at maximum stress (section 7.3)
P_{cro} Critical load, computed on the basis of the initial tangent modulus of elasticity and an uncracked section (section 7.3)
P_k Vertical load capacity when load is applied at the edge of the kern of a wall section (section 7.2.2.1)
P_0 Short wall axial load capacity determined on the basis of prism strength (section 7.2.2.1)
s Ratio of tensile strength to axial compressive strength of masonry (f'_t/f'_m)
T' Resultant tensile force acting on cross section
t Thickness of wall
u Uncracked thickness in cracked section (figure 7.2)
V Horizontal reaction
w Distributed transverse load
Δ Maximum transverse deflection
δ Transverse deflection
Δf Difference in force (figure 7.4)

SI Conversion Units

In view of present accepted practice in this country in this technological area, common U.S. units measurement have been used throughout this paper. In recognition of the position of the USA as a signato to the General Conference on Weights and Measures, which gave official status to the metric SI system units in 1960, we assist readers interested in making use of the coherent system of SI units by giving conve sion factors applicable to U.S. units used in this paper.

Length
1 in = 0.0254* meter
1 ft = 0.3048* meter

Area
1 $in^2 = 6.4516^* \times 10^{-4}$ $meter^2$
1 $ft^2 = 0.09290$ $meter^2$

Force
1 lb(1bf) = 4.448 newton
1 kip = 4448 newton

Pressure, Stress
1 psi = 6895 $newton/meter^2$
1 ksi = 6.895×10^6 $newton/meter^2$

Mass/Volume
1 lb/ft^3 ($1bm/ft^3$) = 16.02 kilogram/mete

Moment
1 kip-in = 113.0 newton-meter

*Exactly

Strength of Masonry Walls Under Compressive and Transverse Loads*

Felix Y. Yokel, Robert G. Mathey, and Robert D. Dikkers

Ninety walls of 10 different types of masonry construction were tested under various combinations of vertical and transverse load. It is shown that the effect of vertical load and wall slenderness on transverse strength can be predicted by rational analysis. The analysis is based on established theory which has been extended to account for the properties of masonry. Similar methods of rational analysis have been adopted for the design of steel structures and are presently being considered for reinforced concrete structures.

Key words: Brick; cavity walls; composite walls; compressive strength; concrete block; flexural strength; masonry; mortar; slenderness effects; standards; structural stability; walls.

1. Introduction and Objective

Until very recently masonry structures were designed by essentially empirical methods, and only limited effort has been devoted in the past to the development of rational design criteria.

A literature search of the state of knowledge on the transverse strength of masonry walls indicated that research was needed on the effect of vertical compressive loads on the transverse flexural strength of masonry walls. To this end a research effort was initiated by the National Bureau of Standards to obtain data on the flexural strength of masonry walls of various types of construction, subjected simultaneously to transverse loads and vertical compressive loads.

The results of tests of 90 walls of various types of masonry construction are reported. The data from these tests are used as a basis for the development of analytical procedures to predict the strength of masonry walls subjected to combined compressive and transverse loads.

A new analytical approach is proposed to evaluate both strength and slenderness effects in masonry walls. The application of this approach would lead to new design procedures, closely paralleling similar procedures recently adopted for steel construction and presently under consideration for reinforced concrete. Present design practice is evaluated and compared with the proposed approach.

*This work was performed with the aid of a financial grant from the Tri-Service Building Materials Investigational Program (Office of the Chief of Engineers; Naval Facilities Engineering Command; Headquarters, U.S. Air Force).

2. Scope

To obtain the desired experimental data on the strength of masonry walls subjected to combined compressive and transverse loads, tests were conducted on the following 10 different types of wall construction:

1. 8-in hollow concrete masonry units with masonry cement mortar.
2. 8-in hollow concrete masonry units with high-bond mortar.
3. 8-in 100 percent solid concrete masonry units with masonry cement mortar.
4. 4-in Brick A with portland cement-lime mortar.
5. 4-in Brick A with high-bond mortar.
6. 4-in Brick S with high-bond mortar.
7. 4-in Brick B with high-bond mortar.
8. 4-2-4-in cavity walls of hollow concrete masonry units with masonry cement mortar.
9. 4-2-4-in cavity walls of Brick B and hollow concrete masonry units with masonry cement mortar.
10. 8-in composite walls of Brick B and hollow concrete masonry units with masonry cement mortar.

Eight or more wall panel specimens of each of the 10 types listed above were tested by applying uniform transverse loads, uniform axial compressive loads, or a combination of both types of loading. The wall specimens were nominally 4-ft wide and 8-ft high. Two wall specimens of each type were axially loaded to compressive failure with no transverse loading. These walls were 4×8 ft except for two walls of each

of the 4 types of brick walls given in the preceding list, which were nominally 2-ft wide and 8-ft high. The capacity of the testing machine used in the tests was not sufficient to develop the compressive strength of 4 × 8-ft brick wall panels.

For the 10 wall systems listed above, companion prism specimens were constructed. These prisms were tested to determine their strength in compression and in flexure.

In the subsequent analysis in section 8, wall panel strength is compared to prism strength. The data from both the wall and prism tests are used to develop analytical methods for the determination of the transverse strength of various types of masonry wall construction.

The conclusions from this investigation are compared with present design practice in section 9.

3. Materials

All materials used in the wall panel construction were available commercially and were representative of those commonly used in building construction.

3.1. Brick

Three types of brick designated as A, B, and S were used in the construction of the wall panel specimens. The dimensions and physical properties of these types of brick are presented in table 3.1, and brick units are shown in figure 3.1.

The three types of brick were selected to cover a reasonable range of compressive strengths and absorption rates that represent high-strength brick currently used in building construction. Brick A were cream colored, extruded, wire-cut units with 3 round cores. Brick B were gray, extruded, wire-cut units with 5 oval cores. Brick S were red, extruded, wir cut units, having no cores.

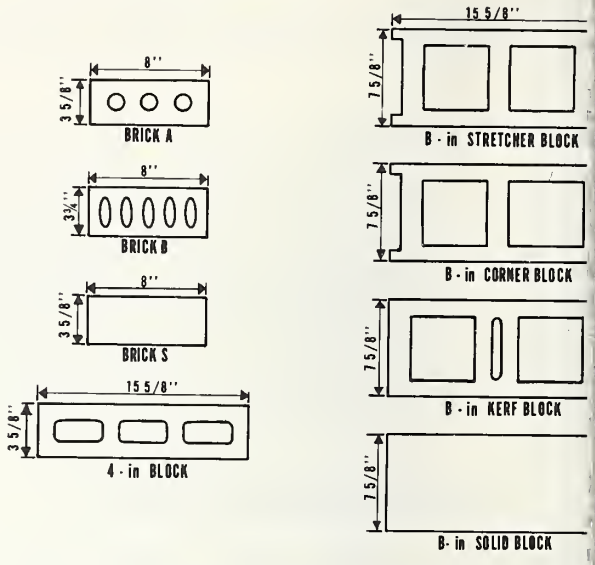

FIGURE 3.1. *Masonry units.*

3.2. Concrete Masonry Units

Three types of concrete masonry units were use in the construction of the wall panel specimens:

1. 8-in, 2-core hollow block
2. 4-in, 3-core hollow block
3. 8-in solid block

The dimensions and physical properties of thes units are given in table 3.2. The units are illustrate in figure 3.1. The 8-in hollow block, 4-in hollo block, and the 8-in solid block were made lightweight expanded-slag aggregate and portlan cement. Three shapes of 8-in hollow units were use in the wall panels: 1. stretcher block (two ope ends), 2. corner block (single open ends), and 3. ke

TABLE 3.1. *Dimensions and physical properties of brick* [a]

Brick designation	Width	Length	Height	Gross area	Net solid area	Compressive strength (Gross area)	Modulus of rupture	Absorption per cent		Saturation coefficient	Initial rate of absorption
	in	*in*	*in*	*in²*	*%*	*psi*	*psi*	*24-hr cold*	*5-hr boil*		*g per 30 in² per min*
A	3.63	7.97	2.25	28.9	89.7	14,480	850	3.33	5.1	0.65	6.2
B	3.75	8.08	2.25	30.0	80.8	20,660	760	2.7	3.3	0.82	2.6
S	3.62	8.00	2.26	29.0	100.0	17,560	740	7.6	10.5	0.72	19.8

[a] Brick were tested in accordance to ASTM C67–66 [1].[1] Each value in the table represents the results of tests of measurement of five specimens.

[1] Figures in brackets indicate literature references given in section 12.

TABLE 3.2. *Dimensions and physical properties of concrete masonry units* [a]

Masonry unit designation	Width	Length	Height	Minimum face shell thickness	Gross area	Net solid area	Compressive strength (Gross area)	Weight of concrete	Absorption
	in	*in*	*in*	*in*	in^2	%	*psi*	lb/ft^3	lb/ft^3
8-in hollow expanded slag block	7⅝	15⅝	7⅝	1¼	119.1	52.2	1100	103.0	14.5
4-in hollow expanded slag block	3⅝	15⅝	7⅝	1	56.6	72.4	1530	101.7	14.9
8-in solid expanded slag block	7⅝	15⅝	7⅝	.....	119.1	100.0	3370	[b]	.....

[a] Concrete masonry units were tested in accordance to ASTM C140–65T [2]. Each value in the table represents the results of tests or measurements of five specimens.

[b] Since the units were acquired at the same time from the same producer of the other two types of expanded slag block, it is assumed that the weight of concrete and the absorption are approximately the same as for the other two units.

block. The kerf block units were cut into two pieces and used at the ends of alternate courses. All values for 8 × 8 × 16-in block given in table 3.2 are for stretcher block.

3.3. Mortar

Three types of mortar were used in the wall panels:

1. Masonry cement mortar
2. Portland cement-lime mortar
3. High-bond mortar

The masonry cement and portland cement-lime mortars were selected to represent conventional masonry construction, and serve as a basis for comparison with masonry containing high-bond mortar. The masonry cement mortar contained 1 part by volume of masonry cement and 3 parts [2] by volume of masonry sand and met the requirements for type N mortar described in ASTM C270-68 [3]. This mortar will be referred to as 1:3 mortar. The portland cement-lime mortar contained (by volume) 1 part of Type 1 portland cement, 1 part hydrated lime, and 4 parts of sand. This mortar will be referred to as 1:1:4 mortar.

The high-bond mortar contained 1-ft^3 (1 part) of Type 1 portland cement, 1-ft^3 (1 part) fine limestone (passing a No. 200 sieve), 4-ft^3 (4 parts) of masonry sand, and 4 gallons of liquid additive. This additive, was a commercially available polyvinylidene chloride having the trade name of Sarabond.[3]

The washed river silica sand used in the three types of mortars had a gradation conforming to the requirements of ASTM C144-66T [4]. The fineness modulus of the sand was 1.95.

The mortar materials were obtained from the same source during fabrication of the wall panel specimens, and were essentially uniform.

The mortars were mixed in a conventional barrel type mixer with rotating blades. Retempering was permitted, but mortar was not used that was more than three hours old. Two-inch mortar cubes were made along with the wall panels and prism specimens. The mortar cubes were air cured in the laboratory under the same conditions as the wall panels and prism specimens. Compressive strengths of the mortar cubes with respect to the type of wall construction and type of mortar are given in table 3.3. The compressive strengths of the mortar cubes representing mortar in the prism specimens are given in table 3.4. The mortar cubes were tested at approximately the same age as the corresponding wall panel or prism specimen.

4. Test Specimens

A detailed description of the wall and prism specimens and the methods of fabrication of these specimens are presented in this section.

4.1. Description of Walls

All the wall panel specimens in this series of tests were constructed in running bond[4] and were

[2] Sand was proportioned on the basis of an average (loose volume) unit weight of 90 lb/ft^3.

[3] A proprietary commercial product produced by The Dow Chemical Company.

[4] Units in adjacent courses overlap by 50 percent and head joints in alternate courses are in vertical alignment.

TABLE 3.3. *Mortar cube compressive strengths for different wall construction* [a]

8-in Hollow block [b] (1:3)	8-in Hollow block (h.b.)	8-in Solid block (1:3)	4-in Brick A (1:1:4)	4-in Brick A (h.b.)	4-in Brick S (h.b.)	4-in Brick B (h.b.)	4-2-4 in Cavity block and block (1:3)	4-2-4 in Cavity brick and block (1:3)	8-in Comp. brick and block (1:3)
660	7590	400	900	7410	8010	8210	480	720	530
500	9460	490	1500	7580	6640	7490	810	910	510
510		430	1080	6850	6980	7830	660	500	780
430		400	930		8480	8430		490	420
		470				7410		430	670
						6930		380	
Average values									
525	8710	440	1100	7280	7530	7720	650	570	580

[a] Mortar cube strengths are given in psi and each value represents the average of 3 tests. The cubes were air cured along with th wall specimens and tested at ages between 35 and 42 days.
[b] Mortar type.

TABLE 3.4. *Mortar cube compressive strengths for prism specimens*

Type of mortar	No. of specimens	Age	Compressive strength
		days	*psi*
1:3	3	180	345
1:3	3	38	460
High-bond	3	180	4920

nominally 4-ft wide and 8-ft high with the exception of eight brick walls which were 2-ft wide and 8-ft high. The thickness and cross section of the wall panels depended on the type of masonry units and the type of construction used. Outside cross-sectional dimensions, areas and moments of inertia of net cross sections for each of the 10 types of masonry walls are shown in figures 4.1 through 4.3. A brief description for each of the 10 types of walls is as follows:

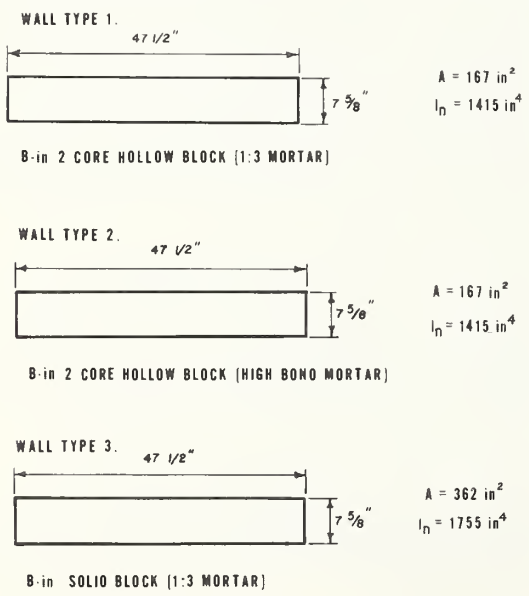

FIGURE 4.1. *Cross-sectional dimensions of block walls.*

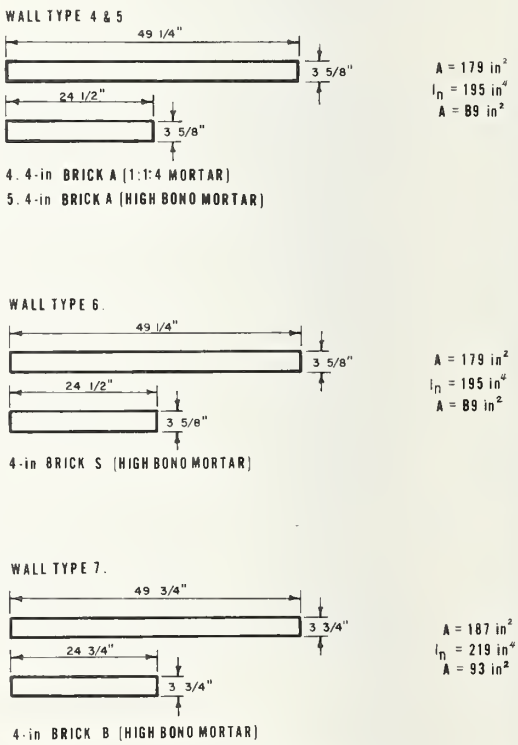

FIGURE 4.2. *Cross-sectional dimensions of brick walls.*

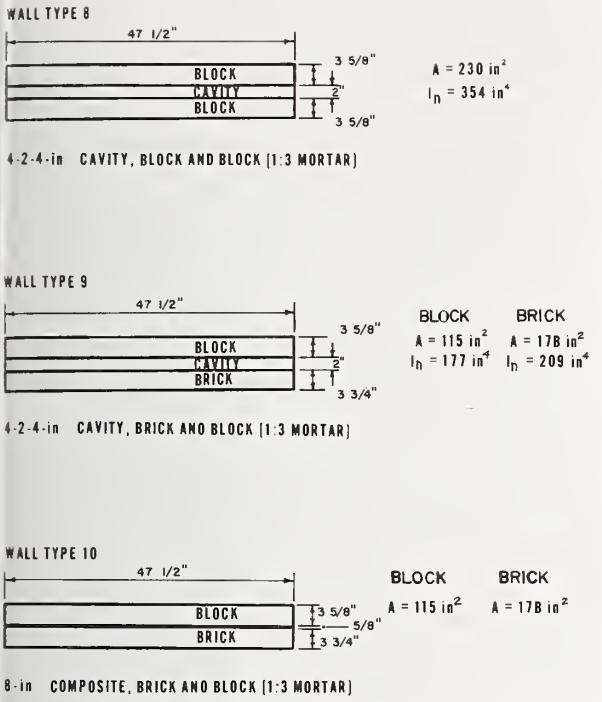

FIGURE 4.3. *Cross-sectional dimensions of cavity and composite walls.*

1. 8-in hollow concrete block walls with type N (1:3) mortar

The walls contained 8 × 8 × 16-in whole units having two cores and half-units that were obtained by cutting kerf block. The walls were constructed in running bond with type N mortar and the bottom course contained a half unit at each end. The bed and head-joint mortar was applied only to the face shells (face-shell bedding) with the exception of the outside edges at the ends of the walls where mortar was applied to the end webs. Stretcher block were used in the wall interior. At the ends, corner block and one-half kerf block, respectively, were used in alternate courses.

2. 8-in hollow concrete block walls with high-bond mortar

This type of wall was constructed in the same way as the 8-in hollow concrete block walls previously described, with the exception that a high bond mortar was used instead of ASTM type N masonry cement mortar.

3. 8-in 100 percent solid concrete block walls with type N (1:3) mortar

These walls were constructed in the same manner as the 8-in hollow block walls except that 100 percent solid block was used. Full bed and head mortar joints were used in constructing these solid wall panels.

4. 4-in brick (A) walls with 1:1:4 mortar

The walls were 4-in thick and were constructed using Brick A and portland cement-lime mortar. Brick were laid in running bond with full bed and head joints. These walls were intended to be control specimens for all four types of single wythe brick walls, all of which were built in a similar manner.

5. 4-in brick brick (A) walls with high bond-mortar

This group of 4-in thick wall panels were made of Brick A and high-bond mortar. Brick were laid as previously described.

6. 4-in brick (S) walls with high-bond mortar

These 4-in thick brick walls were constructed using Brick S and high-bond mortar. Brick were laid as previously described.

7. 4-in brick (B) walls with high-bond mortar

These 4-in thick brick wall panels were constructed using Brick B and high-bond mortar. Brick were laid as previously described.

8. 4-2-4-in cavity walls of hollow concrete block with type N (1:3) mortar

In these cavity walls 4-in hollow concrete block were laid in running bond and mortar was applied to the entire horizontal surfaces and the vertical end surfaces of the block. The head joints of opposite wythes of block were staggered by starting the bottom course of one wythe with a half unit and that of the opposite wythe with a whole unit. Facing and backing wythes were bonded with metal ties in accordance with American Standard A41.1 [5]. Descriptive details of the ties and their locations in the wall are provided in section 4.2 on wall fabrication.

9. 4-2-4-in cavity walls of brick (B) and hollow concrete block with type N (1:3) mortar

The cavity walls containing brick were made with a facing of Brick B and a backing of 3-core 4 × 8 × 16-in hollow concrete block. The brick and block were laid in running bond and the mortar joints were made solid in the brick facing wythe and in the

concrete block backing as previously described. Metal ties were provided as in the previous wall system.

10. 8-in composite brick (B) and hollow concrete block walls with type N (1:3) mortar

In the 8-in composite wall panels the facing was made of Brick B and the backing of 4-in hollow concrete block. Bonding consisted of a brick header course in every seventh brick course.

Full head and bed joints were used in the brick facing and 4-in block backing. The back of the brick facing was pargeted[5] with mortar and when the backup block was laid a conscious effort was made to fill the gap between brick and block with mortar.

4.2. Fabrication of Walls

The masonry wall panels measuring nominally 4 × 8-ft and 2 × 8-ft were fabricated and air cured in a controlled environment laboratory that was maintained at 73 °F ± 3 °F and 50 percent ± 5 percent relative humidity. All of the wall specimens were constructed by the same experienced mason using techniques representative of good workmanship. The walls were built in running bond with the mortar joints on both faces of the walls cut flush and not tooled.

The bottom course of masonry was laid in a full bed of mortar in a steel channel of suitable width and length to facilitate moving and placement of the test panel in the testing machine. Walls were erected between wooden frames that were braced in two planes to keep them perpendicular to the floor. The bed joint locations were marked on the wooden frames in order to control the thickness of these joints through the entire series of tests.

In controlling the bed joints for the various types of walls made of concrete block or clay brick at a thickness of $\frac{3}{8}$ in, the height of 3 brick and 3 joints was taken as 8 in. In a similar manner the height of one concrete masonry unit and one joint was also taken as 8 in.

The mason kept the face of the wall which was away from him in alignment using a horizontal line and level. This face was designated as the outer face of the wall. The near face of the wall to the mason was designated as the inner face.

In all walls the first unit was laid at the end of the course without head joint mortar. Head joints were subsequently formed by buttering one end of a unit just before placing it in the wall. In this way all head joints were "shoved" and there were no closure units or slushed head joints.

Two series of cavity walls were constructed with a 2-in space between inner and outer wythes. One series was built of one wythe of brick and one wythe of 4 × 8 × 16-in hollow concrete units. The other series was built with two wythes of 4 × 8 × 16-in hollow concrete units. The first course of each wythe was set in a common bed of mortar and for the remainder of the wall construction the cavity was kept clear of mortar droppings.

The top course of the cavity walls to be tested with no vertical load was bridged with a 2-in thick course of 8 × 10-in solid units laid in a full bed of mortar, so that the upper courses of the wythes as well as the lower courses would be connected during the flexural tests. Cavity walls which were tested in flexure under vertical load had their upper courses held in place by the application of the vertical load and did not require bridging.

The facing and backing wythes of the cavity walls were tied together in accordance with American Standard A41.1. The commercial ties used in these walls were $\frac{3}{16}$-in diameter steel rods bent into a completely closed rectangle measuring 2 × 6 in with the ends of the rod meeting at the middle of the 2-in sides. The two 6-in sides of the ties contained a $\frac{1}{4}$-in drip crimp[6] at mid-length. Ties were placed in alternate bed joints of block courses starting with the joint above the second course. Lateral spacing of the ties along a bed joint was 30-in on centers starting at points 2 $\frac{1}{2}$-in from opposite ends in alternate tied joints. This spacing resulted in a pattern of 2 ties in alternate joints staggered by 15 inches. The wall panels contained 10 metal ties; therefore, there was nominally one tie for each 3.2 ft² of wall area.

Two-inch mortar cubes were made along with the wall specimens and were air cured in the laboratory under the same conditions as the wall specimens.

4.3. Description and Fabrication of Prisms

Tests were carried out on a large number of small specimens in order to determine the properties of the various types of masonry. Compression tests were conducted on 2-, 3-, and 5-block high prisms and on 5-brick high prisms. The block prisms were

[5] A coat of mortar was applied to the vertical face.

[6] A triangular vertical dent which drains accumulated water.

constructed in stacked[7] bond. The brick prisms were constructed in running bond with a whole unit in the first, third, and fifth courses and 2 half-units in the second and fourth courses.

The prisms constructed using the 8 × 8 × 16-in hollow block contained only face-shell mortar bedding. Full bed joints were used in fabricating the prisms in which the 8 × 8 × 16-in solid and 4 × 8 × 16-in hollow block were used. The brick prisms were constructed with full head and bed mortar joints.

Flexural tests were carried out on 2-block high prisms in accordance with ASTM Standard E149-66 [6]. These prisms were made of both hollow and solid 8 × 8 × 16-in block and 4 × 8 × 16-in hollow block and were constructed in the same manner as the prisms used for compressive tests. Flexural tests were also conducted on 7-course brick prisms tested as beams with the 8-in dimension of the brick horizontal, which were loaded at the third points over a 16-in clear span. These 7-course brick prisms were constructed in stacked bond with full bed mortar joints.

The prisms were constructed from the three types of mortar described in section 3.3. Two-in mortar cubes were made along with the small specimens and were air cured in the laboratory under the same conditions as the prisms.

The decision on size and type of prisms was governed by the following considerations:

Concrete block

(a) Compression: At the present time there is no standard ASTM test for determining the compressive strength of concrete block prisms. The National Concrete Masonry Association (NCMA) presently recommends a prism not less than 16 inches in height with a height-to-thickness ratio of two. It was felt that end restraints may have too much effect on the strength of a two-block high prism. Most of the tests were, therefore, conducted on three-block high prisms, but some tests on two-block and five-block high prisms were also conducted for comparison.

Traditionally, block prisms are built in stacked bond and not in running bond. This construction is more practical and stacked bond prisms were, therefore, used in this program.

(b) Flexure: It was decided that flexure tests of prisms would be conducted in accordance with established ASTM Standard E149-66 which requires two-block high prisms laid in stacked bond.

Brick

(a) Compression: At the present time there is no standard ASTM test for determining the compressive strength of brick prisms. The Structural Clay Products Institute (SCPI) presently recommends a prism not less than 12 inches in height with a height-to-thickness ratio of 5 but not less than 2. The 5-brick high prisms used in this program had a height-to-thickness ratio of 3.5 and a height of 12.8 in.

(b) Flexure: There is presently no standard test for the flexural strength of brick prisms. The 7-brick stacked bond prism which is convenient for fabrication and testing was adopted as a specimen for determining the modulus of rupture of brick masonry.

5. Testing Procedures

5.1. Wall Tests

A wall panel in position for testing is shown in figure 5.1. The vertical load was applied concentrically to the wall and was transmitted from the head of the 600,000-lb capacity hydraulic testing machine through a 12 ½-in deep loading beam, a 1-in square steel bar centered along the width of the wall, and a 2-in steel plate that covered the top area of the wall. A piece of ½-in fiberboard was used between the top of the wall and the 2-in steel plate to provide a uniformly distributed load to the top of the wall. The bottom of the wall was built inside a steel channel which rested on a ½-in fiberboard.

The transverse load was applied uniformly by an air bag, made of 20-mil polyvinyl sheeting, that was 84 in long and extended across the entire width of the wall. A steel reaction frame attached to three wheels provided the support for the air bag on one side of the wall specimen. On the opposite side of the wall, upper and lower horizontal reaction bars were spaced 82 ½-in apart, and attached to another reaction frame on wheels.

The two reaction frames were rolled into position on either side of the wall and bolted together at the four corners. On the loaded side of the wall the air

[7] Units in adjacent courses do not overlap, so that all head joints are in vertical alignment.

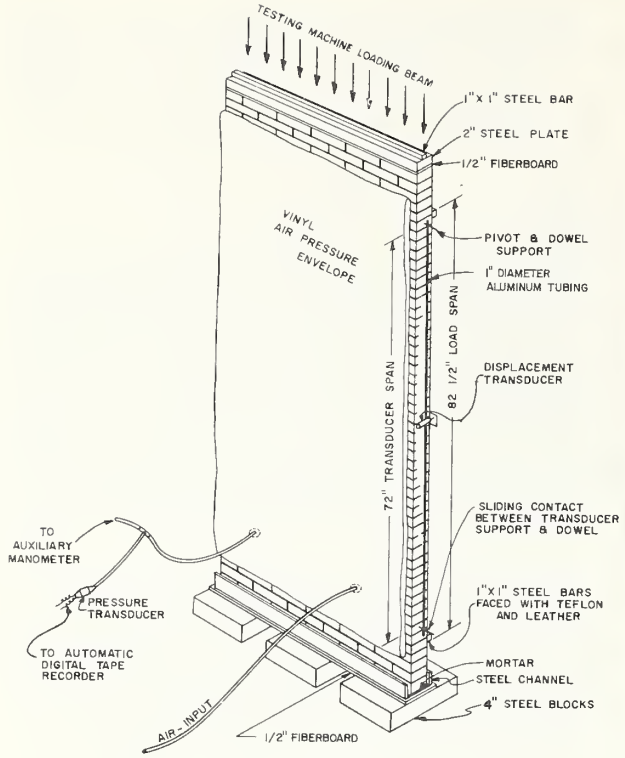

FIGURE 5.1. *Experimental setup for flexural test.*

FIGURE 5.2 *Test apparatus prior to installation of wall panel.*

bag was held against a sheet of plywood attached to the reaction frame. A sheet of rubber on both sides of the air bag provided protection from abrasion. The reaction bars on the opposite face of the wall were 1-in wide, extended across the entire width of the wall specimen, and were faced with teflon over leather to provide a quarter-inch thick resilient material. The steel reaction frame, which has the air bag connected to it, is shown in figure 5.2 prior to its connection to a specimen.

The compressive load was applied vertically to the wall specimens at a rate of 60,000 lb per minute up to failure or to a load level that was maintained while the transverse load was applied.

The inlet tube to the air bag was connected to a hand-regulated compressed air line (100 psi maximum pressure) to apply the transverse load. Air bag pressure was recorded by using a piezo-resistive pressure transducer connected to the air bag outlet tube. Continuous visual monitoring of the air bag pressure was accomplished by using a mercury manometer that was also connected to the outlet tube. The wall specimens were loaded transversely at a rate of approximately 0.30 to 0.35 psi of air pressure per minute.

In all tests where vertical loads were applied, the vertical compressive load was applied first. When the desired vertical load level was reached, the transverse load was applied and gradually increased until the specimen failed.

The walls were tested at an approximate age of 35 days after being air cured in the controlled environment laboratory. They were moved from the fabrication area to the testing machine by a forklift truck. In positioning a wall specimen in the testing machine, the steel channel in which it was built rested on $\frac{1}{2}$-in fiberboard that was placed on top of 4-in thick steel blocks. The steel blocks can be seen in figure 5.2. The 4-in thick steel blocks bore on the platen of the testing machine and were spaced 8 in apart to allow the withdrawal of the forklift truck prongs after positioning of a wall for test.

5.2. Instrumentation for Wall Tests

Vertical applied loads, horizontal applied loads, and lateral deflections of the wall specimens were measured and recorded digitally on paper tape by an automatic electronic multichannel data logging system. The vertical loads were measured with a bonded-foil strain gage pressure transducer that was attached to the hydraulic load measuring system of the testing machine. The pressure in the air bag that was used to apply the uniformly distributed horizon-

tal load was measured with a solid-state pressure transducer having a range of 0-50 psi.

The lateral deflection of the wall specimens was measured with two transformer-type displacement transducers (LVDT's), calibrated to read increments of ± 0.0001 in. which were clamped at mid-height to 6-ft lengths of 1-in diameter aluminum tubing. As shown in figure 5.1., the tubing was attached along the centerline of the two vertical edges of the wall at points near the reaction bars in a manner that allowed it to pivot at each end. The lower end of the tubing was allowed to slide in a vertical direction without lateral movement. The end of the core of the displacement transducers was threaded and loosely screwed into a tapped hole in an aluminum plate that was attached to the face of the wall at mid-height. The attached plate extended beyond the edge of the wall so that the core of the transducer was free to move in or out of the transducer coil. In most wall tests, the displacement transducers were removed just prior to failure to prevent damage to equipment. However, in most cases, deflections were measured beyond the maximum load.

The output from the pressure transducers and the displacement transducers provided signals that were recorded on automatic data-recording equipment. A complete cycle of scanning and recording took 5 seconds. Data were recorded at 5-second intervals during transverse loading for walls without any compressive load or those failing at transverse loads of 1 psi or less. For the wall tests requiring larger transverse loads before failure, data were recorded every 30 seconds. The printed tape record was converted to load-deflection plots by use of conventional high speed digital computers.

5.3. Prism Tests

A description of the various types of prisms is given in section 4.3.

The prisms subjected to compressive tests were loaded at a rate of 50,000 lb per minute. Most of the compressive prisms were capped at top and bottom with high-strength plaster. Since fiberboard was used at the top and bottom of all wall panels to distribute evenly the compressive load, some of the prisms were tested using fiberboard instead of high-strength plaster to investigate the effect of different capping materials on the prism strength.

The flexural strength of the masonry prisms was determined by a flexural bond test and a beam test for concrete masonry and brick masonry, respectively. The flexural bond strength was determined by testing two-block high prisms that were clamped in metal frames at both the top and bottom of the prism and loaded eccentrically 10 in from the longitudinal centerline of the prism. This test method is described in ASTM Standard E149-66.

The 7-course brick prisms were tested as beams with the 8-in dimension of the brick horizontal. The prisms were supported approximately along the centerline of the two end bricks as simple beams with 16-in spans. Symmetrical loads were applied at the third points of the beams.

5.4. Instrumentation for Prism Tests

The modulus of elasticity of the concrete masonry was determined by testing 8-in hollow block prisms. Three-block high prisms constructed in stacked bond were instrumented. The change in length of the prisms subjected to compressive loads was measured with LVDT's which were mounted vertically on the sides of the specimens along the centerline. The gage length extended between the centers of the top and bottom units and was 16 in.

This report also presents test data on the modulus of elasticity of brick masonry. These tests were performed by the National Bureau of Standards in a different testing program. Specimens for these tests were 16 × 16-in and 24 × 24-in monowythe brick piers built in running bond. Brick A with portland cement-lime mortar and Brick A with high-bond mortar were used in two series of pier tests. These piers were instrumented by LVDT's mounted vertically on both faces along the centerline of the long side of the piers. Gage lengths of 10 in and 16 in were used for the 16 × 16-in and the 24 × 24-in piers, respectively.

6. Test Results

6.1. Wall Test Results

A summary of results of the wall tests is given in tables 6.1 through 6.5. Values of the transverse load and midspan deflection corresponding to the point where the load-deflection curves deviated from linearity and values of the maximum transverse load and deflection corresponding to that load are given for various levels of imposed compressive vertical load. It may be noted that the maximum transverse load usually does not represent the final failure load, since transverse loads dropped off before failure.

TABLE 6.1. *Summary of test results on 8-in hollow concrete block walls*

Wall panel desig.	Type construction	Type mortar	Compressive vertical load	Deviation from a linear load-deflection curve occurred at:		Maximum transverse load	Midspan deflection at maximum transverse load
				Transverse load	Midspan deflection		
			lb	*psi*	*in*	*psi*	*in*
1–1	8-in hollow block	1:3	0	0.12	0.00	0.12	0.23
1–2			20,000	1.82	0.02	2.63	0.83
1–3			40,000	3.05	0.05	4.65	0.86
1–4			60,000	4.28	0.07	6.03	.....
1–5			120,000	6.31	0.13	6.31	0.13
1–6			135,000	[a] 95,000	0.01	[a]135,000	0.06
1–7			148,000	[a]115,000	0.00	[a]148,000	0.06
2–1	8-in hollow block	high-bond	0	1.90	0.02	1.90	0.02
2–2			0	1.54	0.02	1.58	0.02
2–3			0	2.00	0.03	2.00	0.03
2–4			40,000	4.48	0.05	5.17	0.91
2–5			75,000	6.93	0.08	6.93	0.08
2–6			130,000	6.13	0.09	6.30	0.09
2–7			150,000	4.41	0.07	5.27	0.08
2–8			150,000	5.32	0.05	5.41	0.05
2–9			150,000	.....	.....	[a]150,000	0.01

[a]Walls were tested by application of only vertical loads. Values given are for vertical loads.

TABLE 6.2. *Summary of test results on 8-in solid concrete block walls*

Wall panel desig.	Type construction	Type mortar	Compressive vertical load	Deviation from a linear load-deflection curve occurred at:		Maximum transverse load	Midspan deflection at maximum transverse load
				Transverse load	Midspan deflection		
			lb	*psi*	*in*	*psi*	*in*
3–1	8-in solid block	1 : 3	0	0.15	0.00	0.34	0.34
3–2			0	0.22	0.01	0.29	0.91
3–3			25,000	1.66	0.05	3.29	0.49
3–4			50,000	3.07	0.06	5.94	0.61
3–5			100,000	2.23	0.02	8.17	0.23
3–6			150,000	6.79	0.07	15.12	0.79
3–7			200,000	7.65	0.10	[b] 15.26	0.40
3–8			300,000	7.65	0.04	[b] 13.80	0.20
3–9			400,000	11.43	0.13	[b] 15.59	0.19
3–10			500,000	5.04	0.08	6.10	0.29
3–11			530,000	.....	.....	13.70	.....
3–12			490,000	.....	.....	.....	.....
3–13			597,000	[a] 395,000	0.04	[a] 597,000	0.03

[a] Walls were tested by application of only vertical loads. Values given are for vertical loads.
[b] Specimen did not fail, testing was halted because the loading mechanism capacity was exceeded.

Deflections at the actual point of failure are in most cases not recorded, since the instrumentation was removed prior to this point.

In some of the wall tests the transverse loading had to be terminated due to the limited capacity of the plastic air bags. Loading was halted for this reason at a horizontal load of approximately 15 psi. Three wall tests which were stopped in this manner are noted in table 6.2, and one such test appears in table 6.5.

The brick wall specimens subjected only to compressive load had a nominal width of 2 ft because of limited testing-machine capacity. In the test data given in tables 6.3 and 6.4 the results were adjusted to correspond to the other wall data, which were obtained from 4-ft wide wall panels, by doubling the measured test loads.

For most of the different types of wall panels at least two specimens of each type were tested at zero compressive load to determine flexural tensile strength.

Table 6.6 contains a summary of computed average compressive stresses and moduli of rupture for the 10 different wall systems. Figures 6.1 through

TABLE 6.3. *Summary of test results on brick A walls*

Wall panel desig.	Type construction	Type mortar	Compressive vertical load	Deviation from a linear load-deflection curve occurred at:		Maximum transverse load	Midspan deflection at maximum transverse load
				Transverse load	Midspan deflection		
			lb	*psi*	*in*	*psi*	*in*
4–1	4-in brick A	1 : 1 : 4	0	0.12	0.01	0.20	0.02
4–2			0	0.20	0.03	0.20	0.03
4–3			100,000	2.21	0.12	3.38	0.51
4–4			200,000	3.70	0.18	5.20	0.54
4–5			250,000	2.82	0.16	5.48	0.61
4–6			300,000	3.90	0.31	5.14	0.58
4–7			350,000	1.78	0.10	4.47	0.55
4–8			[a] 562,000	.....	.....	.....	.....
4–9			[a] 576,000	.....	.....	.....	.....
5–1	4-in brick A	high-bond	0	0.60	0.02	0.80	0.03
5–2			0	0.58	0.02	0.80	0.03
5–3			100,000	2.70	0.11	3.88	0.42
5–4			200,000	4.88	0.20	6.84	0.65
5–5			250,000	4.90	0.21	7.00	0.53
5–6			300,000	5.62	0.31	6.90	0.59
5–7			350,000	5.44	0.31	6.73	0.59
5–8			400,000	5.10	0.23	8.29	0.67
5–9			[a] 844,000	.....	.....	.....	.....
5–10			[a] 872,000	.....	.....	.....	.....

[a] Actual test was performed on 2-ft wide panel and values were adjusted for 4-ft width.

TABLE 6.4. *Summary of test results on brick B and brick S walls*

Wall panel desig.	Type construction	Type mortar	Compressive vertical load	Deviation from a linear load-deflection curve occurred at:		Maximum transverse load	Midspan deflection at maximum transverse load
				Transverse load	Midspan deflection		
			lb	*psi*	*in*	*psi*	*in*
6–1	4-in brick S	high-bond	0	0.40	0.02	0.40	0.02
6–2			0	0.45	0.02	0.54	0.03
6–3			140,000	2.95	0.20	3.94	0.58
6–4			220,000	4.02	0.28	7.10	0.72
6–5			290,000	4.08	0.24	7.10	0.72
6–6			350,000	4.94	0.29	7.13	0.60
6–7			400,000	3.99	0.22	6.94	0.69
6–8			[a] 1,088,000	.....	.....	.....	.....
6–9			[a] 1,050,000	.....	.....	.....	.....
7–1	4-in brick B	high-bond	0	1.10	0.03	1.10	0.03
7–2			0	1.34	0.04	1.34	0.04
7–3			160,000	4.67	0.13	6.91	0.56
7–4			320,000	7.98	0.21	11.29	0.59
7–5			320,000	6.54	0.25	9.68	0.70
7–6			600,000	6.52	0.23	11.21	0.63
7–7			[a] 948,000	.....	.....	.....	.....
7–8			[a] 970,000	.....	.....	.....	.....

[a] Actual test was performed on 2-ft wide panel and values were adjusted for 4-ft width.

TABLE 6.5. *Summary of test results on cavity and composite walls*

Wall panel desig.	Type construction	Type mortar	Compressive vertical load	Deviation from a linear load-deflection curve occurred at:		Maximum transverse load	Midspan deflection at maximum transverse load
				Transverse load	Midspan deflection		
			lb	*psi*	*in*	*psi*	*in*
8–1	4-2-4-in cavity block-block	1 : 3	0	0.23	0.01	0.23	0.01
8–2			0	0.21	0.01	0.21	0.39
8–3			50,000	1.74	0.09	2.63	0.37
8–4			100,000	2.87	0.13	4.27	0.43
8–5			150,000	4.00	0.22	5.42	0.56
8–6			200,000	4.60	0.32	5.02	0.39
8–7			238,000	[a] 145,000	0.01	[a] 238,000	0.02
8–8			254,000	[a] 155,000	0.02	[a] 254,000	
9–1	4-2-4-in cavity brick-block	1 : 3	0	0.26	0.01	0.26	0.01
9–2			35,000	1.15	0.08	2.20	0.76
9–3			70,000	2.05	0.08	3.97	0.56
9–4			100,000	3.38	0.10	5.16	0.48
9–5			200,000	4.64	0.14	7.50	0.40
9–6			250,000	3.65	0.09	8.18	0.34
9–7			300,000	3.87	0.14	6.53	0.36
9–8			360,000	[a] 175,000	0.01	[a] 360,000	0.15
10–1	8-in composite brick-block	1 : 3	0	0.57	0.02	0.75	0.03
10–2			40,000	3.04	0.05	4.73	1.14
10–3			85,000	5.46	0.05	10.16	0.76
10–4			90,000	5.92	0.10	10.54	0.69
10–5			130,000	6.38	0.06	12.76	0.56
10–6			180,000	6.83	0.03	[b] 14.59	0.28
10–7			350,000	9.11	0.09	13.87	0.21
10–8			400,000	[a] 315,000	0.06	[a] 400,000	0.10
10–9			465,000	[a] 355,000	0.09	[a] 465,000	0.26

[a] Walls were tested by application of only vertical loads. Values given are for vertical loads.
[b] Specimen did not fail, testing was halted because the loading mechanism capacity was exceeded.

TABLE 6.6. *Summary of average compressive and flexural strengths of walls* [a]

Wall panel desig.	Type of construction	Average compressive load	Average compressive strength	Average modulus of rupture	
				Partial fixity assumed	Pin ended assumed
		kip	*psi*	*psi*	*psi*
1	8-in hollow block, 1 : 3 mortar	141.5	847	6	9
2	8-in hollow block, high-bond mortar	150.0	898	130	191
3	8-in solid block, 1 : 3 mortar	543.5	1500	15	22
4	4-in Brick A, 1 : 1 : 4 mortar	569.0	3187	50	75
5	4-in Brick A, high-bond mortar	858.0	4806	210	310
6	4-in Brick S, high-bond mortar	1069.0	6050	120	180
7	4-in Brick B, high-bond mortar	959.0	5140	300	440
8	4-2-4 in cavity block-block, 1 : 3 mortar	246.0	1071	23	34
9	4-2-4 in cavity brick-block, 1 : 3 mortar	360.0	1229	([b])	.....
10	8-in composite brick-block, 1 : 3 mortar	432.5	1476	[c] 30	[c] 44

[a] Average stress on net cross section; see figures 4–1, 4–2, and 4–3.
[b] No meaningful average stress can be computed.
[c] Based on I of transformed section.

5.10 are plots of transverse load versus vertical compressive load for all the wall systems. The curves shown in these figures approximately represent the general trend of the maximum load data.

6.2. Description of Wall Failures

A brief, general description of the manner in which the walls failed is given hereafter for each type of wall construction. As indicated previously, the walls were loaded axially with a uniform load and the transverse load was applied uniformly over the face of the wall that normally is considered the exterior face. The walls were loaded in compression only, flexure only, or a combination of compression and flexure.

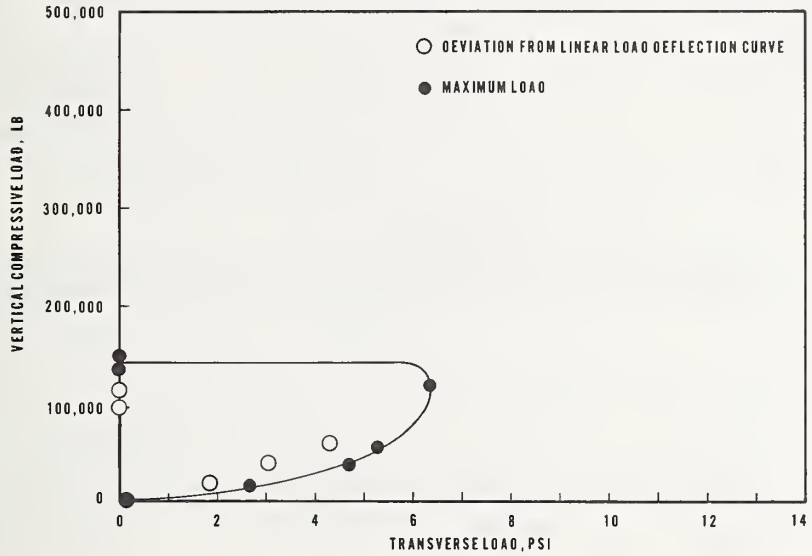

FIGURE 6.1. *Relationship between vertical compressive load and transverse load for 8-in hollow concrete block walls with Type N(1:3) mortar.*

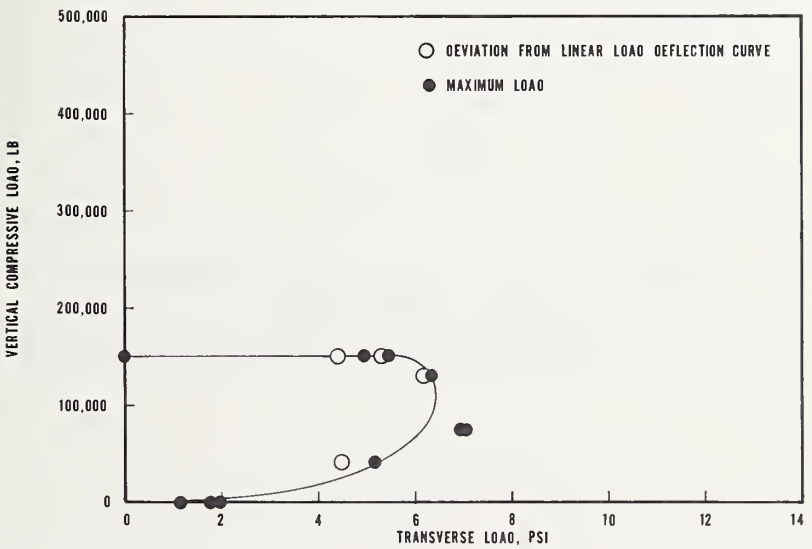

FIGURE 6.2. *Relationship between vertical compressive load and transverse load for 8-in hollow concrete block walls with high bond mortar.*

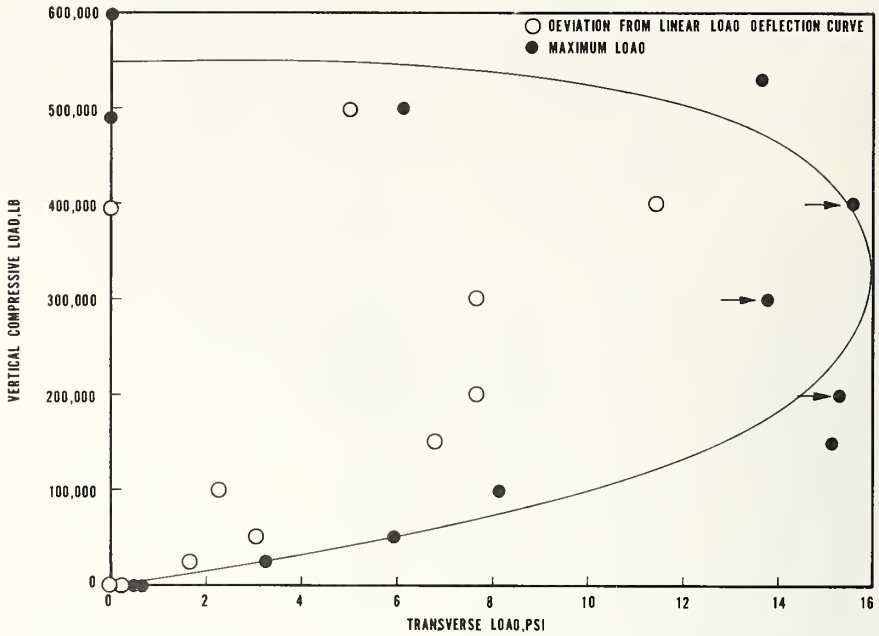

FIGURE 6.3. *Relationship between vertical compressive load and transverse load for 8-in solid concrete block walls with Type N(1:3) mortar.*

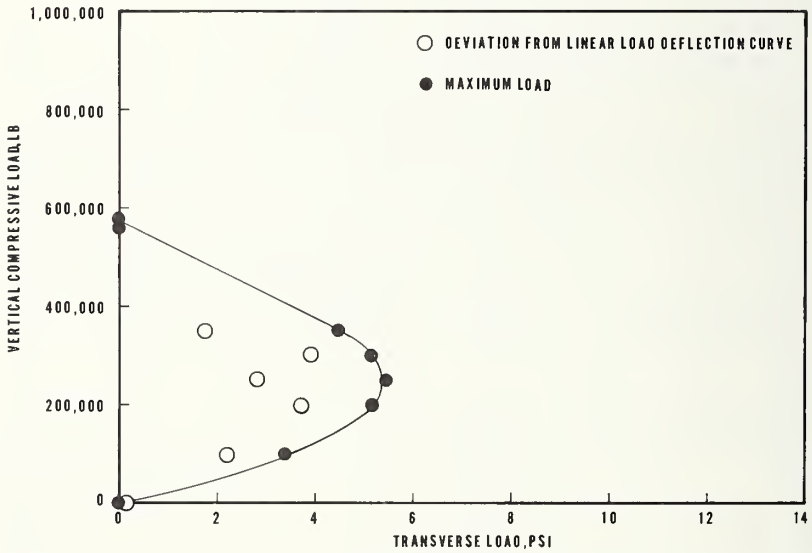

FIGURE 6.4. *Relationship between vertical compressive load and transverse load for 4-in Brick A walls with 1:1:4 mortar.*

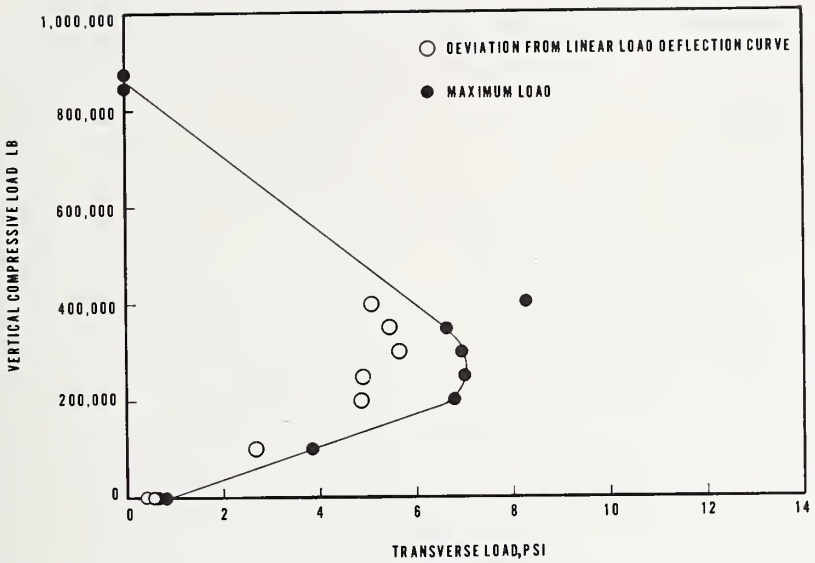

URE 6.5. *Relationship between vertical compressive load and transverse load for 4-in Brick A walls with high bond mortar.*

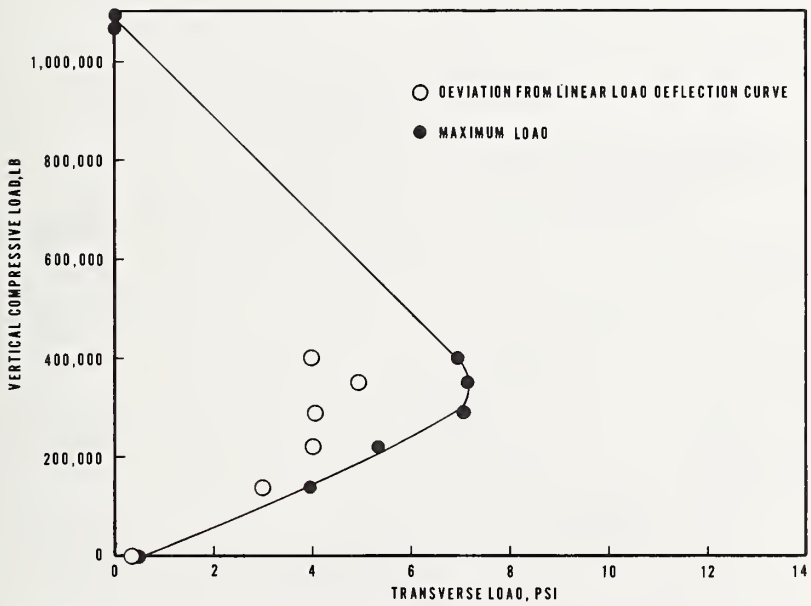

IRE 6.6. *Relationship between vertical compressive load and transverse load for 4-in Brick S walls with high bond mortar.*

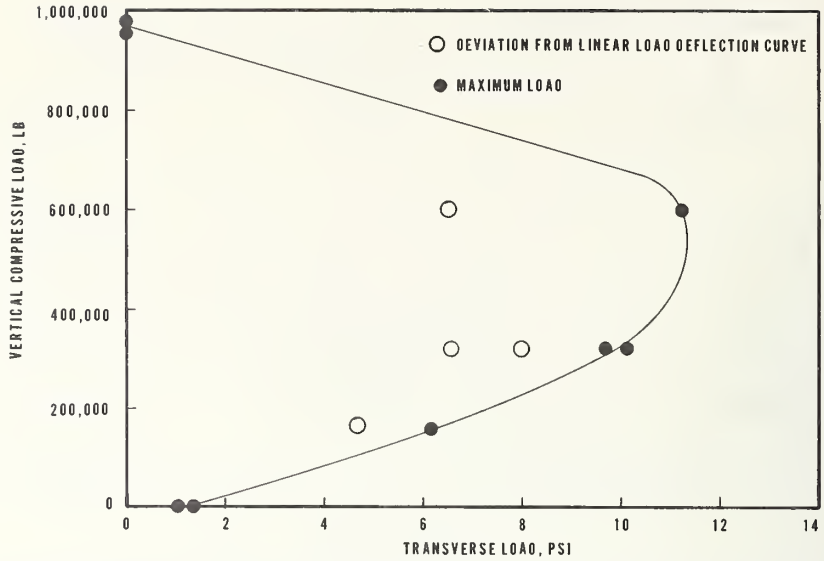

FIGURE 6.7. *Relationship between vertical compressive load and transverse load for 4-in Brick B walls with high bond mortar.*

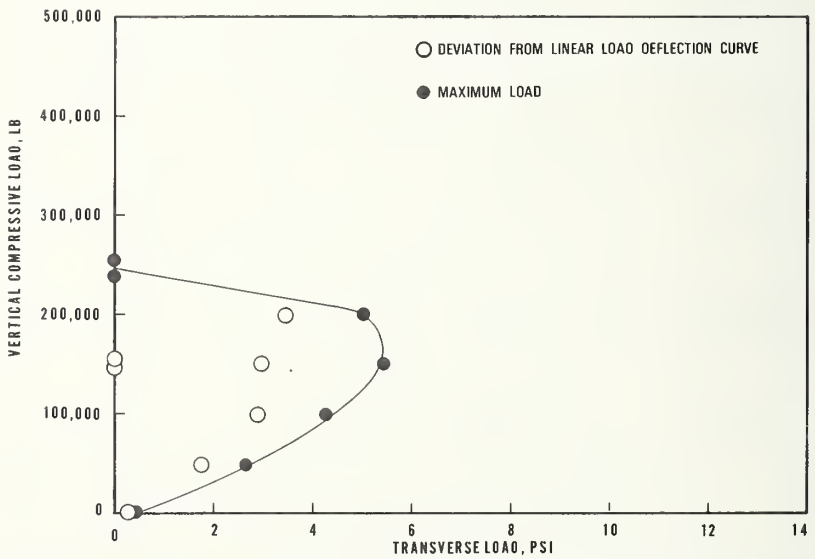

FIGURE 6.8. *Relationship between vertical compressive load for 4-2-4-in cavity block and block walls with Type N(1:3) mortar.*

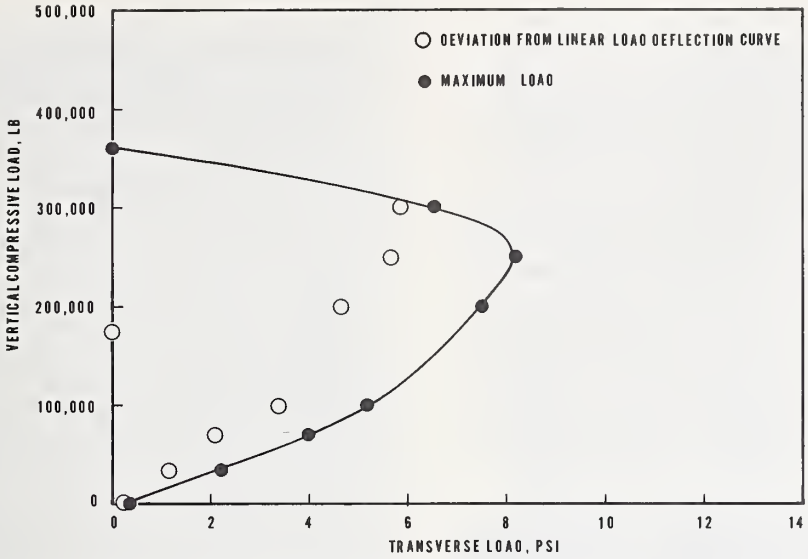

FIGURE 6.9. *Relationship between vertical compressive load and transverse load for 4-2-4-in cavity brick and concrete block walls with Type N(1:3) mortar.*

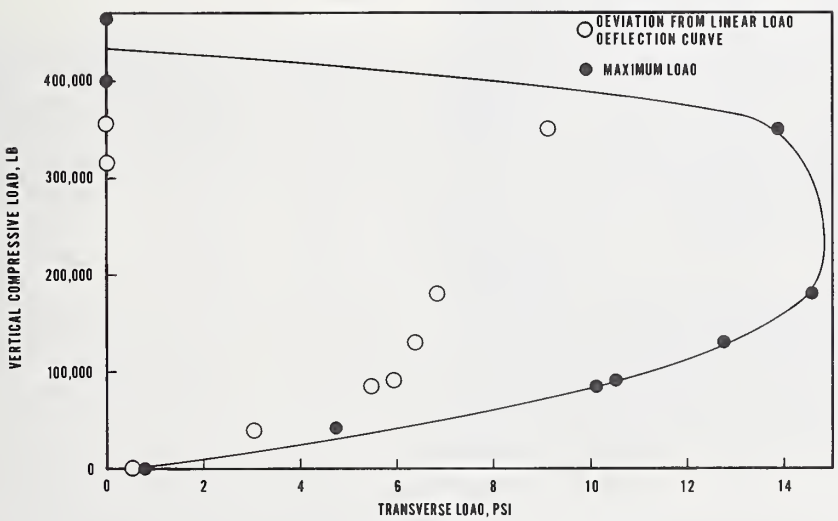

FIGURE 6.10. *Relationship between vertical compressive load and transverse load for 8-in composite brick and concrete block walls with Type N(1:3) mortar.*

1. 8-in hollow concrete block walls (1:3 mortar)

Under combined compressive and flexural loads, the walls failed by tensile cracking along horizontal joints near midspan when the vertical compressive load ranged from 0 to 60,000 lb.

For vertical compressive loads greater than 60,000 lb, vertical splitting occurred along the ends of the walls near the top or the bottom. Generally the end splitting extended from 4 to 6 courses from the top of the wall. This type of end splitting failure was also observed in the 3-block high prism tests. The failure of wall 1-4 is shown in figure 6.11. This wall was subjected to a 60,000 lb compressive load prior to the application of the transverse uniform load.

FIGURE 6.11. *Failure of 8-in hollow concrete block wall.*

2. 8-in hollow concrete block walls (high-bond mortar)

Tensile failure occurred along a horizontal joint at midspan or near midspan in walls under combined loading in which the vertical compressive load ranged from 0 to 75,000 lb. Walls that were subjected to vertical compressive loads greater than 75,000 lb failed by splitting of the end webs of the concrete masonry units near the top or near the bottom of the wall. The failure of wall 2-8 is shown in figure 6.12. This wall had a compressive load of 150,000 lb prior to the application of the transverse load.

3. 8-in solid concrete block walls (1:3 mortar)

Cracking along a horizontal joint at midspan or near midspan occurred in all wall panel specimens under combined loading in which the superimposed vertical compressive load ranged from 0 to 200,000 lb. At vertical compressive loads of 25,000 lb and 200,000 lb, initial cracking was observed at transverse air pressures of 2.8 psi and 11.4 psi, respectively. Walls subjected to vertical compressive loads ranging from 300,000 to 400,000 lb did not exhibit any cracking prior to stopping the application of transverse loads. In all wall tests in which the compressive load ranged from 200,000 to 400,000 lb, the transverse loading was stopped because of either excessive deflection of the wall or limitations on the capacity of the transverse loading system. The system was capable of applying a uniform load of 15 psi over the face of the walls. In walls subjected to vertical compressive loads greater than 400,000 lb, failure occurred by crushing accompanied by splitting in the top one to three courses. Typical failures for 3 different vertical compressive loads are shown in figure 6.13.

4. 4-in brick (A) walls (1:1:4 mortar)

5. 4-in brick (A) walls (high-bond mortar)

6. 4-in brick (S) walls (high-bond mortar)

7. 4-in brick (B) walls (high-bond mortar)

The following general comments apply to the four types of brick walls listed above. Under combined loading conditions with low vertical compressive loads, failure occurred on the tensile face of the wall by cracking along a horizontal joint near midspan as shown in figure 6.14. An increase in the vertical compressive load resulted in flexural failures that were initiated on the compressive side of the wall panel specimen. At very high vertical loads, failure occurred suddenly by crushing. A typical crushing failure is shown in figure 6.15.

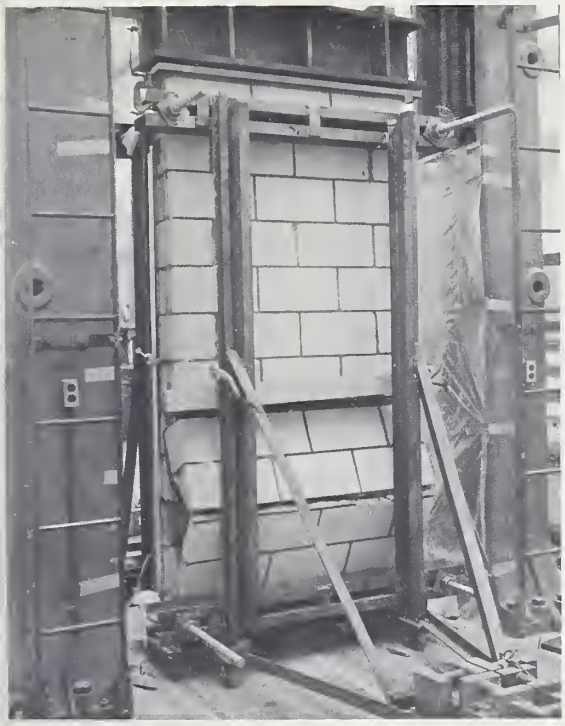

OVERALL VIEW

CLOSE UP VIEW

FIGURE 6.12. *Failure of 8-in hollow concrete block wall (specimen 2-8).*

WALL SPECMEN 3-6

WALL SPECIMEN 3-8

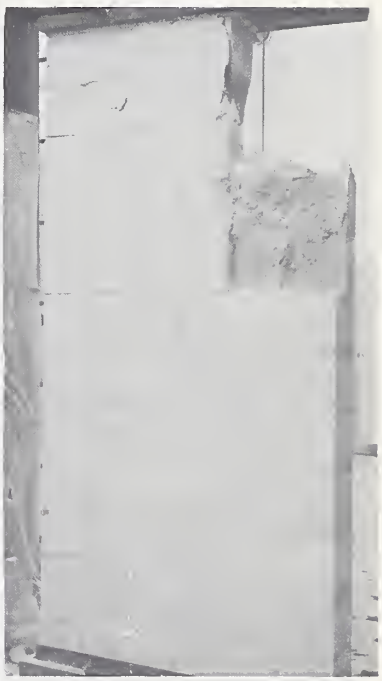

WALL SPECIMEN 3-12

FIGURE 6.13. *Failures of 8-in solid concrete masonry walls.*

410-021 OL - 71 - 4

FIGURE 6.14. *Typical failure of brick walls with low vertical compressive loads.*

FIGURE 6.15. *Typical failure of brick walls with high vertical compressive loads.*

TENSION FACE

COMPRESSION FACE

FIGURE 6.16. *Failure of block-block cavity wall (specimen 8-5).*

FIGURE 6.17. *Failures of brick-block cavity walls.*

8. 4-2-4-in cavity walls of hollow concrete block (1:3 mortar)

Tensile failure due to combined loading occurred in walls in which the applied compressive loads ranged from 0 to 100,000 lb. This type failure was in the horizontal joint on the tensile face of both wythes of the wall near midspan. In tests where the compressive load was greater than 100,000 lb, failure of the wall occurred by crushing. These crushing-type failures generally occurred near the top of the wall. The tensile face and compressive face of wall 8-5 are shown in figure 6.16. This wall was subjected to a vertical compressive load of 150,000 lb prior to transverse load application.

9. 4-2-4-in cavity walls of brick (B) and hollow concrete block (1:3 mortar)

Tensile failure due to combined loading occurred in walls in which the applied compressive load ranged from 0 to 100,000 lb. For the wall subjected to 200,000 lb compressive load, failure occurred by buckling of the ties and subsequent crushing of the masonry. In tests in which the compressive load exceeded 250,000 lb, failure occurred by crushing accompanied by some splitting of the concrete masonry units near the top of the wall. The failures of walls 9-6 and 9-7 are shown in figure 6.17. These walls were loaded with vertical compressive loads of 250,000 and 300,000 lb, respectively, prior to application of transverse loads.

10. 8-in composite brick and hollow concrete block walls (1:3 mortar)

Under combined loading, tensile failures occurred on the block face along a horizontal joint near midspan for walls having vertical compressive loads that ranged from 0 to 130,000 lb. In wall tests where the vertical compressive load exceeded 130,000 lb, the walls either failed by crushing of the concrete masonry units or flexural loading had to be suspended because of the capacity of the horizontal loading equipment. The failures of walls 10-4 and 10-5 are shown in figure 6.18. The vertical compressive loads on these walls were 90,000 and 130,000 lb, respectively.

6.3. Prism Test Results

The results of tests of masonry prisms in compression and flexure are presented in tables 6.7 and 6.8.

TABLE 6.7. *Summary of compressive tests of prisms*

Specimen designation	Mortar type	Capping material	Number of specimens tested	Age at time of test	Compressive strength (Gross area)[a]	Compressive strength (Net area)[b]
				days	*psi*	*psi*
3-block high prisms						
8-in hollow	1 : 3	plaster	3	180	440	840
8-in hollow	high-bond	plaster	3	180	760	1460
8-in hollow	high-bond	fiberboard	4	66	420	800
8-in hollow	high-bond	plaster	1	66	780	1490
8-in hollow	1 : 3	plaster	2	37	400	770
8-in hollow	high-bond	plaster	2	37	760	1460
8-in solid	1 : 3	plaster	3	180	1560	1560
8-in solid	1 : 3	plaster	2	37	1790	1790
4-in hollow	1 : 3	plaster	3	180	860	1190
4-in hollow	1 : 3	fiberboard	4	66	1020	1410
4-in hollow	1 : 3	fiberboard	4	66	960	1330
2-block high prisms						
8-in hollow	high-bond	plaster	3	180	780	1490
5-block high prisms						
8-in hollow	high-bond	fiberboard	4	66	440	840
5-course brick prisms						
brick A	1 : 1 : 4	plaster	3	35	5400	
brick A	high-bond	plaster	3	35	6240	
brick B	1 : 3	plaster	3	180	3010	
brick B	1 : 3	plaster	2	63	4870	
brick B	1 : 3	fiberboard	3	63	4520	
brick B	1 : 3	plaster	2	38	3160	
brick B	high-bond	plaster	3	35	7650	
brick S	high-bond	plaster	3	35	7320	

[a] Values were based on measured gross cross-sectional area.
[b] Values were based on measured net cross-sectional area.

TABLE 6.8. *Summary of flexural tests of prisms*

Specimen designation	Mortar type	Number of specimens tested	Age at time of test	Flexural modulus of rupture [b]	Flexural modulus of rupture [c]
			days	*psi*	*psi*
2-block high prisms					
8-in hollow	1 : 3	3	180	6	9
8-in hollow	high-bond	5	38	192	231
8-in solid	1 : 3	5	180	25	25
4-in hollow	1 : 3	8	180	26	27
7-course brick prisms [a]					
brick A	1 : 1 : 4	3	35	35	
brick A	high-bond	3	35	370	
brick B	1 : 3	5	180	54	
brick B	high-bond	3	35	430	
brick S	high-bond	3	35	220	

[a] Tested over 16-in clear span and loaded at the third points.
[b] Values were based on the gross cross-sectional area.
[c] Values based on the net cross-sectional area.

TABLE 6.9. *Values of average strengths of prisms*

Specimen designation	Mortar type	Number of specimens tested	Compressive strength (gross area)	Compressive strength (net area)	Flexural strength (gross area)	Flexural strength (net area)
			psi	*psi*	*psi*	*psi*
3-block high prisms						
8-in hollow	1 : 3	5	420	810	.....	.....
8-in hollow	high-bond	6	760	1460	.....	.....
8-in solid	1 : 3	5	1650	1650	.....	.....
4-in hollow	1 : 3	11	950	1320	.....	.....
5-course brick prisms						
brick A	1 : 1 : 4	3	5400	.....	.....	.....
brick A	high-bond	3	6240	.....	.....	.....
brick B	1 : 3	7	3580	.....	.....	.....
brick B	high-bond	3	7650	.....	.....	.....
brick S	high-bond	3	7320	.....	.....	.....
2-block high prisms						
8-in hollow	1 : 3	3	.....	.....	6	9
8-in hollow	high-bond	5	.....	.....	192	231
8-in solid	1 : 3	5	.....	.....	25	.....
4-in hollow	1 : 3	8	.....	.....	26	27
7-course brick prisms						
brick A	1 : 1 : 4	3	.....	.....	35	.....
brick A	high-bond	3	.....	.....	370	.....
brick B	1 : 3	5	.....	.....	54	.....
brick B	high-bond	3	.....	.....	430	.....
brick S	high-bond	3	.....	.....	220	.....

respectively. Table 6.9 summarizes average values of strength that were used in the evaluation of the correlation between wall and prism tests.

From the values given in table 6.7, the compressive strength of the 3-block high prisms of 8-in hollow block with high-bond mortar was 44 percent less when fiberboard was used as a capping material instead of high strength plaster.

It is also noted from table 6.7 that the compressive strength was approximately the same for both the 3-block and 5-block high prisms constructed from 8-in hollow block and high bond mortar when fiberboard was used as a capping material. The type of capping material had little effect on the compressive strength of the 3-block high prisms constructed of 4-in hollow block and the 5-course prisms made of Brick B.

When fiberboard was used as a capping material, failure occurred in the prisms constructed of 8-in hollow block and high bond mortar by vertical splitting along the middle of the end webs of the block. Vertical splitting accompanied by crushing occurred in similiar specimens capped with high strength plaster. Failure cracking in 3- and 5-block high prisms constructed of hollow block is shown in figure 6.19.

7. Theoretical Discussion

7.1. Introduction

The theoretical approach developed in this section parallels similar methods recently adopted for the design of compression members in steel structures, and proposed for reinforced concrete structures. The theory is subsequently used in the analysis of the test results in this investigation and it is demonstrated that the general trend, as well as the magnitude of these test results, are closely predicted.

7.2. Interaction Between Vertical Loads and Moments

7.2.1. General Discussion

Equilibrium conditions of short prismatic walls acted on by a combination of vertical and horizontal loads are shown in figure 7.1. The effect of deflections on the short-wall equilibrium condition is of second-order magnitude and can, therefore, be disregarded. The horizontal forces in this case act normal to the plane of the wall. Flexural tensile strength is assumed to be relatively low when compared with compressive strength. Flexural compressive strength is assumed to equal af'_m, where f'_m, is

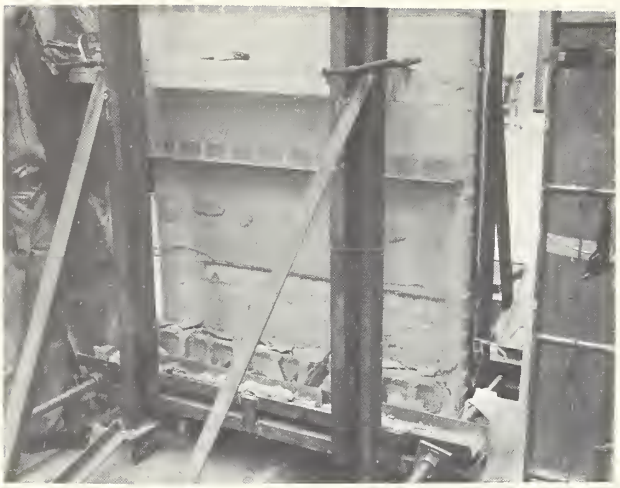

WALL SPECIMEN 10-4

WALL SPECIMEN 10-5

FIGURE 6.18. *Failures of composite walls.*

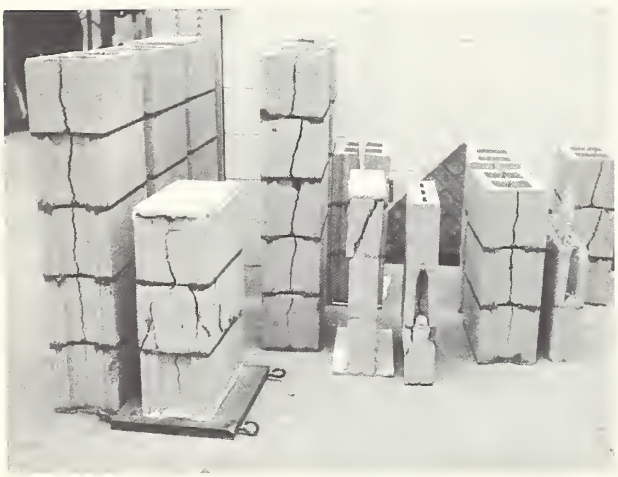

FIGURE 6.19. *Failure cracking in 3- and 5-block high prisms constructed with hollow block.*

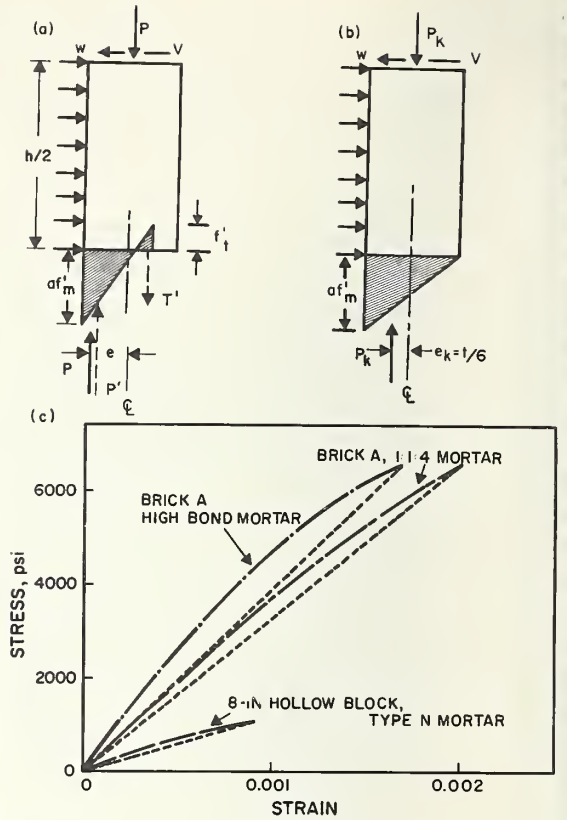

FIGURE 7.1. *Equilibrium conditions of a short wall under combined transverse and axial loads and stress-strain curves for masonry.*

the compressive strength of masonry as determined by tests on axially loaded three-block or five-brick prisms. It will be demonstrated in section 8.3 that the flexural strength factor "a" is not necessarily equal to unity and may depend on strain gradient.

In figures 7.1(a) and 7.1(b) the simplified assumption is made that the stress-strain relationship of masonry is linear up to the point of failure stress.

Typical stress-strain curves for brick and concrete block masonry used in the test specimens of this experiment are shown in figure 7.1(c). The dotted lines drawn from the origin to the end points of these curves correspond to a stress-strain relationship that would lead to the linear stress block shown in figures 7.1(a) and (b). Note that while the stress-strain relations observed in the specimens are not linear, the linear approximation does not depart very much from the actual curves. A stress block similar to the actual curves would in all cases result in an ultimate moment greater than the elastic moment represented by figures 7.1(a) and (b). The linear approximation to the stress block will therefore result in a conservative prediction of moment capacity.

It must be emphasized that the conclusions drawn from figure 7.1(c) are limited to the information available for masonry used in this testing program. Figure 7.1(c) is not necessarily typical for all types of masonry. Neither can it be stated with certainty that stress-strain relationships derived from axial loading of walls are similar to the stress-strain relationship in flexure, when there is a strain gradient. However, within the limits of the present state of knowledge, the linear stress block represents a reasonable and conservative approximation.

In figures 7.1(a) and (b) a free body is shown for a section of a wall from its top to mid-height. Figure 7.1(a) illustrates the case of a cracked section at mid-height. Figure 7.1(b) illustrates the case of an uncracked section, where the vertical resultant force at mid-height acts at the edge of the kern[8]. If the wall is assumed pin connected at its ends and therefore does not develop any moments at its end supports, the horizontal force V acting at the top of the wall can be determined as $V = wh/2$. The internal forces at mid-height must resist a moment: $M = wh^2/8$. All compressive forces P' and tensile forces T' acting on the base of the free body shown in figure 7.1(a) can be replaced by a single resultant compressive force which is equal and opposite to the axial force P and acts at an eccentricity with respect to the line of action of P, such that: $Pe = wh^2/8$.

Moments produced by linear stress blocks with a maximum stress of af'_m as illustrated in figures 7.1(a) and (b) will be referred to as "elastic ultimate moments" (M_e).

7.2.2. Cross-Sectional Moment Capacity

7.2.2.1. Solid Prismatic Sections

It has been noted in the previous section that observed stress-strain properties of the masonry tested justify the conservative assumption of a linear distribution of flexural bending stresses at failure. This proposition is also based on the assumption that plane sections remain plane under flexure and that the presence of strain gradients will not materially affect the linearity of the stress-strain relationships shown in figure 7.1(c). Equations for the moment capacity of solid prismatic sections derived herein are based on the above assumptions.

[8] The kern is the portion of the area of the cross section through which a resultant compressive force must pass if it causes no tensile stress in the cross section.

Figure 7.2(a) shows a solid prismatic section of width b and thickness t, acted upon by a vertical load P at an eccentricity e relative to the section centroid as shown in the figure.

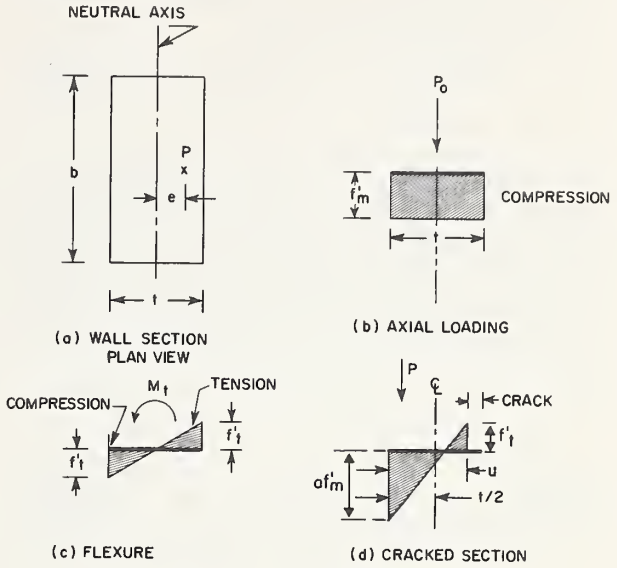

FIGURE 7.2. *Stress distribution.*

Figure 7.2(b) shows the stress distribution at failure under axial compressive load. The axial load capacity P_0 can be derived by equilibrium:

$$P_0 = f'_m bt = Af'_m \qquad (7.1)$$

where: f'_m = Compressive strength of masonry determined from axial prism test,
A = Area of net section.

Figure 7.1(b) illustrates the stress distribution when a section is loaded to capacity by a vertical load, applied at the edge of the kern. At this stress distribution there will be zero stress at the outer fibers on one side of the section.

Thus:
$$\frac{P_k e_k c}{I_n} = \frac{P_k}{A}$$

$$\therefore e_k = \frac{I_n}{Ac} = \frac{t}{6}$$

where: e_k = Distance from centroid to edge of kern,
P_k = Vertical load capacity when load is applied at the edge of the kern,
c = Distance from centroid to outer fiber,
I_n = Moment of inertia of section based on uncracked net section.

The vertical load capacity P_k is:

$$P_k = (1)/(2af'_m bt) = \frac{aP_0}{2} \tag{7.2}$$

The moment capacity at eccentricity e_k, M_k, can be derived in terms of P_k and e_k:

$$M_k = P_k e_k = \frac{aP_0 t}{12} \tag{7.3}$$

The stress distribution at flexural failure, when no resultant vertical load acts on the section, is illustrated in figure 7.2(c). Since the flexural tensile strength of masonry is generally very low compared to the flexural compressive strength, failure will be controlled by tensile strength. The moment capacity at this stress distribution, M_t, is derived below:

if: $s = \frac{f'_t}{f'_m}$

where: f'_t = Tensile strength of masonry determined from modulus of rupture test.

$$M_t = \frac{f'_t I}{c} = sf'_m \frac{bt^2}{6}$$

but: $f'_m bt = P_0$

$$\therefore M_t = \frac{sP_0 t}{6} \tag{7.4}$$

When the tensile strength at the extreme fiber of a section is exceeded the section will crack. However, initial cracking does not necessarily constitute structural failure, since the ultimate moment of the cracked section at any particular axial load may exceed the cracking moment. Equations for the ultimate moment of cracked sections are derived below.

Figure 7.2(d) shows the stress distribution on a cracked section at maximum tensile and flexural compressive stresses. Length "u" is the uncracked depth of the section and P the resultant vertical compressive force acting on the section. The following equation can be written for P:

$$P = (af'_m + f'_t)\frac{bu}{2} - f'_t bu$$
$$= \frac{bu}{2}(af'_m - f'_t) \tag{1}$$

The resultant moment acting on the section, M_e, can be defined in terms of af'_m, f'_t, and u, as:

$$M_e = \frac{bu}{2}(af'_m + f'_t)\left(\frac{t}{2} - \frac{u}{3}\right) - f'_t bu\left(\frac{t}{2} - \frac{u}{2}\right)$$
$$= \frac{bu}{2}(af'_m + f'_t)\left(\frac{t}{2} - \frac{u}{3}\right)$$
$$- \frac{bu}{2} \cdot 2f'_t\left(\frac{t}{2} - \frac{u}{3}\right) + \frac{bu}{2} 2f'_t \frac{u}{6} \tag{2}$$

Substituting (1) into (2), M_e can be expressed in terms of P:

$$M_e = P\left(\frac{t}{2} - \frac{u}{3}\right) + buf'_t \cdot \frac{u}{6} \tag{3}$$

from (1): $$bu = \frac{2P}{af'_m - f'_t}$$

and $$af'_m = \frac{aP_0}{bt}$$

$$f'_t = \frac{sP_0}{bt}$$

$$\therefore bu = \frac{2Pbt}{P_0(a-s)}$$

$$u = \frac{2Pt}{P_0(a-s)} \tag{4}$$

from (4): $$P\frac{u}{3} = \frac{P}{3}\frac{P}{P_0} \cdot \frac{2t}{(a-s)}$$

and $$buf'_t \cdot \frac{u}{6} = \frac{1}{6} \cdot \frac{sP_0}{bt} \cdot \frac{2Pbt}{P_0(a-s)} \cdot \frac{2Pt}{P_0(a-s)}$$
$$= \frac{2}{3} \cdot \frac{P^2}{P_0} \cdot \frac{ts}{(a-s)^2} \tag{5}$$

Substituting (4) and (5) into (3):

$$M_e = P\left(\frac{t}{2} - \frac{u}{3}\right) + buf'_t \cdot \frac{u}{6}$$
$$= \frac{Pt}{2}\left[1 - \frac{4}{3} \cdot \frac{P}{P_0} \cdot \frac{1}{(a-s)}\right] + \frac{Pt}{2} \cdot \frac{4}{3}\frac{P}{P_0} \cdot \frac{s}{(a-s)^2}$$
$$= \frac{Pt}{2}\left\{1 - \frac{4}{3}\frac{P}{P_0}\left[\frac{1}{a-s} - \frac{s}{(a-s)^2}\right]\right\}$$
$$= \frac{Pt}{2}\left\{1 - 1.33\frac{P}{P_0}\left[\frac{a-2s}{(a-s)^2}\right]\right\} \tag{6}$$

For masonry with no tensile strength or negligible tensile strength ($s \simeq 0$), eq (6) reduces to:

$$M_e \simeq \frac{Pt}{2}\left(1-1.33\,\frac{P}{aP_0}\right) \qquad (7)$$

It is also interesting to examine eq (6) for relatively small tensile strength, which is typical for most kinds of masonry:

the term: $\dfrac{a-2s}{(a-s)^2}$

can be rewritten as: $\dfrac{a-2s}{a^2-2as+s^2}$

but if s is very small, s^2 is of second order magnitude, and:

$$\frac{a-2s}{(a-s)^2} \simeq \frac{a-2s}{a(a-2s)} = \frac{1}{a}$$

thus: $$\frac{a-2s}{(a-s)^2} \simeq \frac{1}{a}$$

for most practical cases. This result indicates that the tensile strength of masonry has a relatively minor effect on the moment capacity of cracked sections. The equation for the moment capacity of cracked sections can thus be written as:

$$M_e = \frac{Pt}{2}\left\{1-1.33\,\frac{P}{P_0}\left[\frac{a-2s}{(a-s)^2}\right]\right\}$$

$$\simeq \frac{Pt}{2}\left(1-1.33\,\frac{P}{aP_0}\right) \qquad (7.5)$$

As noted above the ultimate cracked moment is not necessarily the greatest moment that a section can support at a given vertical load. For instance, at $P = 0$ the ultimate moment capacity of a cross section equals $M_t \neq 0$, while eq (7.5) converges to 0 as P goes to 0. Figures 7.3(a) and (b) show two different modes of stress distribution which have a resultant force P and a resultant moment Pe. In both cases the moment shown at the top of the figure is the maximum moment at which section cracking is about to occur, M_c', which occurs at the cracking load P_c. In figure 7.3(a) this vertical load is gradually decreased and always placed at an eccentricity which will generate the maximum tensile stress f_t' at the outer fiber but not cause section cracking. In figure 7.3(b) the vertical load is also decreased, but it is placed at an eccentricity at which maximum tensile and compressive stresses are developed simultaneously. The moments developed

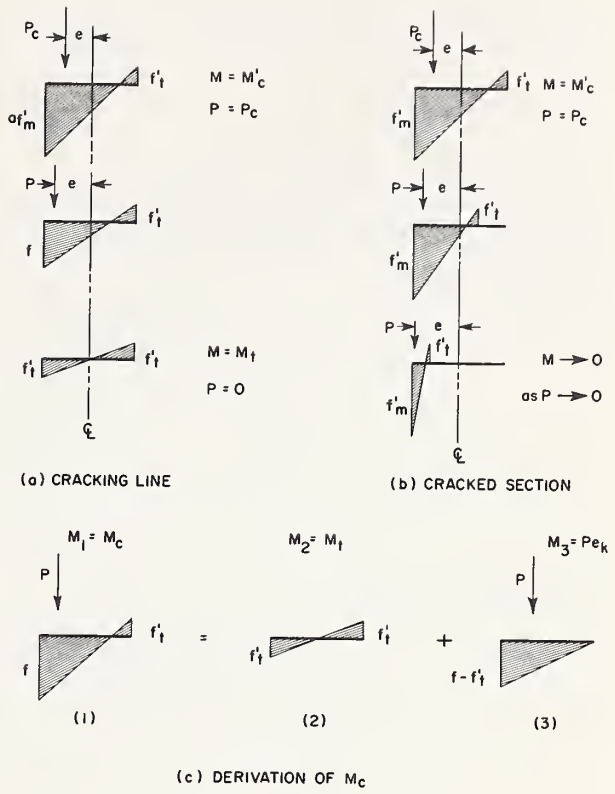

FIGURE 7.3. *Moments at $P \leq P_c$.*

by the stress distribution shown in figure 7.3(b) can be computed by eq (7.5). An equation for the stress distribution shown in figure 7.3(a) can be derived by resolving the stress block into two separate components as shown in figure 7.3(c). This moment, which is hereafter defined as the cracking moment (M_c), is given as:

$$M_c = M_{(1)} = M_{(2)} + M_{(3)}$$

$$M_{(2)} = M_t = sP_0\,\frac{t}{6} \text{ (from eq 7.4)}$$

$$M_{(3)} = Pe_k.$$

since the resultant force P is applied at the edge of the kern.

therefore: $$M_c = Pe_k + \frac{sP_0t}{6}$$

but: $$e_k = \frac{t}{6}$$

Thus: $$M_c = \frac{t}{6}\,(sP_0 + P) \qquad (7.6)$$

For masonry with no tensile strength: $M_c = Pt/6$. Since eq (7.5) converges to 0 at $P = 0$, and eq (7.6) converges to M_t at $P = 0$, there is a range of vertical loads between $P = 0$ and some value of P where the cracking moments exceed the ultimate cracked moment computed by approximate eq (7.5).

The complete equation for M_e for axial loads smaller than the cracking load (P_c) can therefore be written as follows:

$$M_e = \frac{Pt}{2}\left\{1 - 1.33\,\frac{P}{P_0}\left[\frac{a-2s}{(a-s)^2}\right]\right\}$$

$$\simeq \frac{Pt}{2}\left(1 - 1.33\,\frac{P}{aP_0}\right) \qquad (7.7)$$

or:

$$M_e = \frac{t}{6}\,(sP_0 + P)$$

whichever is greater.

At loads greater than P_c the section will not crack. Figure 7.4 shows a typical stress block at such a load. The load P acting on the section will be:

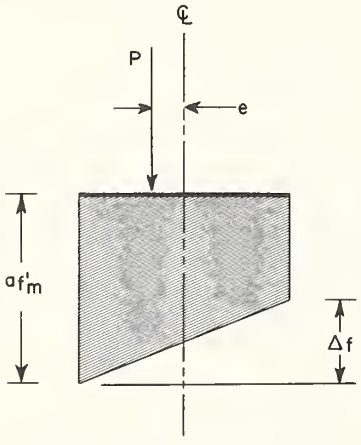

FIGURE 7.4. *Moment at $P > P_c$.*

$$P = bt\left(af'_m - \frac{\Delta f}{2}\right)$$

$$= aP_0 - \frac{\Delta f bt}{2}$$

The ultimate moment will be:

$$M_e = \frac{\Delta f bt}{2} \cdot e_k = \frac{\Delta f bt}{2} \cdot \frac{t}{6}$$

but:

$$\frac{\Delta f bt}{2} = aP_0 - P$$

therefore at $P \geq P_c$:

$$M_e = (aP_0 - P) \quad e_k = (aP_0 - P)\,\frac{t}{6} \qquad (7.8)$$

It is evident from the equations developed above that cross-sectional moment capacity is a function of the vertical load acting on the cross section. An interaction diagram can therefore be constructed by plotting ultimate moments (M_e) against vertical load. Figure 7.5 shows an interaction diagram for solid prismatic sections. In order to make this plot generally applicable, axial loads and moments were plotted in non-dimensional form. Axial loads P were divided by the axial load capacity $P_0 = f'_m\,bt$, while moments were divided by the moment capacity when the vertical load is applied at the edge of the kern, $M_k = P_0 t/12$, which corresponds to the stress distribution in figure 7.1(b). Figure 7.5 has been developed on the assumption that "a", the flexural compressive strength factor, equals unity. This is a conservative assumption which will be further discussed in section 8.3.

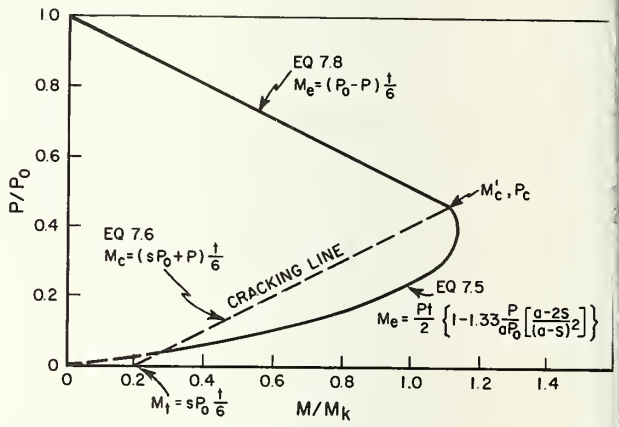

FIGURE 7.5. *Cross-sectional capacity of solid prismatic section at $f'_t = 0.1 f'_m$.*

Figure 7.5 shows the interaction diagram for masonry capable of developing a tensile strength $f'_t = 0.1\,f'_m$. The line connecting M_t at $P = 0$ with M'_c at $P = P_c$ is the locus of all moments which will bring the section to the verge of section cracking. This line, which was computed by eq (7.6) will be referred to as the "cracking line". The curve connecting the origin with M'_c is the locus of the cracked moments, computed by approximate eq (7.5). From $P = 0$ to the intersection of the cracking line with the curve, moment M_c exceeds the cracked moment and therefore represents, for all practical purposes, the section capacity. Between this intersection point and M'_c the section capacity is for all practical purposes represented by the cracked moment [eq(7.5)]. Thus a general expression for M_e between $P = 0$ and $P = P_c$ is provided by eq (7.7). The straight line connect-

ing M_c with $M = 0$ at $P/P_o = 1$ is a plot of eq (7.8) and represents section capacity above P_c.

The effect of tensile strength on section capacity is illustrated in figure 7.6. This figure shows an interaction curve for $f_t' = 0$. Note that in this case the cracking line connects the origin with M_k. The dotted lines show M_c for the case of $f_t' = 0.1\ f_m'$, which would represent a masonry of relatively high tensile strength. Note that the interaction curves differ appreciably only between $P = 0$ and a very low value of P where the cracking line intersects the curve for cracked moments. Above this point the difference between the two curves is not significant. Approximate eq (7.5) which does not consider tensile strength is therefore sufficiently accurate for all practical purposes.

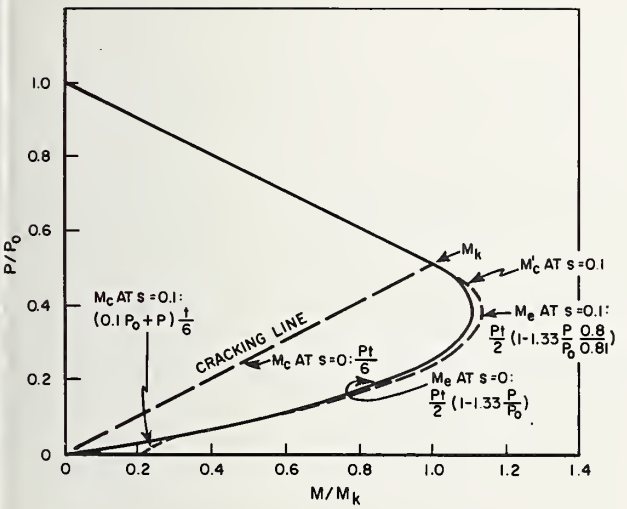

FIGURE 7.6. *Cross-sectional capacity of solid prismatic section at $f_t' = 0$.*

7.2.2.2. Symmetrical Hollow Sections

Equations developed in section 7.2.2.1 cannot be directly applied to walls which do not have a solid cross section. Similar equations can be derived for the case of hollow symmetrical cross sections (hollow block walls).

The distance from the section centroid to the edge of the kern, e_k, can be expressed as:

$$e_k = \frac{I_n}{Ac} = \frac{2I_n}{At} \tag{7.9}$$

The load capacity when a vertical load is applied at the edge of the kern, P_k, as illustrated in figure 7.1(b), can be determined by symmetry:

$$P_k = \frac{aP_0}{2} \tag{7.10}$$

Similarly, M_k, the ultimate moment associated with the stress block in figure 7.1(b) equals:

$$M_k = P_k e_k = \frac{aP_0 I_n}{At} \tag{7.11}$$

An exact continuous equation for the cracked moment, applicable to all hollow symmetrical sections, can not be derived because of the discontinuities in these sections. However, an approximate equation, sufficiently accurate for all practical purposes and applicable to any cross section, is developed below:

Eq (7.5) can be rewritten as follows:

$$M_e \simeq \frac{Pt}{2}\left(1 - 1.33\frac{P}{aP_0}\right) = Pc\left(1 - g\frac{P}{aP_0}\right)$$

where c = distance from centroid to outer fiber, and
g = a constant dependent on section geometry.

at $P = P_k$, $M = M_k = P_k e_k$

$$\therefore P_k e_k = P_k c\left(1 - g\frac{P}{aP_0}\right)$$

$$e_k = c\left(1 - g\frac{P_k}{aP_0}\right)$$

$$g = \frac{aP_0}{P_k}\left(1 - \frac{e_k}{c}\right)$$

For symmetrical sections:

$$\frac{aP_0}{P_k} = 2, \qquad \text{and} \qquad \frac{e_k}{c} = \frac{4I_n}{At^2}$$

$$\therefore g = 2\left(1 - \frac{4I_n}{At^2}\right)$$

A general approximate equation for the cracked moment can therefore be written as:

$$M_e \simeq Pc\left(1 - g\frac{P}{aP_0}\right)$$

where:
$$g = \frac{aP_0}{P_k}\left(1 - \frac{e_k}{c}\right) \tag{7.12}$$

and for symmetrical sections:

$$g = 2\left(1 - \frac{4I_n}{At^2}\right)$$

M_t, the ultimate moment at $P=0$, can be computed from the tensile strength of the material:

$$M_t = f_t' \cdot \frac{I_n}{c} = sP_0 e_k = 2sP_0 \frac{I_n}{At} \qquad (7.13)$$

It should be noted that, for hollow block with face-shell bedding, the moment of inertia I_n to be used in combination with tensile stress should be based on the face-shell area alone. However, the difference between I_n based on the face-shell area alone and I_n based on the entire net section of the masonry unit is not very great for most hollow block. In this report, I_n for the entire net section of the block is therefore used throughout.

The equation for the cracking line, can be derived from figure 7.3(c) as:

$$M_c = M_t + Pe_k \simeq sP_0 e_k + Pe_k$$

$$= e_k(sP_0 + P) = \frac{2I_n}{At}(sP_0 + P) \qquad (7.14)$$

The approximate equation for M_e between $P=0$ and $P=P_k$ can therefore be written:

$$M_e \simeq P_c\left(1 - g\frac{P}{aP_0}\right)$$

where: $$g = 2\left(1 - \frac{4I_n}{At^2}\right) \qquad (7.15)$$

or: $$M_e = \frac{2I_n}{At}(sP_0 + P)$$

whichever is greater.

An equation for M_e for vertical loads greater than P_c can be derived, as in the case of solid sections, from figure 7.4:

if: $P \geq P_c$

$$M_e = e_k(aP_0 - P) = \frac{2I_n}{At}(aP_0 - P) \qquad (7.16)$$

Note that eq (7.15) covers the range of vertieal loads from 0 to P_k, while eq (7.16) is valid from P_c to P. P_c is slightly lower than P_k and the range between P_c and P_k is covered by both equations. This redundancy results from the approximate nature of eq (7.15), which does not account for tensile strength. Eq (7.15) is a conservative approximation.

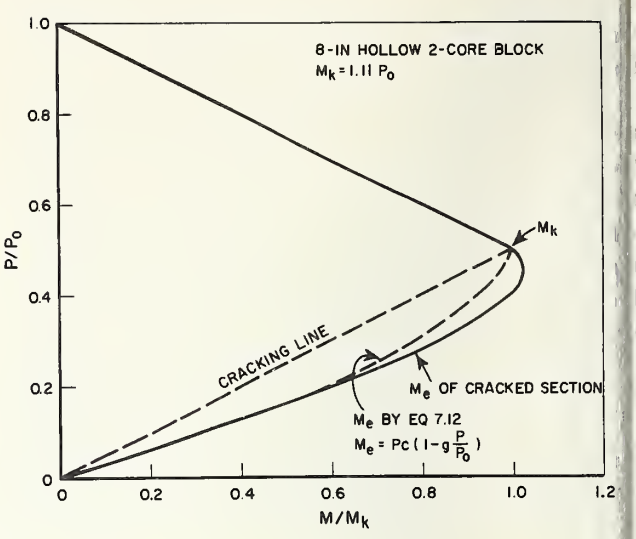

FIGURE 7.7. *Cross-sectional capacity of symmetrical hollow section.*

Figure 7.7 shows an interaction diagram for a symmetrical hollow wall section. This particular figure illustrates the case of 2-core hollow masonry block. The curve is plotted for $f_t' = 0$, since only the location of the cracking line would be significantly affected by tensile strength. The curve is plotted for the case where $af_m' = f_m'$; $(a = 1)$. As in the solid section, M_k occurs at one half the maximum axial load (P_0). However, the eccentricity of the vertical load corresponding to that moment (e_k) will be greater than was the case for the solid section. Note that in this case the maximum cracked moment only slightly exceeds M_k (1.02 M_k), while in the solid section the maximum cracked moment was 1.12 M_k (see fig. 7.5).

The interaction curve shown by the solid line in this figure has been developed by computing axial loads and moments associated with various stress blocks and is thus theoretically correct. The broken line is a plot of eq (7.12) which purports to approximate the interaction curve. Note that up to $P/P_0 = 0.2$ there is good agreement. For higher values of P/P_0, eq (7.12) begins to deviate on the conservative side; however, the maximum deviation never exceeds 8 percent. Considering that in present design practice the maximum allowable axial load is $0.2P_0$ it may be concluded that for all practical purposes eq (7.12) is sufficiently accurate.

7.2.2.3. Asymmetric Sections

The third case of interest in addition to symmetrical solid and symmetrical hollow walls is that of an asymmetric wall cross section. In this investigation

this case is represented by the composite brick and block walls.

Figure 7.8 shows an idealized asymmetric section, with the neutral axis closer to one face of the wall. Such a section would result by transforming a section composed of two kinds of masonry which have different stiffness. In the case of figure 7.8 the stiffer material would be on side 1. Transformation would be made in accordance with the ratio of the moduli of elasticity: $m = E_1/E_2$.

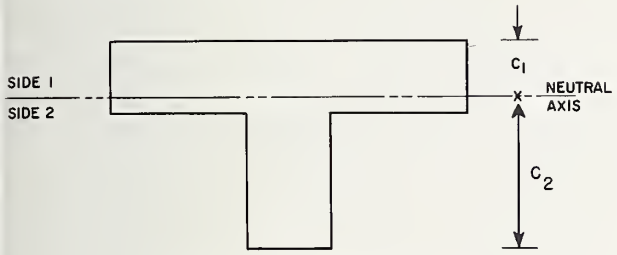

FIGURE 7.8. *Asymmetrical section.*

The area of side 1 would be multiplied by "m". Compressive strengths associated with the transformed section would be $a_1 f'_{m1}/m$ and f'_{t1}/m on side 1 and $a_2 f'_{m2}$ and f'_{t2} on side 2.

The distances from the neutral axis to the edge of the kern, e_k, can be computed as follows: When a load P is applied at the kern eccentricity, the stress at the outer fiber opposite to that eccentricity will be zero.

Therefore:

$$\frac{P_{k1}}{A} = \frac{P_{k1} e_{k1} c_2}{I_n}$$

Loads P_k, the load capacities at kern eccentricity, which will be different for sides 1 and 2 can be determined from e_k as:

$$e_{k1} = \frac{I_n}{Ac_2}$$

Similarly
$$e_{k2} = \frac{I_n}{Ac_1} \qquad (7.17)$$

$$a_2 f'_{m2} = \frac{P_{k2}}{A} + \frac{P_{k2} e_{k2} c_2}{I_n}$$

$$= P_{k2}\left(\frac{1}{A} + \frac{I_n c_2}{A I_n c_1}\right) = \frac{P_{k2}}{A}\left(\frac{c_1 + c_2}{c_1}\right)$$

$$\therefore P_{k2} = a_2 f'_{m2} \cdot \frac{Ac_1}{t};$$

Similarly:
$$P_{k1} = \frac{a_1}{m} f'_{m1} \cdot \frac{Ac_2}{t}$$

therefore:
$$\frac{P_{k1}}{P_{k2}} = \frac{a_1 f'_{m1}}{m a_2 f'_{m2}} \cdot \frac{c_2}{c_1} \qquad (7.18)$$

Values for M_k, the ultimate moment at kern eccentricity, can be derived from equations (7.17) and (7.18):

$$M_{k2} = P_{k2} e_{k2} = a_2 f'_{m2} \cdot \frac{Ac_1}{t} \cdot \frac{I_n}{Ac_1} = a_2 f'_{m2} \cdot \frac{I_n}{t}$$

Similarly:
$$M_{k1} = a_1 f'_{m1} \cdot \frac{I_n}{mt}$$

and:
$$\frac{M_{k1}}{M_{k2}} = \frac{a_1 f'_{m1}}{m a_2 f'_{m2}} \qquad (7.19)$$

The ultimate moment of a cracked section for this case can be computed by approximate eq (7.12) as:

$$M_{c1} = Pc_1\left(1 - g_1 \cdot \frac{P}{aP_{01}}\right)$$

where:
$$g_1 = \frac{a_1 P_{01}}{P_{k1}}\left(1 - \frac{e_{k1}}{c_1}\right)$$

and
$$M_{c2} = Pc_2\left(1 - g_2 \cdot \frac{P}{aP_{02}}\right)$$

where
$$g_2 = \frac{a_2 P_{02}}{P_{k2}}\left(1 - \frac{e_{k2}}{c_2}\right) \qquad (7.20)$$

Values for P_{01} and P_{02} are hypothetical values of axial strength based on the respective material components on sides 1 and 2. An actual specimen would develop only the lower of these two computed strengths.

Equations for ultimate tensile moments M_t at $P = 0$ can also be derived as:

$$M_{t1} = \frac{f'_{t2} I_n}{c_2}$$

$$M_{t2} = \frac{f'_{t1} I_n}{mc_1} \qquad (7.21)$$

Expressions for the cracking lines will therefore be:

$$M_{c1} = M_{t1} + Pe_{k1}$$
$$M_{c2} = M_{t2} + Pe_{k2} \qquad (7.22)$$

Equations (7.18) through (7.20) have been derived for the general case where the ratio of the moduli of elasticity of the two materials differs from the ratio of the flexural compressive strengths ($E_1/E_2 \neq a_1 f'_{m1}/a_2 f'_{m2}$). However, in the particular case of the composite brick and block walls tested in this study, and also for a wide range of different masonry systems, the expression:

$$\frac{E_1}{E_2} \simeq \frac{a_1 f'_{m1}}{a_2 f'_{m2}}$$

is approximately correct, or E is approximately proportional to af'_m. This relationship makes it possible to greatly simplify equations (7.18) to (7.20). These simplified equations are summarized below:

Loads P_k:

$$P_{k1} = \frac{aP_0}{1+\frac{c_1}{c_2}}; \quad P_{k2} = \frac{aP_0}{1+\frac{c_2}{c_1}}$$

$$\frac{P_{k1}}{P_{k2}} = \frac{c_2}{c_1} \tag{7.23}$$

Moments M_k:

$$M_{k1} = M_{k2} = P_{k1}e_{k1} = P_{k2}e_{k2} \tag{7.24}$$

Cracked Moments:

$$\left.\begin{aligned} M_{e1} &= Pc_1\left(1 - g_1 \cdot \frac{P}{aP_0}\right) \\ \text{where:} \quad g_1 &= \frac{aP_0}{P_{k1}}\left(1 - \frac{e_{k1}}{c_1}\right) \\ M_{e2} &= Pc_2\left(1 - g_2 \cdot \frac{P}{aP_0}\right) \\ \text{where:} \quad g_2 &= \frac{aP_0}{P_{k2}}\left(1 - \frac{e_{k2}}{c_2}\right) \end{aligned}\right\} \tag{7.25}$$

An interaction diagram for an asymmetric section is shown in figure 7.9. This figure applies to the composite brick and block walls used in this program. In this case the ratio of the moduli of elasticity approximately equals the ratio of the masonry strengths, and simplified equations (7.23), (7.24) and (7.25) are applicable. The conservative assumption was also made that $a = 1$. The diagram shown on side 1 applies to moments which cause block compression and side 2 applies to moments that cause brick compression. It will be seen later in this report that moment capacity in both directions must be considered in order to predict the strength of this wall system. Cracking lines were drawn for $f'_t = 0$. Note that P_k depends on the direction of eccentricity; however, for the case where f'_m is proportional to E the values for M_k and P_0 are unique. Accurately computed interaction curves are drawn as solid lines. These are compared with interaction curves which are computed by approximate eq (7.25). Note that the agreement for brick compressive moments is excellent. For block compressive moments the approximate equation closely predicts moments up to $P/P_0 = 0.15$. For higher values of P moments are slightly overestimated; however, the largest discrepancy does not exceed 5 percent. Again it may be concluded that the approximate equation is sufficiently accurate for all practical purposes.

7.3. Slenderness Effects

Slenderness effects on the moment capacity of walls are illustrated in figure 7.10. This figure shows the free body of the upper half of a deflected wall subjected to axial and transverse loads. The effective moment at any point along the height of this wall will be determined by the location of the line of action of the vertical force, relative to the location of the deflected centerline of the wall. Hence, the moment acting on any section of the wall is magnified by an added moment equal to the product of the axial force and the centerline deflection.

A similar problem has been analyzed for the case of eccentrically loaded reinforced concrete columns [7], where it has been shown that the external moments acting on a column are magnified and that this effect can be predicted quite reasonably by the following equation:

$$M_e = M_0 \frac{C_m}{1 - \frac{P}{P_{cr}}} \tag{7.26}$$

where C_m is a moment correction factor, depending on the ratio of the end moments and the shape of the primary moment diagram and $P_{cr} = \pi^2 EI/(kh)^2$ is the axial load that will cause a stability-induced compression failure. This method of computing the total moment is designated as the "Moment Magnifier Method". A similar method may be applied to the loading conditions of the tests reported herein.

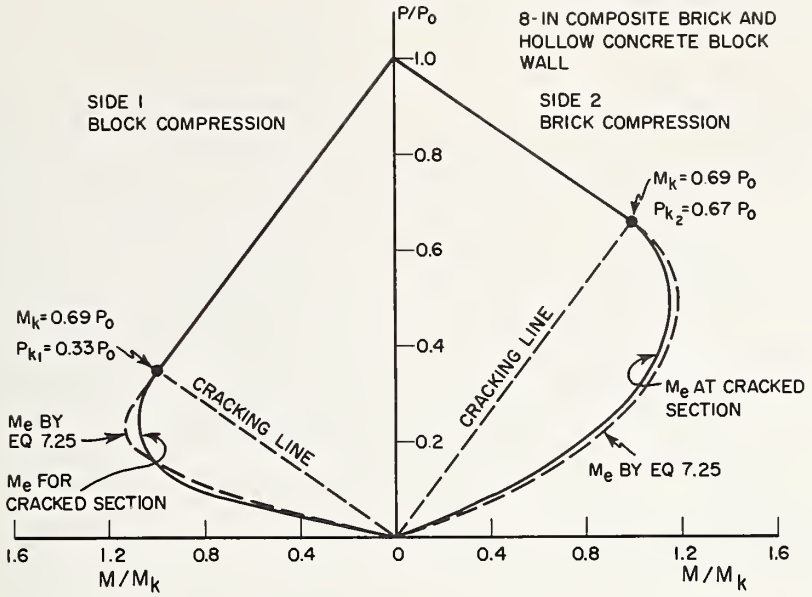

FIGURE 7.9. *Cross-sectional moment capacity of asymmetrical section.*

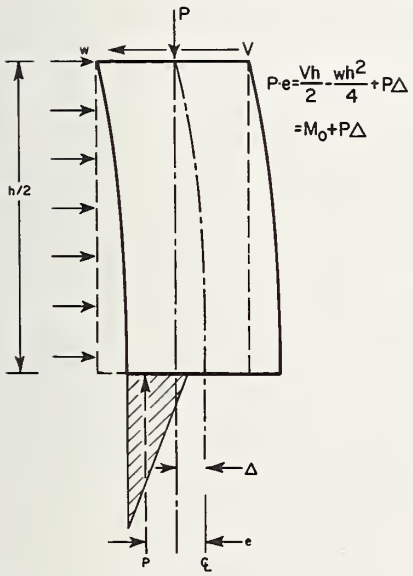

FIGURE 7.10. *Slenderness effects on equilibrium.*

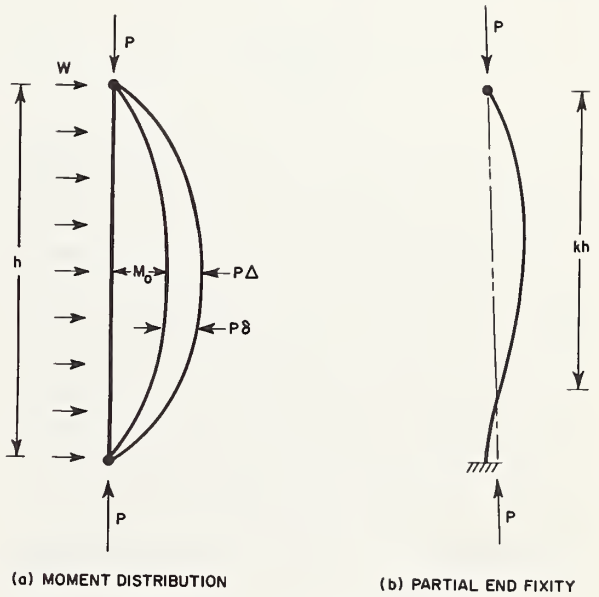

FIGURE 7.11. *Slenderness effects.*

Figure 7.11(a) shows the moment diagram acting on a wall which is subjected to combined axial and transverse loading. If it is assumed that the wall section is pin-ended, the moment due to transverse load will be parabolically distributed over the height of the wall with a maximum moment at mid-height, $M_0 = (1/8)wh^2$. If it is in turn assumed that the deflection curve of the wall is also parabolic,[9] the added moment caused by the action of the axial load on the deflected wall, $P\delta$, will also be distributed parabolically with a maximum moment $P\Delta$ at mid-height. Thus the maximum total moment acting on the wall at mid-height, which at failure will equal the section capacity M_e, equals $M_e = M_o + P\Delta$. If it is assumed that the stiffness EI is constant over the height of the wall the following equation can be written for Δ, the mid-height deflection:

$$\Delta = \frac{5}{48}\frac{h^2}{EI}(M_0 + P\Delta)$$

[9] A parabolic curve is a close approximation to the actual deflection curve.

The maximum added moment acting at mid-height, $P\Delta$, can be expressed in terms of Δ:

$$P\Delta = \frac{5Ph^2}{48EI}(M_0 + P\Delta)$$

If it is now assumed that the maximum moment: $M_e = M_0 + P\Delta$, then:

$$M_e = M_0 + \frac{5Ph^2}{48EI} \cdot M_e$$

$$\therefore M_e = M_0 \frac{1}{1 - \frac{5Ph^2}{48EI}}$$

but:

$$\frac{48EI}{5h^2} \simeq \frac{\pi^2 EI}{h^2} = P_{cr}$$

The equation for section capacity for pin-ended conditions can therefore be rewritten:

$$M_e = M_0 \frac{1}{1 - \frac{5Ph^2}{48EI}} \simeq M_0 \frac{1}{1 - \frac{P}{P_{cr}}} \qquad (7.27)$$

Under conditions of partial end-fixity the deflection curve, and thus the magnitude of the added moment, will change. For the particular case of transverse loading, the equation for pin-ended conditions can be modified by substituting the "effective" wall height, kh, at which a pin-ended member of equal stiffness (EI) would develop similar slenderness effects, for the wall height h. Effective heights for different conditions of end-fixity for braced members, as well as members which are free to sway at the top, may be conveniently determined by referring to the Jackson and Moreland Alignment Charts [8]. Partial end-fixity is illustrated in figure 7.11(b), and eq (7.26) thus becomes:

$$M_e = M'_0 \frac{1}{1 - \frac{P}{P_{cr}}} \qquad (7.28)$$

where: $$P_{cr} \simeq \frac{\pi^2 EI}{(kh)^2}$$

and M'_0 is the maximum moment in the direction of the transverse loads at the given end-fixity.

The equation must be modified for section cracking (change in I), and change in E with increasing stresses. For a material with a relatively small tensile strength, the section will be cracked within the range of vertical loads where section capacity is governed by the ultimate moment for a cracked section. Thus, the stiffness (EI) of the section is a function of vertical load. Consequently, EI in the moment magnification equation is a function of P/P_0.

It has been shown for lightly reinforced concrete columns [7] that slenderness effects can reasonably be approximated by using an "equivalent" EI of $E_i I_n/2.5$. Observation of the magnitude of deflections of the slender brick walls tested in this study indicates that at axial loads up to about $0.25P_0$ an "equivalent" EI of $E_i I_n/3$ will fit the test results reasonably well. For this case eq (7.28) can thus be modified as:

$$M'_0 = M_e \left(1 - \frac{P}{P_{cr}}\right)$$

where: $$P_{cr} \simeq \frac{\pi^2 E_i I_n}{3(kh)^2} \qquad (7.29)$$

This equation accounts also for partial end-fixity.

The above equation is a good approximation for the range of vertical loads between $P = 0$ and $P = 0.25P_0$. For higher vertical loads section capacity is underestimated by eq (7.29). Closer examination of the test results on brick walls indicated that an equivalent EI of:

$$EI = E_i I_n \left(0.2 + \frac{P}{P_0}\right) \leq 0.7 E_i I_n \qquad (7.30)$$

will approximate the actual test results of slender walls over the entire range of vertical loads.

Reduced interaction curves can be developed by plotting $M_e - P\Delta$ for each value of P. Such reduced curves will show the value of M'_0, the moment that can be imposed on the wall by external forces at any particular value of P.

These interaction curves can be used to determine the moment capacity of slender walls since they have been in effect corrected for effects of deflections. Reduced interaction curves using equations (7.29) and (7.30) are compared with test results in the following sections.

Figure 7.12 illustrates the effect of different slenderness ratios on an interaction diagram for a solid prismatic section. While slenderness is traditionally expressed by the parameter kh/t, slenderness effects, computed by the moment magnifier method, depend on the parameter P_0/P_{cro}

where: $$P_{cro} = \frac{\pi^2 E_i I_n}{(kh)^2}$$

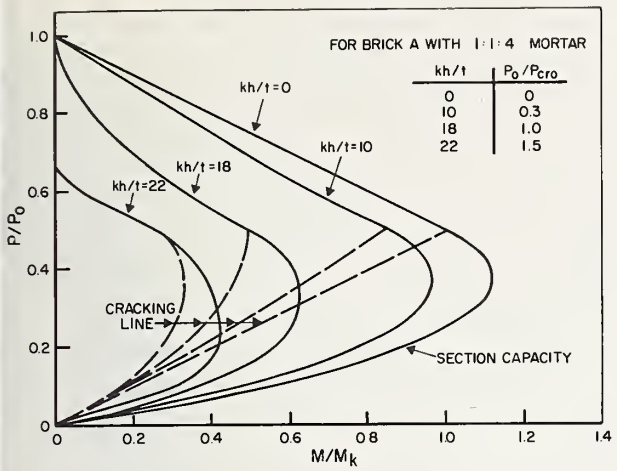

FIGURE 7.12. *Slenderness effects on moment capacity of solid prismatic section.*

The figure illustrates the order of magnitude of slenderness effects for different kh/t ratios of Type A Brick with 1:1:4 mortar. Note that the location of the cracking line is also affected by slenderness.

8. Analysis of Test Results

8.1. Introduction

In this section the test results are analyzed and compared with the theory developed in section 7.

Section 8.2 deals with the observed stress-strain properties of the different types of masonry tested in this investigation. In section 8.3, section capacity is evaluated on the basis of test results on small prism specimens. In section 8.4 the strength and rigidity of the wall panels tested are evaluated. The magnitude of measured slenderness effects is determined and compared with theoretically predicted slenderness effects.

8.2. Stress-Strain Relationships

Stress-strain curves for concrete block and brick, developed from tests of axially loaded block prisms and brick piers are shown in figures 8.1, 8.2, and 8.3.

Figure 8.1 shows the stress-strain curve obtained from an axially loaded 8-in hollow block prism with 1:3 mortar. An initial tangent modulus of elasticity of 1.5×10^6 psi was developed, and at failure a secant modulus of elasticity of 1.3×10^6 psi and a tangent modulus of elasticity of 650,000 psi. It should be realized that stress-strain relations may be different if masonry is subjected to strain gradients associated with flexural stress. Nevertheless, on the basis of this information, which is the only information

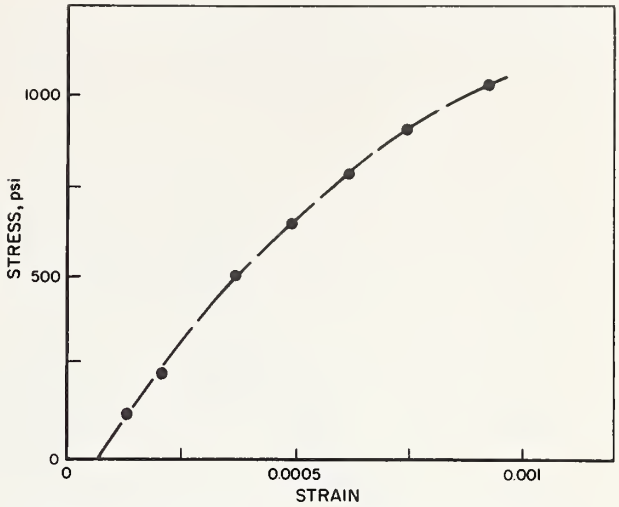

FIGURE 8.1. *Stress-strain diagram from axially loaded 8 × 8 × 16-in hollow block prism with Type N(1:3) mortar.*

available for the concrete block test specimens used, it appears that the simplified assumption of linear stress distribution at failure is a reasonably good and slightly conservative approximation.

Stress-strain curves obtained from a series of tests on 16 × 16-in and 24 × 24-in piers made of Brick A with 1:1:4 mortar are shown in figure 8.2.[10] The average initial tangent modulus of elasticity from these tests is 3.65×10^6 psi, and the average secant modulus of elasticity at failure is 3.25×10^6 psi. The results from these tests are reasonably consistent, except that one specimen appeared to have significantly less stiffness. Again, the assumption of a linear stress distribution at flexural failure appears justified, even though strain gradients may have an effect on stress-strain relationships in compression.

Figure 8.3 shows a similar family of curves for specimens made of Brick A with high-bond mortar.[10] The average initial modulus of elasticity of these specimens was 4.2×10^6 psi and the average secant modulus at failure was 3.6×10^6 psi. Some of these specimens developed significantly more deformation than other specimens, but on the whole it again appears that the approximation of a linear stress distribution at flexural failure is justified.

8.3. Cross-Sectional Capacity

It has been noted in section 7.2 that compressive strength of masonry in flexure does not necessarily equal the compressive strength in pure compression.

[10] A study of high-bond mortars, conducted at the National Bureau of Standards in June 1968.

This relationship can be investigated by examining the cross-sectional capacity of short walls where slenderness effects are negligible.

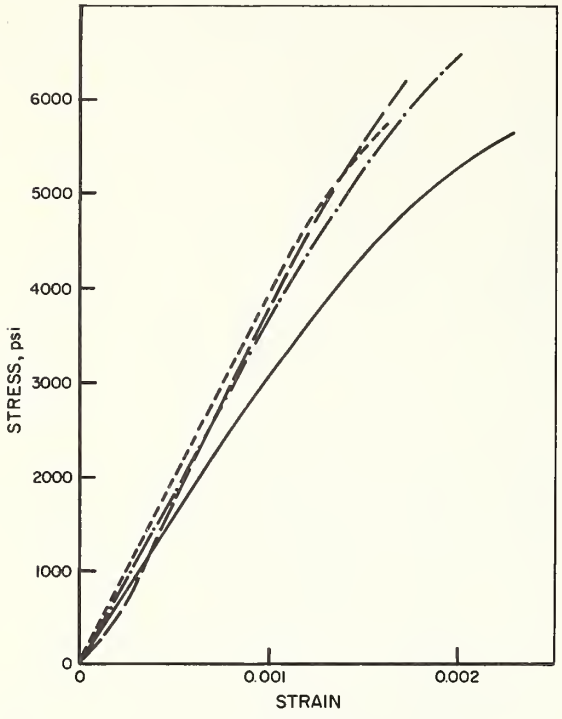

FIGURE 8.2. *Stress-strain diagrams from axially loaded piers, Brick A with Type N(1:1:4) mortar.*

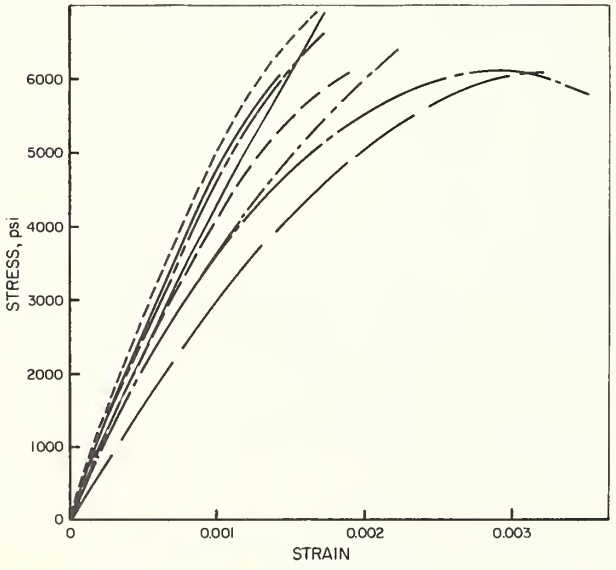

FIGURE 8.3. *Stress-strain diagrams from axially loaded piers, Brick A with high bond mortar.*

Short-wall section capacity for hollow concrete block, solid concrete block, and brick was investigated in a series of tests on eccentrically loaded prisms. The masonry units used in these tests had somewhat different properties than the masonry units used in the full scale walls. The information conveyed therefore, is of a qualitative, rather than a quantitative nature. Other prism tests with masonry units and mortars similar to the ones used in the wall specimens were conducted while the testing program was in progress and were used to determine section capacity of the wall systems tested, however, these prisms were subjected only to axial loads.

The results of tests on eccentrically loaded prisms made of hollow 8 × 8 × 16-in concrete block, solid 8 × 8 × 16-in concrete block and 4-in brick are shown in figures 8.4, 8.5, and 8.6, respectively.

Figure 8.4 shows a plot of 12 tests that were conducted on three-block prism specimens made of hollow 8-in concrete masonry units using type N mortar. Vertical loads were applied at different eccentricities, as shown in the sketch, in order to determine the cross-sectional capacity to resist combined vertical loads and moments. The solid curve is a theoretical interaction curve developed on the assumption that $f'_m = af'_m$ or $a = 1$. Comparison of this interaction curve with test results indicates that the load capacity under eccentric loading exceeds the capacity predicted on the assumption that $a = 1$ by a considerable margin.

A second theoretical curve, shown by the dashed line is the theoretical interaction curve corresponding to the average apparent flexural compressive strength developed at the $t/3$ eccentricity, which exceeds the compressive strength under axial load by 40 percent ($a = 1.4$). Comparison of this second interaction curve with the test results at eccentricities smaller than $t/3$ indicates that apparently factor "a" increases with increasing strain gradients.

The observed mode of failure in these tests was generally vertical splitting of the webs which originated at the corners of the intersection between the webs and the face shells, followed at the larger eccentricities by crushing of the face shells.

Figure 8.5 shows a plot of 12 tests on eccentrically loaded 8 × 8 × 16-in solid concrete block prisms. In these tests the strength increase at increasing load eccentricity is even greater, since the apparent compressive strength developed at maximum load eccentricity exceeded the compressive strength under axial loading by 145 percent.

Tests results from eccentrically loaded brick prisms are illustrated in figure 8.6. A similar phenomenon can be observed in this case, where ap-

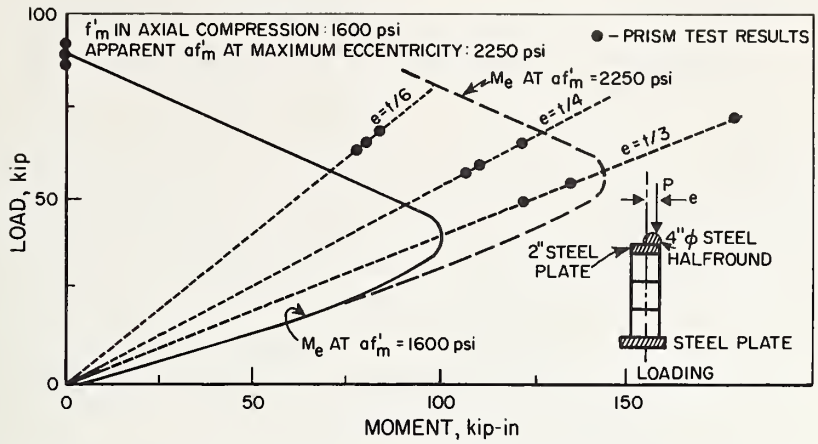

FIGURE 8.4. *8-in hollow concrete block prisms with Type N mortar under eccentric loading.*

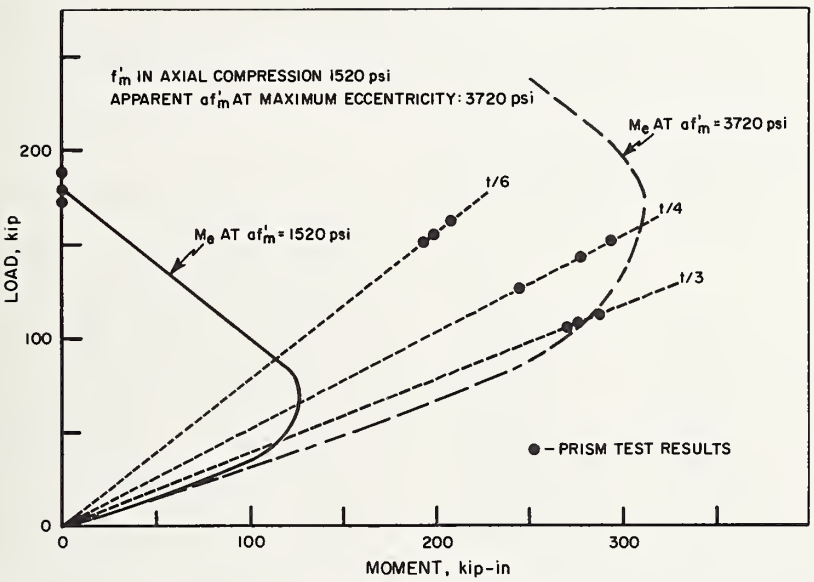

FIGURE 8.5. *8-in solid concrete block prisms with Type N mortar under eccentric loading.*

parent compressive strength developed under maximum eccentricity exceeds compressive strength under axial loading by 144 percent.

It should be noted that the preceding test results may be affected to some extent by end fixity conditions. It is also important to note that in all the preceding cases the apparent compressive strength in flexure was computed on the assumption of a linear stress distribution at flexural failure. If the stress distribution at failure was not linear, flexural compressive stresses may have been overestimated. But even had the specimens developed a fully plastic moment, compressive flexural strength would exceed compressive strength under axial loading by a considerable margin. It is also apparent from figures 8.4, 8.5, and 8.6, that in all cases "a" increases with increasing strain gradients. This can be seen by comparing the test results with the dashed interaction curves, which were computed for the average flexural strength at the $t/3$ eccentricity.

It has been noted above that prisms constructed during this testing program as companion specimens to the wall panels were tested in axial compression only. While the test results illustrated in figures 8.4, 8.5, and 8.6 provide qualitative information to the effect that $af'_m > f'_m$ and that the factor "a" seems to increase with increasing strain gradients, the magnitude of factor "a" for the wall panels tested cannot be estimated on the basis of available information. In the subsequent interpretation of test results, wall panel strength will be analytically predicted on the basis of prism strength, making the conservative as-

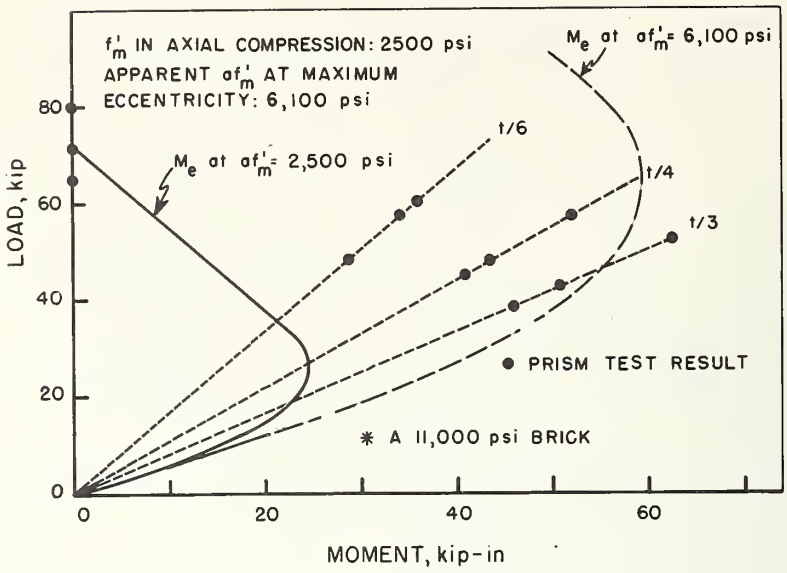

FIGURE 8.6. *4-in brick* prisms with 1:1:4 mortar under eccentric loading.*

sumption that $a = 1$, and that wall panel strength will therefore equal or exceed the strength predicted on the basis of compressive tests on axially loaded prisms.

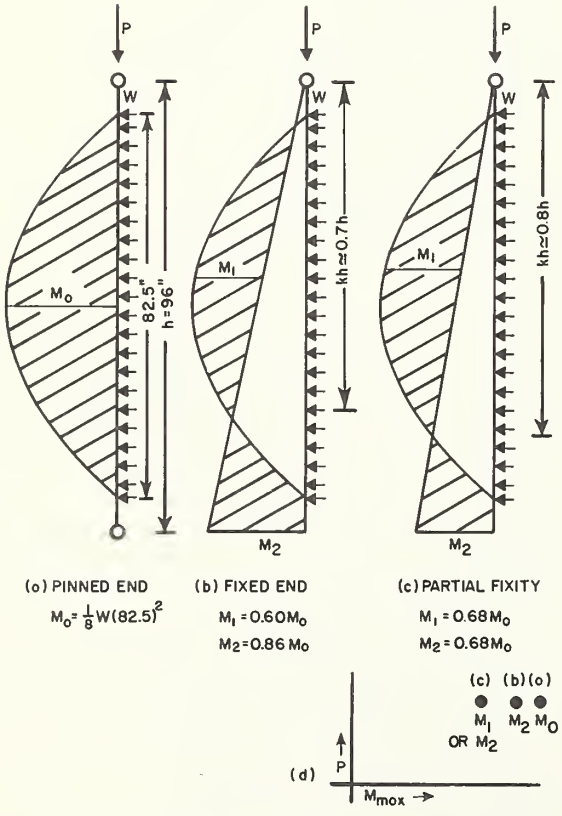

FIGURE 8.7. *Influence of end conditions.*

8.4. Wall Strength

8.4.1. General Discussion of the Test Conditions

Figure 5.1 illustrates the test setup and the loading conditions. The top of the wall is free to rotate but is restrained from lateral movement and may be considered as pin connected. The bottom of the wall rests on a fiberboard which does permit rotation, but may impose some restraint on the rotation, particularly under large vertical loads. While these test conditions attempt to simulate actual conditions in a structure, they also impose a varying degree of restraint on the wall base, which will tend to reduce the maximum moment caused by superimposed loads when compared to a wall with a pinned base.

Figure 8.7 illustrates the approximate influence of end conditions on moments due to superimposed lateral loads for three hypothetical cases. In figure 8.7(a), the wall base is free to rotate and the maximum moment due to lateral load is developed. Figure 8.7(b) illustrates the case of complete fixity of the wall base. In the latter case, the maximum moment occurs at the wall base and equals approximately 86 percent of the maximum moment in figure 8.7(a).[11]

[11] The magnitude of this moment will be influenced by the effects of the vertical load, section cracking, and changes of the modulus of elasticity with changing stress. These factors were not considered when the approximate fixed ended moment was determined.

Figure 8.7(c) illustrates the case of partial restraint of the wall base which produces the least possible moments due to superimposed lateral loads. Note that in this case the lateral load produces only 68 percent of the moment that is produced in the case of a pin connection at the bottom of the wall. Figure 8.7(d) illustrates the effect that the assumed end conditions would have on the determination of the moment that acted on the wall at a given lateral load. End conditions will also significantly influence slenderness effects as discussed in section 7.3.

In the subsequent interpretation of results it has been assumed that partial end restraint reduced moments in the walls to 68 percent of the pin-ended moments. Slenderness effects for the conditions illustrated in figure 8.7(c) were assumed to correspond to an "effective" wall height of 80 percent of actual height ($k = 0.8$). Wall strength computed in this way will be the lowest strength that the walls could have developed.

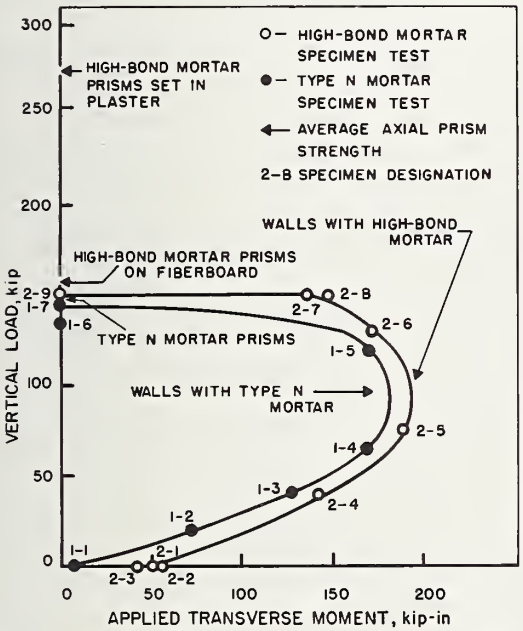

FIGURE 8.8. *Comparative strength of 8-in hollow concrete block walls with Type N and high bond mortars.*

8.4.2. Concrete Block Walls

8.4.2.1. 8-in Hollow Concrete Block Walls

Figure 8.8 shows a comparative plot of the test results on hollow 8-in concrete masonry walls with ASTM type N (1:3) mortar, and walls built of the same masonry units using high-bond mortar. Moments plotted in the figure are the moments imposed by transverse loads, assuming partial fixity as illustrated in figure 8.7(c). The curves shown in the figure show the average trend of the test results.

Note that at $P = 0$ the three high-bond mortar walls tested developed moments of 42.3 kip-in, 52.2 kip-in and 54.8 kip-in while the wall with type N mortar developed a 3.3 kip-in moment. These moments correspond to an average masonry tensile strength of 130 psi for high-bond mortar walls and a tensile strength of 6 psi for the regular mortar wall tested. (Correction has been made for the weight of the wall.) The average tensile strength for these wall systems, as determined by flexure tests on two-block prisms, was 231 psi for high-bond mortar and 9 psi for regular mortar. Thus the full-scale walls developed at least 50 percent of the tensile strength determined by prism tests for high-bond mortar, and 60 percent of the tensile strength for regular mortar.

Further comparison of the test results for the two wall systems indicates that, at higher vertical loads, the moment capacities of the two wall systems did not differ significantly and that the maximum axial load bearing capacity of the two systems was about equal.

Wall strength in pure compression, computed on the basis of the average strength obtained from prism tests, is also shown in figure 8.8. Note that there is good agreement between compressive strength of conventional mortar prisms and strength of the full scale wall system. In the case of high-bond mortar, the strength of prisms set in plaster exceeded wall strength by a considerable margin. The strength was correctly predicted by prisms set on fiberboard. This difference in strength may be caused by the added lateral restraint imposed by the friction between the prism support and the capping. The combined effect of the stronger high-bond mortar and the end restraints will prevent failure of the masonry units by vertical splitting, which is the usual mode of failure. It should also be noted that in the test panels, fiberboards were set at the top and bottom of the wall panels.

In order to make a meaningful comparison between the interaction curve, predicted for a short wall on the basis of prism strength, and the strength of a more slender wall, the added moment attributable to deflections must be taken into consideration. This can be done approximately by adding to the moment imposed on the wall by transverse loads an additional moment which equals the axial load times

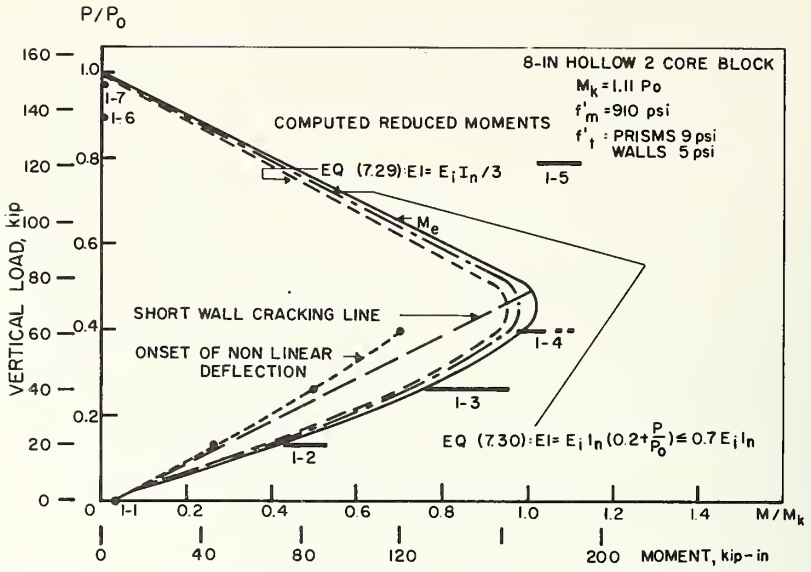

FIGURE 8.9. *8-in hollow block walls with Type N mortar, correlation with prism strength.*

the maximum deflection of the wall at failure, relative to the line of action of the axial load.

Figure 8.9 compares the experimental strength of the 8-in walls constructed using conventional mortar with an analytical prediction based on prism tests. In this analytical prediction the prism strength under axial compression was used as a basis of computing $f'_m (af'_m = f'_m)$.

To bring prism tests and wall tests to a common denominator, and to afford comparison, all vertical loads are divided by P_0, the load-bearing capacity under axial loading computed on the basis of the average prism strength, and all moments are divided by the maximum theoretical moment capacity if the vertical load is applied at the edge of the kern of the section (M_k), based on the assumption that flexural compressive strength is equal to compressive strength in pure compression. The actual magnitude of loads and moments is also shown in figure 8.9 by additional scales.

For each test point, both the moment imposed by transverse loads and the added moment imposed by deflection are shown. The part of the moment attributable to deflection is shown by the solid black horizontal lines. These lines illustrate the magnitude of the measured slenderness effect.

The solid curve in figure 8.9, (M_e), is a short-wall interaction curve, computed on the basis of axial prism strength. The two dotted curves represent reduced interaction curves, computed by eq (7.29) and (7.30), respectively. Note that the theoretical short-wall interaction curve underestimates wall strength for all panels. The reduced interaction curves predict moment capacities equal to or smaller than the observed reduced capacity.

For wall 1-4, for which no deflection reading is available at failure, the first solid line of the broken horizontal line is the magnitude of the added moment at the last measured deflection. The great strength developed by most walls, particularly wall 1-5, tends to indicate that the flexural compressive strength exceeded f'_m by a substantial margin.

Added moments due to deflections are in general not very great compared with the total wall strength. Nevertheless, they are of a greater order of magnitude than the predicted added moments. This difference is in part attributable to the great loss in moment of inertia, associated with section cracking of hollow block. Eqs (7.29) and (7.30), which were developed on the basis of brick data, do not account for this effect and may also not account sufficiently for the decrease in the modulus of elasticity of concrete block with increasing stress. Since no data on more slender hollow block walls are available, it was not feasible to develop a special relationship for slenderness effects on hollow block walls within the scope of this investigation. Note that most of the specimens exceeded the computed reduced moment by a rather narrow margin while developing cross-sectional capacities which were considerably greater than the predicted capacity.

It is also interesting to compare the points at which the load-deflection curves deviated from linearity with the location of the theoretical cracking

line. Both lines are shown in figure 8.9. It appears that cracking moments reduced for slenderness effects could be used to closely predict this point. Since the cracking line is a function of the shape of the cross section and the flexural strength in tension, the flexural compressive strength has no effect on the magnitude of cracking moments.

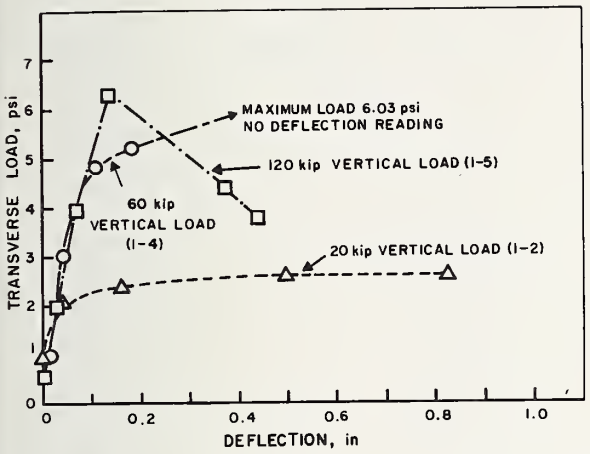

FIGURE 8.10. *Load-deflection curves for 8-in hollow concrete block walls with Type N mortar.*

real ductility of the materials. Thus, great additional deflections will develop without a significant increase in moment. At higher compressive loads, failures tend to be more brittle because of the large added moments associated with each increment of added deflection. This behavior is illustrated by the dashed-dotted line which shows the deflections at a 120-kip vertical load.

The test strength of 8-in hollow block walls with high-bond mortar is compared in figure 8.11 with analytical predictions, based on the results of prism tests. The short-wall interaction curve was developed on the basis of the strength of axially loaded prisms with fiberboard capping. This strength was used since it is realized that the prisms with plaster capping develop deceptively higher strength than the walls.

The solid curve in figure 8.11 shows theoretical short-wall capacities. Up to an axial load of 0.2 P_0, the capacity is controlled by the cracking line, which is based on the average tensile strength developed by the walls. Wall strength, rather than prism strength was used, since flexural tests on high-bond

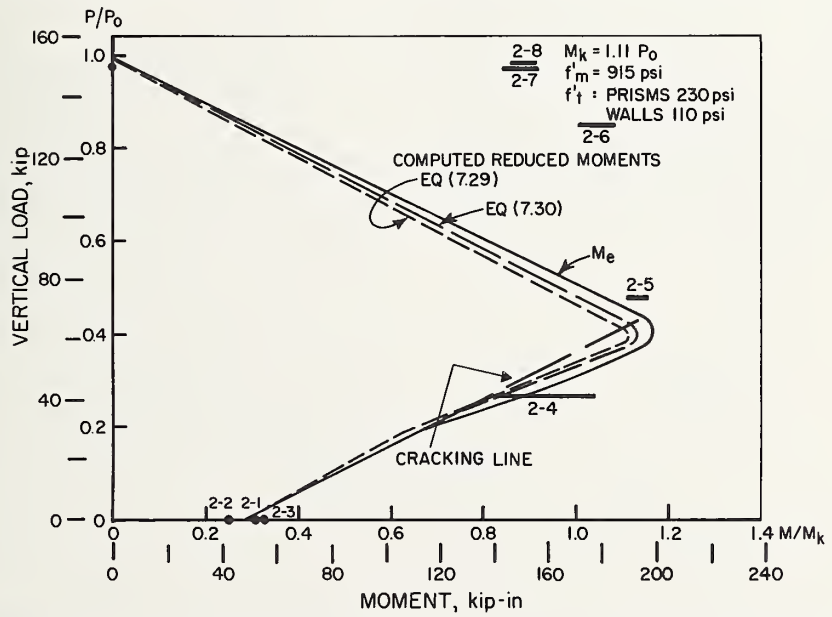

FIGURE 8.11. *8-in hollow concrete block walls with high bond mortar, correlation with prism strength.*

Figure 8.10 shows load-deflection curves for some of the wall specimens. The dashed curve shows the deflections at 20-kip vertical load. Note that at this low vertical load the walls exhibit considerable apparent ductility. This is attributable to the sudden loss in stiffness with section cracking and not to any mortar prisms developed a tensile strength approximately 70 percent higher than the tensile strength developed by wall panels. Note that the tensile strength of this type of construction is so high that the interaction curve at low axial loads can be adequately approximated by the cracking line.

Comparison of test results with the theoretical interaction curves in figure 8.11 shows that all specimens exceeded the predicted strength. In general, added moments due to deflections were small when compared with the total moments developed, and tended to be smaller than in the case of 8-in hollow block walls with conventional mortar. An exception to this behavior is specimen 2-4. Unfortunately no load-deflection curve is available for this specimen, since the instrumentation became jammed at the beginning of the test and only the ultimate deflection was measured. The vertical load on this specimen was within the range of vertical loads such that the ultimate moment occurs at a cracked section. Specimens 2-6, 2-7, and 2-8 indicated that flexural compressive strength is substantially higher than compressive strength under axial load. Indeed, specimens 2-7 and 2-8 carried a vertical load as large as the failure load under axial loading alone.

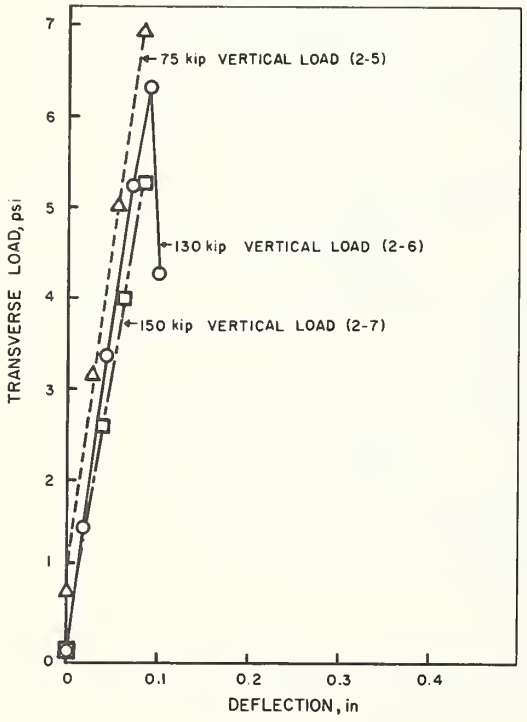

FIGURE 8.12. *Load-deflection curves for 8-in hollow concrete block wall with high bond mortor.*

Typical load-deflection curves for these tests are illustrated in figure 8.12. Note that in this case the load-deflection diagrams are essentially linear until a brittle failure occurs at maximum load. Only specimen 2-4 showed a large deflection at maximum load (0.56 in). The curve for this specimen is not plotted since only maximum deflection readings are available.

Figure 8.13 shows a comparison of load-deflection curves of 8-in hollow block walls built with type N and with high-bond mortar and subjected to vertical loads of 120 and 130 kips, respectively. Note that the high-bond mortar wall is slightly stiffer.

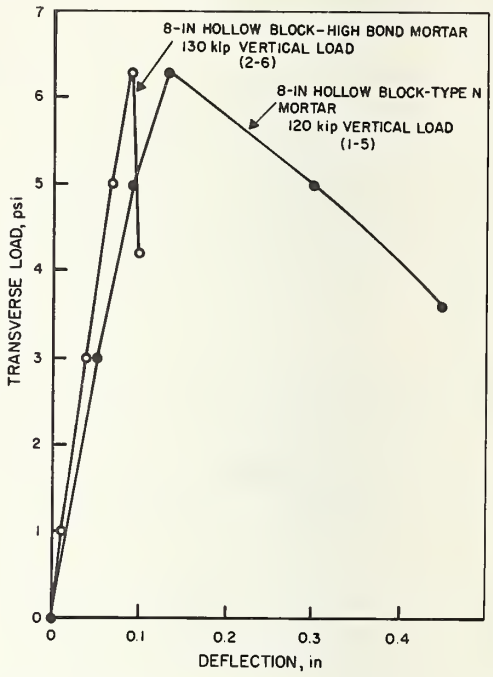

FIGURE 8.13. *Relative stiffness of 8-in hollow concrete block walls.*

Initial tangent moduli of elasticity may be computed from the initial slopes of these load-deflection curves which are not significantly affected by section cracking. To account for some uncertainty about the degree of base fixity, moduli were computed for the extreme cases of partial fixity as in figure 8.7(c) and of pin-ended condition at the base of the wall. The following values were derived in this manner:

	Partial fixity	Pin ended
Hollow block with type N mortar	$E = 0.9 \times 10^6 - 1.6 \times 10^6$ psi	
Hollow block with high-bond mortar	$E = 1.1 \times 10^6 - 2.0 \times 10^6$ psi	

Values for the type N mortar walls are between 0.9 $\times$ 10^6 and 1.6 $\times$ 10^6 psi. The initial modulus of elasticity derived from figure 8.1 for the same type of masonry is 1.5 $\times$ 10^6 psi which is within the computed range and closer to the value corresponding to the pin-ended condition. The value for the high bond

mortar walls appears to be approximately 20 percent higher.

8.4.2.2. 8-in Solid Concrete Block Walls

Figure 8.14 shows a plot of the test results on solid concrete block walls with type N mortar. Moments plotted are the moments imposed by transverse loads (reduced moments). Test results on hollow concrete block walls with type N mortar are plotted in the same figure for comparison, illustrating the great difference in strength between the two systems. The solid curves approximately represent the trend of the data.

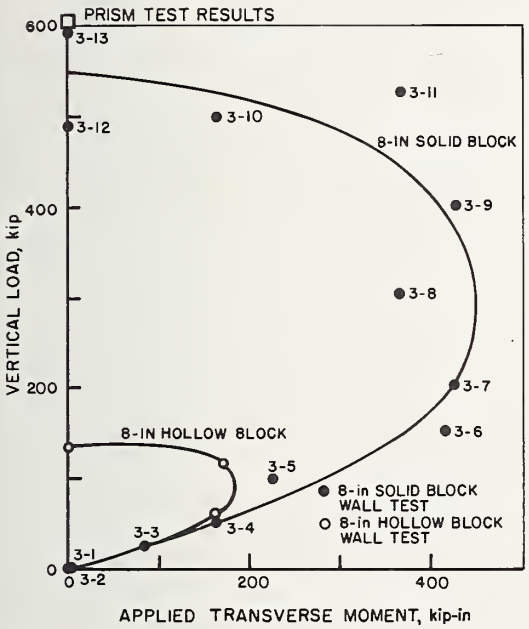

FIGURE 8.14. *Test results for 8-in solid concrete block walls with Type N mortar.*

The average prism test results predicted about 10 percent higher strength than the average of the axial wall test results. This predicted strength is also plotted in figure 8.14.

The two specimens tested at zero vertical load developed moments of 8 kip-in and 9.3 kip-in, respectively. This corresponds to an average tensile strength of 15 psi which may be compared with the average 25 psi tensile strength developed by flexure tests on prisms. Thus the full-scale walls developed approximately 60 percent of the tensile strength computed from two-block prism tests.

Figure 8.15 compares the observed transverse strength of the wall system with an interaction diagram analytically derived from the average prism strength. The solid curve (M_e) shows computed section capacity. Specimens 3-7, 3-8, and 3-9 did not fail since their strength exceeded the capacity of the loading mechanism. Specimens tested at a vertical load of 150 kips or higher in general exceeded the predicted moment capacity by a considerable margin, particularly specimen 3-11 for which no deflection was measured. This behavior again points to the phenomenon that the flexural compressive strength exceeds the axial strength. At smaller axial loads, panels developed capacities which were equal to or slightly smaller than predicted capacity.

Theoretically predicted slenderness reductions by eq (7.29) and (7.30) are also shown in the figure by

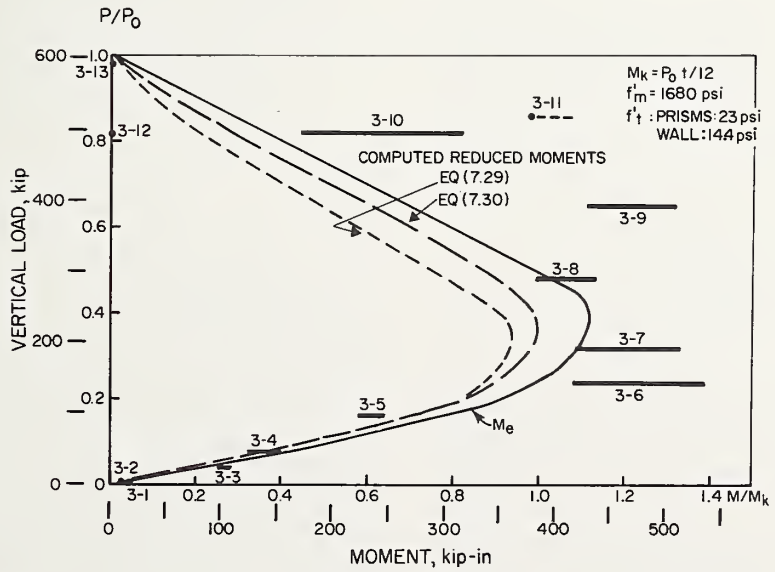

FIGURE 8.15. *8-in solid concrete block walls with Type N mortar, correlation with prism strength.*

the two dashed curves. Except for specimen 3-5, which failed at 90 percent of the predicted strength, all panels developed or exceeded the reduced moment capacity predicted on the basis of axial prism tests.

Typical load-deflection curves for solid 8-in concrete block walls are shown in figure 8.16. These curves indicate that at low axial load there was a significant increase in deflections before the ultimate load was reached.

The load-deflection curves for specimens 3-7, 3-8 and 3-9 must be considered incomplete since their strengths exceeded the loading mechanism capacity.

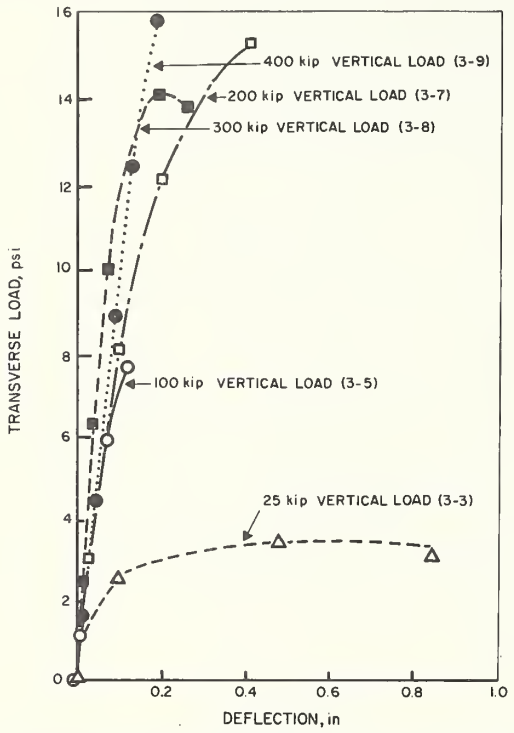

FIGURE 8.16. *Load-deflection curves for solid 8-in concrete block walls with Type N mortar.*

8.4.2.3. Conclusions

The following conclusions can be drawn from the test results on concrete block walls:

(1) The transverse strength of concrete masonry walls was approximately and conservatively predicted by determining cross-sectional moment capacity and reducing that capacity for slenderness effects by the moment magnifier method.

(2) Theoretical moment capacity computed on the basis of axial prism strength and a linear stress-strain relationship correctly predicted the trend of the experimental data. The prediction of moment capacity was conservative, since flexural compressive strength is underestimated by axial prism tests.

(3) Slenderness effects computed by the moment magnifier method, using a modulus of elasticity as derived from experimental results, have orders of magnitude and show trends which are in good agreement with the experimental data.

(4) The ultimate compressive strength of three-block prism specimens made of concrete block and type N mortar and capped with plaster correlated well with the compressive strength of the full scale walls tested under axial loading. Prism specimens made of 8-in hollow block and high-bond mortar and capped with plaster developed significantly greater compressive strength than the full scale walls. However, the same prisms, when set on fiberboard, developed compressive strength which correlated well with the strength of full-scale walls, which were also tested on fiberboard. The added strength of the capped prisms is probably caused by the influence of end restraint.

(5) Full-scale walls, when tested in flexure with no axial load, developed flexural tensile strength in excess of 50 percent of the tensile strength as determined from two-block prism tests in flexure.

(6) Hollow 8-in block walls with high-bond mortar developed significantly higher tensile strength than similar walls with type N mortar. However there was no noticeable difference in compressive strength.

8.4.3. Brick Walls

8.4.3.1. Comparison of Brick Wall Systems

Figure 8.17 shows a comparison of the test results on two wall systems. The solid circles are test results of type A brick walls with 1:1:4 mortar and the hollow circles are test results of type A brick with high-bond mortar. Moments plotted are the moments imposed by transverse loads. The curves show the average trend of the test results. Note that the walls with high-bond mortar developed significantly higher load capacities. This behavior contrasts with that of the hollow block walls, where the wall

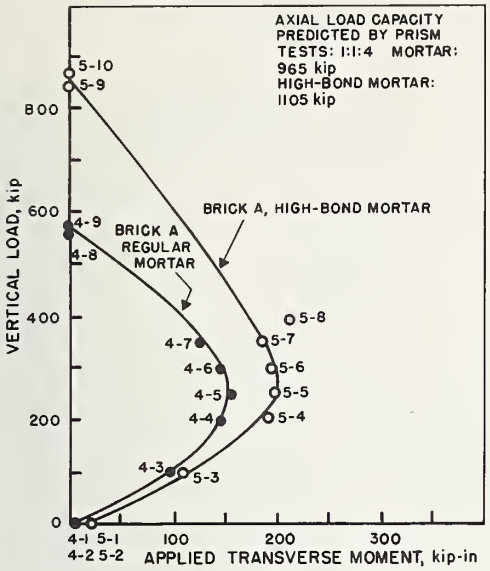

FIGURE 8.17. *Comparative strength of Brick A walls with 1:1:4 and with high bond mortars.*

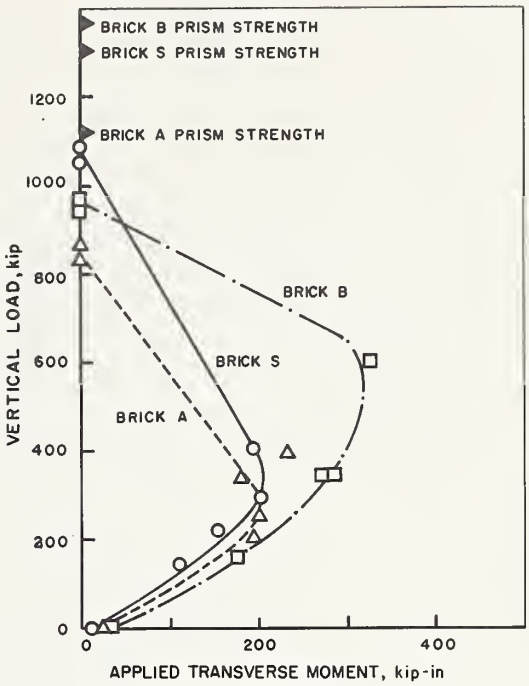

FIGURE 8.18. *Influence of brick units on the strength of high bond mortar walls.*

strength may have been limited by the relatively low strength of the masonry units.

At zero vertical load the two walls with 1:1:4 mortar developed moments of 5.5 kip-in, which correspond to tensile strengths of 50 psi. This value compares with an average tensile strength of 35 psi developed by the seven-brick beam specimens. The two high-bond mortar walls tested at zero compressive loads developed moments of 22 kip-in, which correspond to tensile strengths of 210 psi. This compares with an average tensile strength of 370 psi predicted by seven-brick beam tests. Thus, in this case, the high-bond mortar walls developed 57 percent of the tensile strength predicted by prism tests, and the regular mortar walls exceeded the prism strength.

Figure 8.17 also lists the short-wall axial load capacity predicted from the average prism strength for the two wall systems. The values were not plotted since one lies off the figure. The walls with 1:1:4 mortar developed an average axial load capacity of 567 kip. Short-wall axial load capacity computed on the basis of prism strength would be 965 kip. This result indicates that the wall developed only 59 percent of the short-wall compressive strength. The high-bond mortar walls developed an average axial load capacity of 858 kip or 77 percent of the short-wall axial load capacity of 1105 kip computed from prism tests. These results lead to the conclusion that the axial load capacity of these walls is probably limited by stability induced compression failure, rather than by the compressive strength of the masonry.

The effect of the properties of the brick units on the transverse strength of high-bond masonry walls is illustrated in figure 8.18, which shows a comparative plot of the interaction curves for Brick A, Brick S, and Brick B walls. The curves show the approximate trend of the test results. Compressive strengths of the brick units are 14,480 psi for Brick A, 17,560 psi for Brick S, and 20,000 psi for Brick B. Tensile strengths of the walls, computed from transverse load capacity with zero vertical load and compressive strengths computed from wall failures under axial compressive loads are tabulated with the average prism strengths for each wall system:

	Wall tensile strength	Prism tensile strength	Wall compressive strength	Prism compressive strength
	(*psi*)	(*psi*)	(*psi*)	(*psi*)
Brick A	210	370	4800	6240
Brick S	120	220	6050	7320
Brick B	300	430	5140	7650

Comparison of the tensile strength data for both, wall tests and prism tests, indicates that Brick S masonry was weakest in tensile strength. Since in

compression Brick S is stronger than Brick A, there appears to be no correlation between brick compressive strength and the tensile strength developed by high-bond mortar. It is quite conceivable that other brick properties, for instance, the initial rate of absorption, may effect the tensile strength developed by the mortar. The relative weakness of Brick S masonry in tension may also be related to the fact that Brick S is not cored. There is definite correlation between the tensile strength derived from prism tests and the tensile strength of the walls; however, it is evident that the flexural prism tests overestimate the tensile strength of the walls. Brick S walls developed 55 percent of the prism tensile strength; Brick A walls, 57 percent; and Brick B walls, 70 percent.

Comparison of compressive strength data from full-scale wall tests and from prism tests indicates that while in the prism tests masonry compressive strength increased with the compressive strength of the brick units, the full-scale walls behaved in a different manner. Brick S walls developed the highest compressive strength (the same walls had the lowest tensile strength), which was 83 percent of the prism strength, while Brick B walls developed only 67 percent of the prism strength. As previously noted, the walls probably failed by stability induced compression failure rather than by compression.

In the latter case the axial load capacity of the walls would be a function of the modulus of elasticity and not of masonry compressive strength, and moduli of elasticity do not necessarily increase with compressive strength of masonry. To date, no extensive experimental study on moduli of elasticity of brick masonry with high bond mortar has been conducted. Data available from another research program conducted at the National Bureau of Standards, as shown in figures 8.2 and 8.3, indicate the following average initial tangent moduli of elasticity: Brick A with 1:1:4 mortar, $E_i = 3.65 \times 10^6$ psi; and Brick A with high-bond mortar, $E_i = 4.2 \times 10^6$ psi. In the following table, axial failure loads are listed together with critical loads (Euler) computed on the basis of "pin ended" wall conditions as well as the partial fixity conditions illustrated in figure 8.7(c). Stiffness EI at failure is assumed to equal 0.7 $E_i I_n$ in accordance with eq (7.30).

It appears that axial failure loads tend to occur within the range of computed critical loads and are considerably lower than predicted short-wall strength. It can therefore be assumed that wall failures are attributable to stability rather than strength.

Mortar type	Avg. axial failure load	Computed critical load		Short-wall axial failure load based on prism test
		Pin ended	Partial fixity	
	(*kip*)	(*kip*)	(*kip*)	(*kip*)
1:1:4	567	540	840	960
High-bond	858	640	990	1110

Further comparison of the three interaction curves in figure 8.18 shows that at low axial loads, Brick S, shown by the solid curve, developed lower transverse strength than Brick A which is shown by the dashed curve. This relationship tended to be reversed at high axial loads, even though the Brick A specimen at the 400-kip vertical load developed very high transverse strength. This general trend is consistent with the observation that Brick S masonry had lower tensile strength and higher compressive strength. Brick B walls, shown by the dashed-dotted curve, developed considerably higher transverse strength than the other two wall systems.

Typical load-deflection curves for the four wall systems tested are shown in figures 8.19, 8.20, 8.21, and 8.22. In all cases the initial slope of these curves, which is basically a function of the modulus of

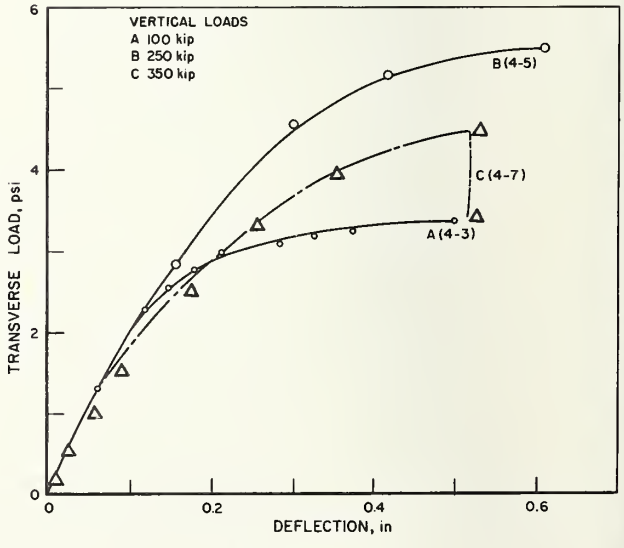

FIGURE 8.19. *Load-deflection curves for Brick A walls with 1:1:4 mortar.*

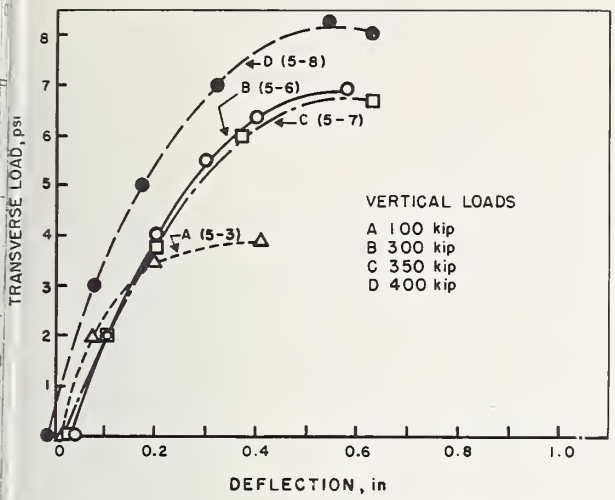

FIGURE 8.20. *Load-deflection curves for Brick A walls with high bond mortar.*

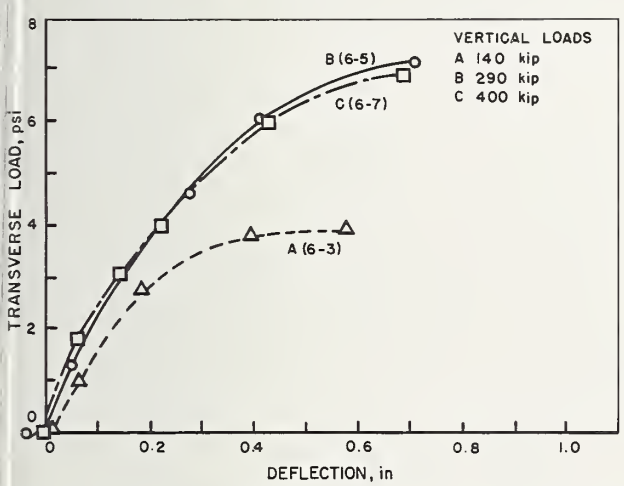

FIGURE 8.21. *Load-deflection curves for Brick S walls with high bond mortar.*

elasticity of the masonry, is similar and seems to be independent of the magnitude of the vertical compressive loads. The subsequent point where the load-deflection curves depart from this initial slope, which is probably the point where section cracking occurs, depends on the magnitude of the vertical load up to the load at which walls fail in compression before section cracking occurs. Above that load an increase in vertical load seems to have no effect on the load-deflection curve. An exception to this is the curve for the 350-kip vertical load in figure 8.19 where inelastic deformations, caused by high compressive stresses, lowered the stiffness of the wall. Curve "D" in figure 8.20 shows the curve for specimen 5-8, which developed higher transverse strength than the other specimens.

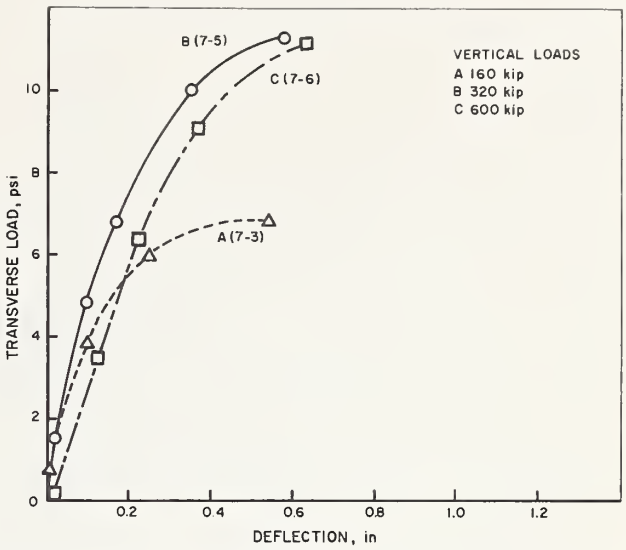

FIGURE 8.22. *Load-deflection curves for Brick B walls with high bond mortar.*

Note that some of the curves do not start at the origin. This behavior is caused by accidental initial eccentricity of the vertical load. If the initial vertical load eccentricity imposes an added moment on the specimen the curve starts to the right of the origin. If initial eccentricity tends to reduce the moments acting on the specimen the curve will start to the left of the origin.

The relative stiffness of the different wall systems is illustrated in figure 8.23, which shows a comparative plot of load-deflection curves for the four wall systems at approximately equal vertical load. Brick

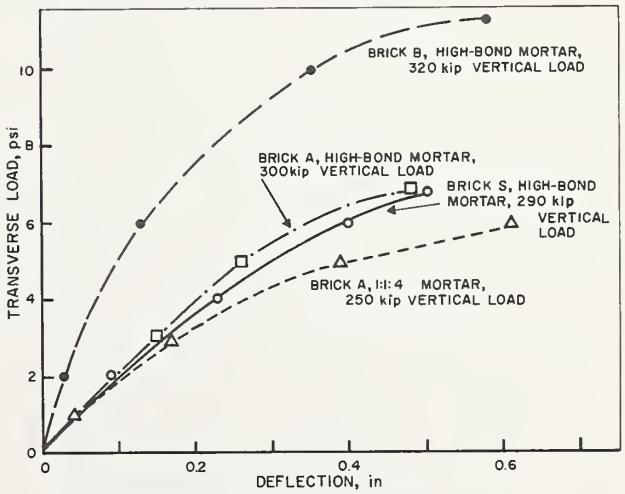

FIGURE 8.23. *Comparative stiffness of brick walls.*

A walls with 1:1:4 mortar were somewhat less stiff than the other wall systems. There is no noticeable difference in stiffness between high-bond mortar walls made of Brick A and Brick S. The Brick B walls, which also developed much higher transverse strength, developed significantly smaller deflections than all other wall systems. This added stiffness must be caused by a higher value of EI which is probably due to the combined effect of a higher modulus of elasticity and a high moment of inertia because of reduced section cracking due to higher tensile strength. This observation is not supported by the relative magnitude of critical loads which was previously discussed, even though reduced section cracking may affect deflection without materially affecting critical loads.

Initial tangent moduli of elasticity may be computed from the initial slope of the load-deflection curves. Since there is some doubt about the degree of end fixity, moduli were computed for the extreme cases of partial fixity as in figure 8.7(c) and of pin ended condition as in figure 8.7(a) at the base of the wall. The following tabulated values were derived in this manner.

	Partial fixity	Pin ended
Brick B (high-bond mortar)	$E = 7.3 \times 10^6 - 12.0 \times 10^6$ psi	
Brick S (high-bond mortar)	$E = 3.0 \times 10^6 - 5.0 \times 10^6$ psi	
Brick A (high-bond mortar)	$E = 3.6 \times 10^6 - 6.3 \times 10^6$ psi	
Brick A (1:1:4 mortar)	$E = 2.2 \times 10^6 - 3.9 \times 10^6$ psi	

Values for Brick A with high-bond mortar are between 3.6×10^6 and 6.3×10^6 psi. The average value of tangent modulus of elasticity derived from figure 8.3 is 4.2×10^6 psi. These values appear reasonably consistent and seem to indicate that fixity may have been somewhat less than the partial fixity which was conservatively assumed in the interpretation of test results. A similar comparison can be made for Brick A with 1:1:4 mortar, even though in this case the specimens on which figure 8.2 is based had a somewhat higher compressive strength than similar prisms taken from the walls tested, and therefore also had a higher modulus of elasticity. The tangent modulus derived from figure 8.2 is 3.6×10^6 psi, while the modulus for Brick A with 1:1:4 mortar computed from deflection curves is between 2.2×10^6 and 3.9×10^6 psi. Again it appears that the values are reasonably consistent and that end fixity was probably somewhat less than the assumed partial fixity. The values of the moduli for the above mentioned masonry walls are also reasonably consistent with observed critical loads. The value for Brick B, on the other hand, appears extremely high considering the low capacity of these walls under axial vertical loads.

8.4.3.2. Correlation of Test Results with Theory

The correlation between prism strength and the strength of full-scale walls for the four wall systems tested is illustrated in figures 8.24, 8.25, 8.26, and 8.27. Again vertical loads are divided by P_0 which is the short wall axial failure load, computed on the basis of prism strength, and moments are divided by $M_k = P_0 t/12$, which is the theoretical maximum elastic moment resulting when a vertical load is applied at the edge of the kern of the section. A dual scale is used to show actual magnitude of loads and moments. The part of the moment caused by deflection is shown by a solid horizontal line. The left end of this line represents the moment caused by transverse loads alone. The right end represents the ultimate moment acting on the wall at failure. Thus, the magnitude of the measured slenderness effect can be clearly seen by the length of the solid lines. The figures illustrate the great magnitude of the added moment caused by deflection, which represents the slenderness effect. Figure 8.24 shows the test results on Brick A walls with conventional mortar. The right-hand end of the solid horizontal lines represents ultimate moment capacity and should be compared with the solid curve marked M_e which was computed on the basis of prism strength. Note that the total ultimate moments developed by the walls closely follow the predicted short wall interaction curve.

Theoretical reduced moments were computed by the two methods represented by the following equations:

$$M_0' = M_e \left(1 - \frac{P}{P_{cr}}\right)$$

where $$P_{cr} = \frac{\pi^2 EI}{(0.8h)^2}.$$

and $$(1)\ EI = \frac{E_i I_n}{3} \qquad (7.29)$$

or $$(2)\ EI = E_i I_n \left(0.2 + \frac{P}{P_0}\right) \leq 0.7 E_i I_n \qquad (7.30)$$

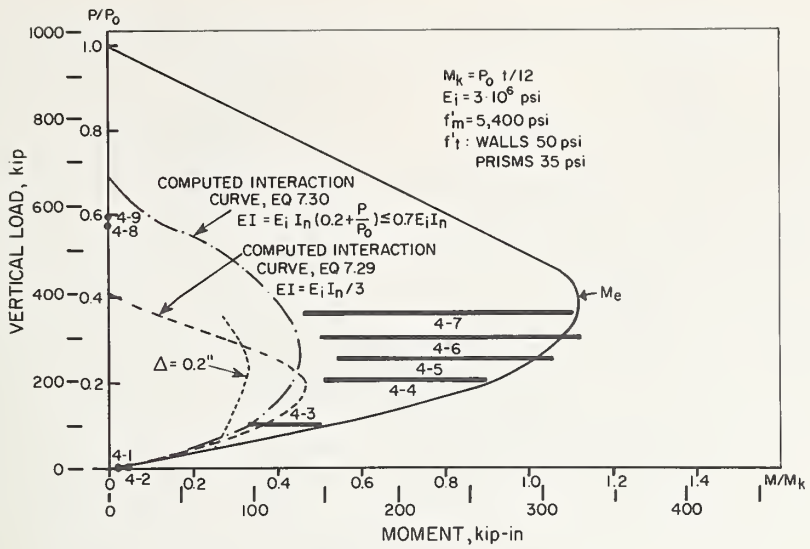

FIGURE 8.24. *Brick A walls with 1:1:4 mortar, correlation with prism strength.*

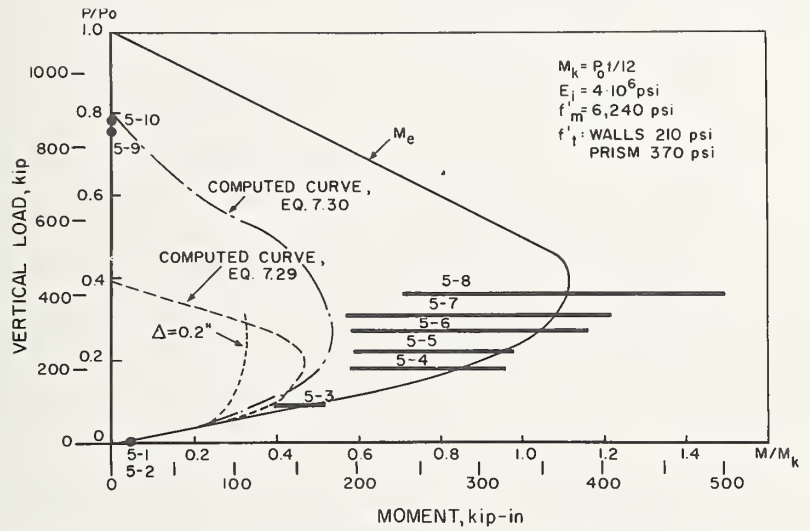

FIGURE 8.25. *Brick A walls with high bond mortar, correlation with prism strength.*

These theoretical curves were developed by reducing the ultimate value of M_e shown by the solid curve in figure 8.24. For Brick A, values of f'_m and E used in arriving at these reduced curves were independently derived on the basis of prism tests and the stress-strain values in figures 8.2 and 8.3, except that the value of E_i for Brick A with 1:1:4 mortar was slightly modified as noted below. For Brick S and B values for f'_m were available only from physical tests. Values for E were assumed to equal the value for Brick A with high-bond mortar. The theoretical reduced curves thus computed, which are shown in figure 8.24 by the dashed and the dashed-dotted curves for eq (7.29) and eq (7.30), respectively, should be compared with the left end of the solid horizontal lines. Examination of these two theoretical curves shows that eq (7.29) slightly overestimates the moments at low axial loads and underestimates the moments at high axial loads. This difference should be expected since cracking will increase with decreasing axial loads, causing a reduction in the moment of inertia, while at high axial loads the total gross section will be effective. Eq (7.30) was derived to fit the test results of all the brick wall systems and in general shows good agreement. Nevertheless, eq (7.29) shows reasonably good agreement with test results within the range below 0.2 P_0, which is the maximum axial load presently permitted in conven-

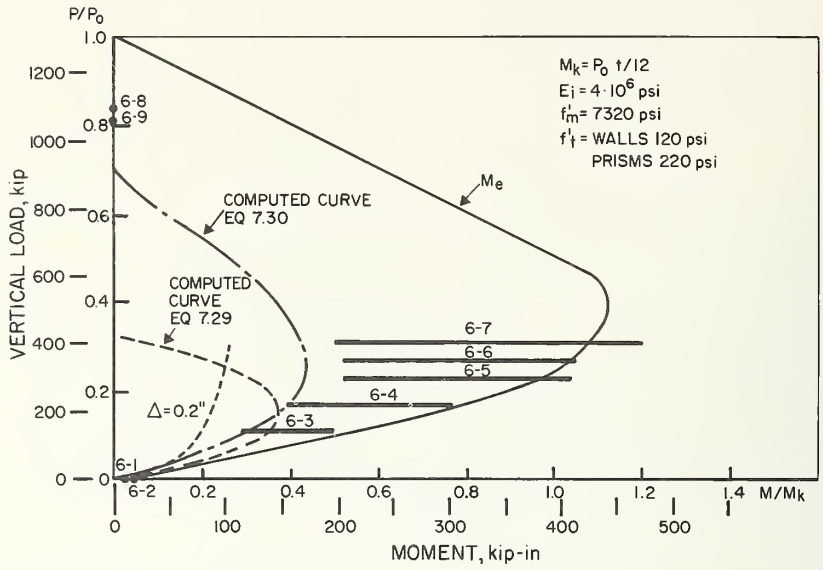

FIGURE 8.26. *Brick S walls with high bond mortar, correlation with prism strength.*

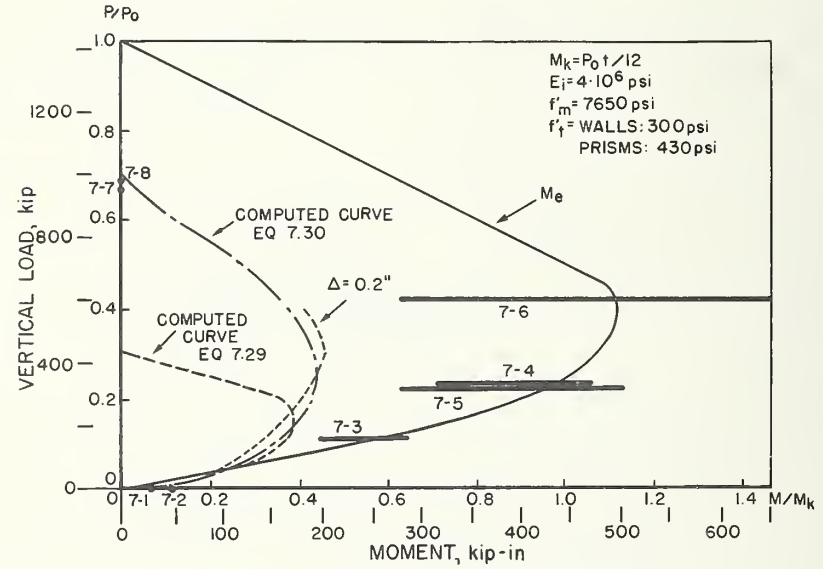

FIGURE 8.27. *Brick B walls with high bond mortar, correlation with prism strength.*

tional design, and it has the advantage of greater simplicity. All calculations were based on partial end fixity, as illustrated in figure 8.7(c). The magnitude of moments at a deflection of 0.2-in which is 1/480 of the wall height, has also been shown on the plot by the dotted curve. This would be a reasonable value for a maximum permissible deflection under service loads in present design practice. The position of that line relative to ultimate load capacity of the wall indicates that even though deflection does not seem to be critical in this case, maximum deflection should be given some consideration, since, at a load level of 0.2 P_0, it occurred at less than 2/3 of the ultimate moment.

For the moment reduction computations for Brick A walls with 1:1:4 mortar, an E of 3×10^6 psi, rather than the 3.65×10^6 psi previously mentioned has been used. The data shown in figure 8.2, which were developed in another testing program came from specimens with a compressive strength over 6000 psi, compared with a 5400 psi strength of prisms tested in this program. This fact, as well as the measured load-deflection curves, seem to indicate that the masonry in the walls used in this program had a

lower modulus of elasticity than the masonry used to develop the stress-strain curves shown in figure 8.2.

Test results on high-bond mortar walls are plotted in figures 8.25, 8.26, and 8.27 in a similar manner. For all these wall systems, theoretical reduced-moment interaction curves were computed using a modulus of elasticity of $E = 4 \times 10^6$ psi. In general, these specimens developed or exceeded the theoretical moment capacity computed from compressive prism strength, indicating that "a" was greater than 1. Computed theoretical reduced curves show reasonably good correlation with test results, except that the strengths of the Brick B walls (figure 8.27) were underestimated. These walls developed deflection curves corresponding to a much higher modulus of elasticity, but their buckling load was rather low. These walls also exceeded their predicted section capacity by a substantial margin.

8.4.3.3. Conclusions

The following conclusions can be drawn from the test results on brick walls:

(1) The load capacity of the brick walls tested was closely predicted by the moment magnifier method, using compressive prism strength as the basis for predicting short-wall section capacity, and a stiffness EI in accordance with eq (7.29) or (7.30). The trend of the relationship between vertical loads and moments was correctly predicted by theoretical interaction curves and the order of magnitude of observed slenderness effects shows good agreement with the predicted slenderness effects.

(2) All brick walls tested behaved as slender walls. They failed by stability induced compression and their moment capacity was significantly reduced by slenderness effects.

(3) Compressive and flexural tensile strengths of prisms built from Brick A with 1:1:4 mortar were smaller than the strengths of prisms from the same brick built with high-bond mortar. Compressive strength of high-bond mortar prisms increased with the compressive strength of the brick units. Flexural tensile strength of high-bond mortar prisms did not correlate with the compressive strength of the brick units.

(4) Full-scale walls built with 1:1:4 mortar developed flexural tensile strength which exceeded the average tensile strength determined from prism tests. Full-scale high-bond mortar walls developed 50 percent or more of the prism tensile strength.

(5) Walls built of Brick A with high-bond mortar developed significantly higher ultimate load capacity under combinations of vertical and transverse loads than walls built of the same brick with 1:1:4 mortar.

(6) Walls built with high-bond mortar and Brick B developed significantly higher transverse strength than the high-bond mortar walls built with lower strength brick. However, under compressive loads alone these walls did not develop increased strength.

(7) Maximum permissible deflection as well as wall strength should be considered when permissible transverse service loads are determined for brick walls with slenderness ratios similar to or greater than the ratios of the walls tested.

8.4.4. Cavity and Composite Walls

Cavity and composite wall systems consist of separate wythes which may or may not act monolithically. The strengths of these systems depend not only on the strengths of the wythes of which they are composed but also on the manner in which these wythes interact.

8.4.4.1. Comparative Strength of Walls

Figure 8.28 shows a plot of the three composite and cavity wall systems tested. In addition, Brick A walls with 1:1:4 mortar and 8-in solid concrete block walls are shown for the sake of comparison. As expected, the 4-2-4-in hollow concrete block cavity wall had the least strength. The difference in strength between the 4-2-4-in brick and the hollow concrete

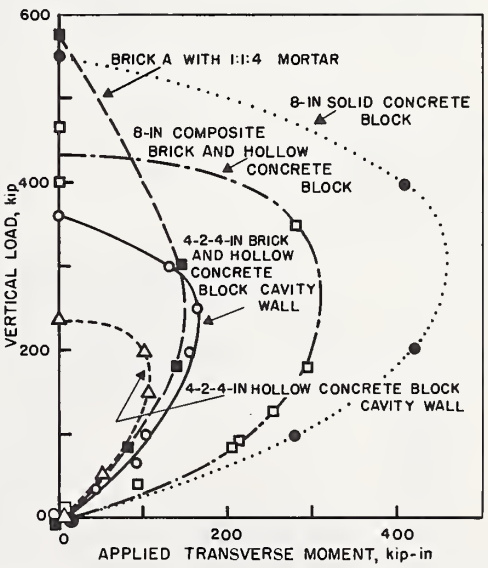

FIGURE 8.28. *Comparative strength of cavity and composite walls.*

block cavity walls shown by the solid curve and the 8-in composite brick and block walls shown by the dashed-dotted curve, which consist of brick and block components of equal dimension and strength, is an indication that the composite walls acted as monolithic composite sections while there was no composite action by the cavity walls. Another interesting comparison can be made between the interaction curve for Brick A with 1:1:4 mortar shown by the dashed curve, in figure 8.28 and the 4-2-4-in brick and hollow concrete block cavity wall. The curve for Brick A has been plotted even though the brick in the cavity wall is Brick B, since no observed interaction curve for Brick B with conventional mortar is available. Note that the Brick A walls acting alone developed almost as much moment capacity as the cavity walls and higher axial load capacity than the cavity walls. It is evident from this comparison that the cavity walls will develop greater axial load capacity and almost the same moment capacity if the entire vertical load is supported by the brick alone instead of resting on both wall components.

Figure 8.29 shows the comparative stiffness of these walls under transverse loading. The load-deflection curves were measured at slightly different load levels, since the systems were not tested at equal vertical load levels. As expected, the concrete

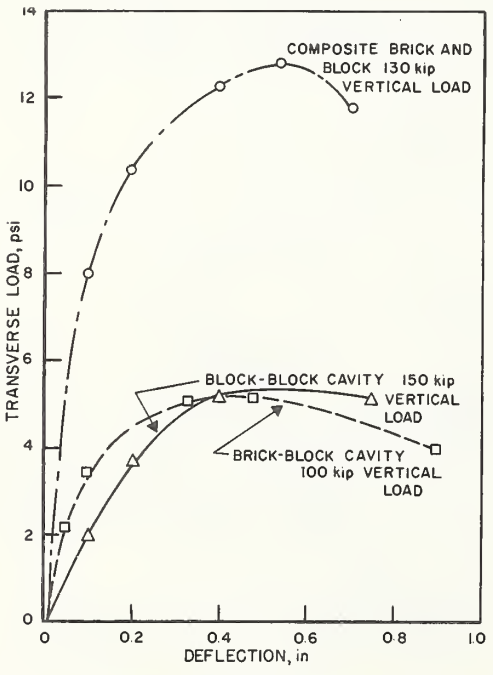

FIGURE 8.29. *Comparative stiffness of cavity and composite walls.*

block cavity wall was the least stiff and the composite 8-in wall was much stiffer than the cavity walls.

In the subsequent sections it is attempted to predict the strength of these composite walls on the basis of section properties, slenderness and the prism strength of the different material components. Prism tests were conducted on brick and block prisms separately, and no composite short-wall sections were tested. The results of these prism tests are utilized to predict wall strength analytically, and actual test results are compared with predicted strength.

8.4.4.2. 4-2-4-in Cavity Walls of Hollow Concrete Block

The ties connecting the two wythes across the cavity in this system are not capable of transmitting shear in the plane of the walls. The wall cross section can, therefore, not be considered a monolithic section. The walls were loaded vertically at their geometric center line and it may be assumed that the vertical load was evenly distributed between the two wythes. It is also assumed that the ties were capable of transmitting horizontal loads from one wythe to the other, causing both wythes to participate in resisting transverse loads.

The results of tests on 4-2-4-in block cavity walls are plotted in figure 8.30 together with interaction curves computed on the basis of prism tests. The assumption was made that each block wythe takes one half the vertical load and one half the moment. P_0 was computed on the basis of the average strength obtained from the prism tests on the 4-in hollow block. Moments were computed conservatively, assuming that partial top and bottom fixity existed which produced about one half the pin-ended moment.

While it is difficult to determine the actual moments acting on the wall it may be noted that, since there were in effect two walls, and the vertical load was applied through a pin connection at the center between the two walls, there could have been partial fixity at the top as well as at the bottom. This condition is illustrated in figure 8.30(a). The additional vertical load imposed by this end condition on one of the wythes and the vertical load reduction in the other wythe, as illustrated in figure 8.30(a), will somewhat affect the moment capacity of each of the wythes.

Study of the mode of failure of these walls indicates that walls 8-1 through 8-4 failed by mid-

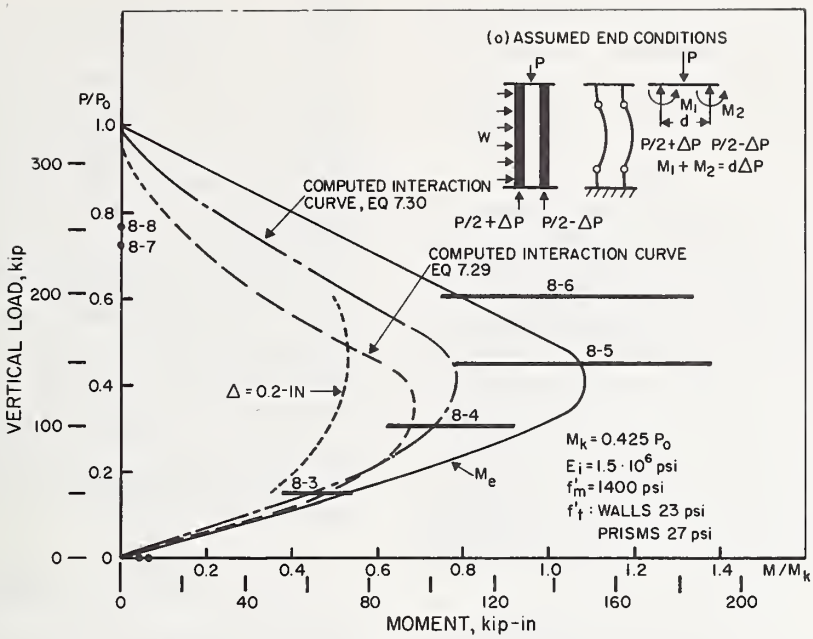

FIGURE 8.30. *4-2-4-in concrete block cavity walls, correlation with prism strength.*

height flexure, whereas walls 8-5 through 8-8 failed by compression near the top. This study suggests that at lower vertical load the amount of end-fixity was less, causing a larger positive moment, whereas at higher vertical load the amount of end-fixity was more than that assumed for the minimum moment condition, causing a specimen failure by negative moment, which in this case occurred near the top.

A study of figure 8.30 reveals that the analytically derived curve for section capacity reflects the trend of the tests reasonably well. This conclusion can be verified by comparing the right end of the horizontal lines with the solid curve. The great strength of specimens 8-5 and 8-6 can be explained by the fact that af'_m exceeds f'_m by a considerable margin. This particularly affects the magnitude of ultimate moments at vertical loads greater than $P_0/2$. It may be seen from the magnitude of the observed added moments due to deflection at failure, which are represented by the length of the horizontal lines, that slenderness effects are an important factor in this wall system. Theoretical reduced interaction curves developed by eq (7.29) and (7.30), which are shown by the dashed and the dashed-dotted curve, respectively, underestimate somewhat slenderness effects at low vertical loads. This difference again indicates, as in the case of the 8-in hollow block walls, that eq (7.30) underestimates slenderness effects for hollow sections where cracking causes a greater reduction in I. The low wall strength under axial load, relative to the prism strength (75 percent of prism strength) cannot be explained by the slenderness, and may be the result of eccentricity caused by unequal load distribution between the wythes. As in the case of the brick walls, moments causing a 0.2-in deflection are shown in figure 8.30.

At zero axial load the walls developed tensile strengths of 24 and 22 psi, or about 74 percent of the average 31 psi tensile strength developed by the 2-block prisms.

Figure 8.31 shows typical load-deflection curves for these walls. As in the cases previously discussed,

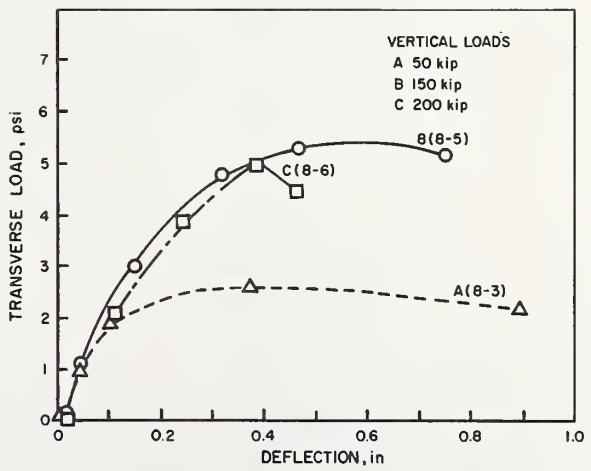

FIGURE 8.31. *Load-deflection curves for 4-2-4-in concrete block cavity walls.*

load-deflection curves tend to have similar initial slopes and tend to depart from these slopes at section cracking, when axial loads are low, while at higher axial load the effect of vertical load on stiffness is not very significant.

8.4.4.3. 4-2-4-in Cavity Walls of Brick and Hollow Concrete Block

It was noted in the previous section that the ties in cavity walls are capable of transmitting transverse forces from wythe to wythe, but that the stiffness of the ties in the plane of the wall is relatively small, so that shear forces acting parallel to the plane of the wall cannot be transmitted. The cavity walls therefore, do not act as monolithic sections. This conclusion is also substantiated by referring to figure 8.28 and comparing the strength of the brick and block cavity walls with that of the composite walls, which developed a much greater moment capacity.

In the brick and block cavity wall there are two wythes of different stiffnesses. The strength of this system can be analyzed by assuming that the ties will cause both wythes to assume the same deflection curve. Equations for the strength of cavity walls are derived using the following assumptions:

(1) Both wythes have equal lateral deflection at all stages of loading.
(2) The moment developed by each wythe is a function of the deflection.
(3) Failure is defined as flexural or compressive failure of one wythe, even though the system may have reserve strength beyond this point by transfer of all the load to the wythe that did not fail.

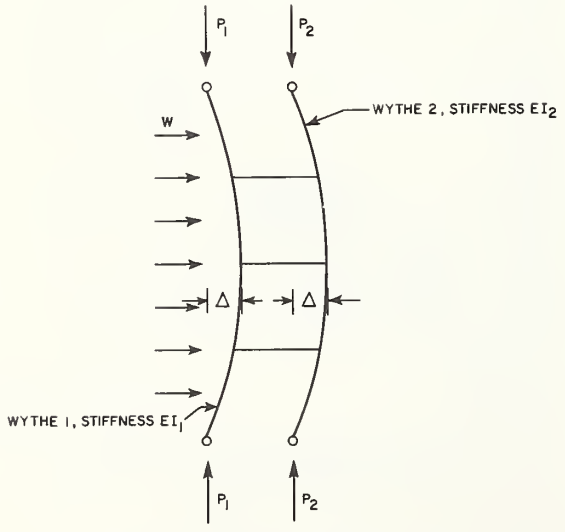

FIGURE 8.32. *Pin-ended cavity wall.*

Figure 8.32 is a schematic sketch of a pin-ended deflected cavity wall. The outside wythe is acted on by the axial force P_1 and by the uniformly distributed transverse load w. The inside wythe is acted on by axial force P_2. Both wythes deflect equally, with a maximum deflection of Δ. The stiffness of the outside wythe is EI_1 and that of the inside wythe EI_2. If it is assumed that the outside wythe develops a maximum internal moment M_1 and the inside wythe a moment M_2, and that the transverse moment due to load w, as well as the added moments due to axial loads P_1 and P_2 are distributed parabolically along the height of the wall, an equation for the relationship between moments M_1 and M_2 can be derived.

The mid-height deflection, Δ can be computed in terms of M_1 or M_2:

$$\Delta=\frac{5h^2}{48EI_1}\cdot M_1=\frac{5h^2}{48EI_2}\cdot M_2 \qquad (1)$$

Moments M_1 and M_2 are therefore related as follows:

$$M_2=M_1\cdot\frac{EI_2}{EI_1}$$

$$M_1=M_2\cdot\frac{EI_1}{EI_2} \qquad (2)$$

The following expressions can be written for the total maximum moment (M_{et}) acting on the wall:

$$M_{et}=\frac{wh^2}{8}+(P_1+P_2)\Delta$$

$$=M_0+(\Sigma P)\Delta \qquad (3)$$

Moment M_{et} can also be expressed in terms of the moments acting on each wythe:

$$M_{et}=M_1+M_2=M_1\left(1+\frac{EI_2}{EI_1}\right)$$

$$=M_2\left(1+\frac{EI_1}{EI_2}\right) \qquad (4)$$

From (1) and (3) and the equation for Δ, the mid-height deflection can be rewritten:

$$\Delta=\frac{5h^2}{48EI_1}M_1=\frac{5h^2}{48EI_1}\cdot M_{et}\frac{1}{1+\frac{EI_2}{EI_1}}$$

The added moment acting on the wall at mid-height, $(\Sigma P)\Delta$ can be expressed as:

$$(\Sigma P)\Delta=M_{et}\frac{5\ h^2\Sigma P}{48\ EI_1\left(1+\frac{EI_2}{EI_1}\right)}$$

$$= M_{et} \cdot \frac{5}{48} \frac{h^2 \Sigma P}{\Sigma EI} \tag{5}$$

but:
$$\frac{48}{5} \cdot \frac{\Sigma EI}{h^2} \simeq \frac{\pi^2 \Sigma EI}{h^2} = \Sigma P_{cr} \tag{6}$$

therefore:
$$(\Sigma P)\Delta = M_{et} \frac{\Sigma P}{\Sigma P_{cr}}$$

The moment due to transverse loads, M_0, is therefore:

$$M_0 = M_{et} - (\Sigma P)\Delta$$
$$= M_{et}\left(1 - \frac{\Sigma P}{\Sigma P_{cr}}\right) \tag{7}$$

The following general equation for the section capacity of a cavity wall can therefore be written:

$$\left.\begin{aligned} M_{et} &= M_{e1}\left(1 + \frac{EI_2}{EI_1}\right) \\ \text{or} \quad M_{et} &= M_{e2}\left(1 + \frac{EI_1}{EI_2}\right) \end{aligned}\right] \tag{8.1}$$

whichever is smaller.

Slenderness effects can be computed by a moment magnifier equation:

$$M_0 = M_{et}\left(1 - \frac{\Sigma P}{\Sigma P_{cr}}\right) \tag{8.2}$$

Eq (8.1) implies that one of the two wythes will probably fail first. The other wythe, at the same time, may or may not have reached its ultimate strength. Since the ultimate moment of each wythe depends on its strength and on the axial load component acting on it, this assumption does not exclude the possibility that after failure of one wythe the second wythe may be able to support all the external loads on the wall and thus prevent collapse at this point. Eq (8.2) indicates that slenderness effects can be evaluated as a function of the total load acting on the wall and the sum of the critical loads of both wythes.

It should be noted that wythe-interaction, as well as slenderness effects depend on the value of EI, and that the value of EI for each wythe is a function of P/P_0 for the wythe. The relationship between the EI values of the two wythes is therefore not fixed and will change with loading conditions.

Hereafter, a theoretical interaction curve for the 4-2-4-in brick and block cavity wall is computed, using the preceding equations. The following masonry parameters are used.

f'_m brick = 3580 psi
f'_m block = 1400 psi
E_i brick = 3.0×10^6 psi[12]
E_i block = 1.3×10^6 psi

Using the above values of f'_m and the cross-sectional areas, the following values for axial load capacity result:

P_0 brick = 637 kip
P_0 block = 161 kip

Moments of inertia computed from cross-sectional dimensions are:

brick wythe $I_n = 209$ in^4
block wythe $I_n = 177$ in^4

Partial top and bottom fixity as illustrated in figure 8.30(a) for the block and block cavity walls has been conservatively assumed in the interpretation of the test results of the brick and block cavity walls.

The same assumption is made in the computations for evaluating slenderness effects using a "k" value of 0.7. Thus:

$$P_{cr} = \frac{\pi^2 EI}{(0.7h)^2}$$

M_e for the brick wythe is computed by eq (7.7):

$$M_e \simeq \frac{Pt}{2}\left(1 - 1.33\frac{P}{P_0}\right)$$

For the brick wythe this becomes:

$$M_e \simeq 1.875P\left(1 - 1.33\frac{P}{P_0}\right)$$

M_e for the block was evaluated by approximate eq (7.12):

if
$$P < \frac{P_0}{2} : M_e \simeq Pc\left(1 - g\frac{P}{P_0}\right),$$

where:
$$g = 2\left(1 - \frac{4I_n}{At^2}\right)$$

[12] The only parameter that was not derived from tests is the modulus of elasticity of brick masonry, which was arbitrarily assumed to be $3 \cdot 10^6$ psi similar to the modulus of Brick A with 1:1:4 mortar. It is realized however, that the lower strength of this brick masonry (3850 psi, as compared with 5400 psi for Brick A) is probably associated with a lower modulus of elasticity.

for the 4-in block:

$$g=2\left(1-\frac{4\cdot 177}{115\cdot 3.63^2}\right)=1.07$$

$$c=\frac{t}{2}=1.81 \text{ in}$$

thus: $$M_e=1.81P\left(1-1.07\frac{P}{P_0}\right)$$

For $$P>\frac{P_0}{2},\ M_e=(P_0-P)e_k$$

for the 4-in block: $e_k=0.85$ in

thus: $$M_e=0.85\ (P-P_0)$$

Table 8.1 shows the steps for computing the section capacity M_{et} for various combinations of axial loads and moments. M_e for each wythe is computed for its appropriate value of P/P_0 by the equations developed above. Then M_{et}, the total section capacity for the cavity wall, is computed on the basis of each of the wythe capacities, using the appropriate stiffness EI, as computed by eq (7.30):

$$EI=E_iI_n\left(0.2+\frac{P}{P_0}\right)\leq 0.7\ E_iI_n$$

M_{et} is computed using eq (8.1):

$$M_{et}=M_{e1}\left(1+\frac{EI_2}{EI_1}\right)$$

The smaller value of M_{et} thus computed will control and is designated by a check mark. Note that up to $\Sigma P = 100$ kip, brick strength controls while block strength controls for axial loads above $\Sigma P = 100$ kip.

Slenderness effects are computed in table 8.2. M_0' is the total net moment capacity of the wall, which in the case of the test specimens corresponds to the maximum moment imposed by the transverse loads.

TABLE 8.2. *Computation of slenderness reduction for brick and block cavity walls*

ΣP	M_{et}	ΣP_{cr}	M_0
	kip−in	*kip*	*kip−in*
50	70	509	63
100	140	643	118
150	159	772	128
200	124	843	95
250	79	898	57
300	25	953	17

A comparison between computed and observed strength is shown in figure 8.33. Specimen tests are plotted by solid bars. The left end of the bars indicates the magnitude of externally applied moments and the length of the bars shows the magnitude of the added moments ($P\Delta$). Moments were computed conservatively, assuming end fixity that would produce 50 percent of the pin-ended moment.

TABLE 8.1. *Section capacity computation for brick and block cavity walls*

Brick							Block					
ΣP	P/P_0	EI	P_{cr}	M_e	$(1+\frac{EI\text{ block}}{EI\text{ brick}})$	M_{et} based on brick	P/P_0	EI	P_{cr}	M_e	$(1+\frac{EI\text{ brick}}{EI\text{ block}})$	M_{et} based on block
kip		*psi×in⁴*	*kip*	*kip−in*		*kip−in*		*psi×in⁴*	*kip*	*kip−in*		*kip−in*
0	0	125×10^6		6.15	1.37	8.4 √	0	46×10^6		2.65	3.7	9.8
50	0.04	150×10^6	330	45	1.55	70 √	0.155	82×10^6	179	38	2.83	108
100	.08	175×10^6	385	84	1.67	140 √	.310	117×10^6	258	61	2.50	152
150	.117	198×10^6	436	119	1.77	211	.465	153×10^6	336	69	2.30	159 √
200	.157	223×10^6	490	148	1.72	255	.620	161×10^6	353	52	2.39	124 √
250	.196	248×10^6	545	173	1.65	286	.775	161×10^6	353	31	2.54	79 √
300	.235	273×10^6	600	194	1.59	308	.93	161×10^6	353	9.4	2.70	25 √

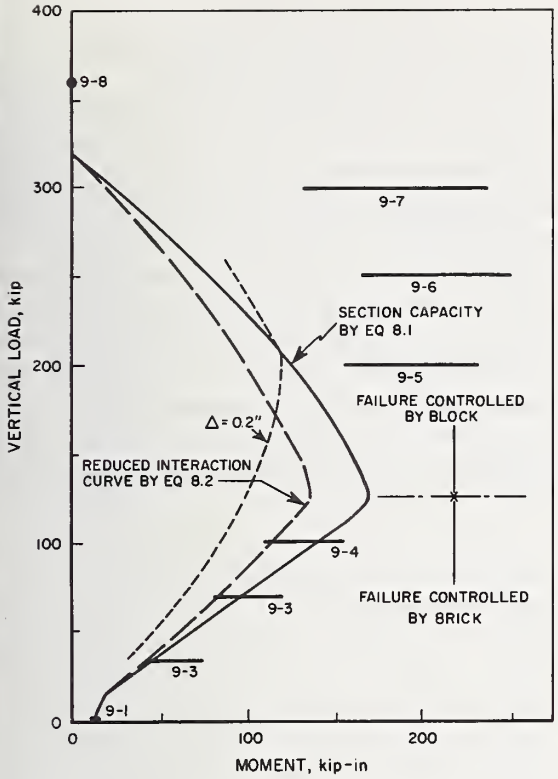

FIGURE 8.33. *4-2-4-in brick and concrete block cavity walls, correlation with prism strength.*

At zero vertical load, the predicted moment, based on the brick, is 8.4 kip-in. This compares with a moment of 5.25 kip-in or higher developed by the specimen. Thus, the wall developed about 60 percent of the moment capacity predicted on the basis of prism strength.

The dashed line in figure 8.33 shows computed reduced moment capacity and should be compared with the left end of the solid bars. Note that this curve is correct or conservative for all the test results except specimen 9-4, where capacity is overestimated by about 7 percent. Up to $P = 100$ kip, the moment capacity is controlled by the brick. In this range the computed reduced moment capacity is in good agreement with the tests. The total moment capacity, which is shown by the solid line and should be compared with the right end of the solid bars, is somewhat less than observed capacity and consequently, the magnitude of the measured slenderness effects is larger than that of the computed effect. This apparent discrepancy is caused by two reasons: First, as noted before, the assumed initial modulus of elasticity probably overestimates somewhat the stiffness of the brick wythe. The second reason is apparent when figure 8.34, which

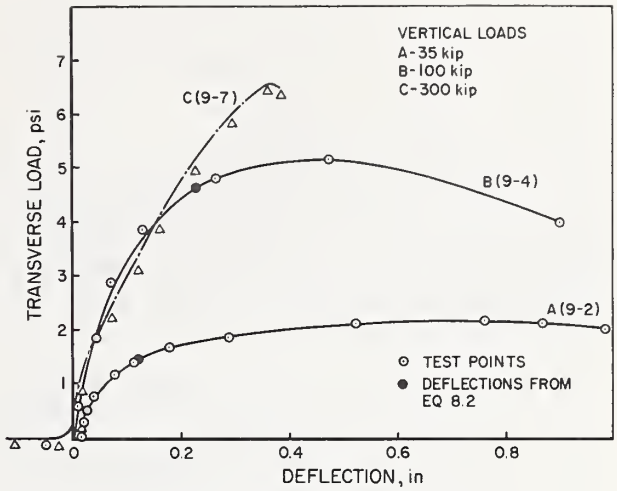

FIGURE 8.34. *Load-deflection curves for 4-2-4-in brick and concrete block cavity walls.*

shows typical load-deflection curves for the brick-block cavity walls, is examined. Note that walls 9-2 and 9-4 show considerable apparent ductility. This behavior is not due to the proximity to a stability failure, since the axial load is small. The cause is a rather significant loss of stiffness due to cracking, combined with the fact that after the beginning of crushing in the brick the wall does not collapse, since added moment capacity is available in the block. The actual deflections associated with the computed failure for these walls are shown in the plot as solid points. These deflections are very small compared with the observed deflections at failure. At these deflections, however, the wall developed from 80 to 90 percent of its ultimate strength.

Above the axial load of 100 kip (figure 8.33), the computed strength underestimates observed wall strength by a very large margin. In this range it is predicted that strength is controlled by the block. Since in this range P/P_0 of the block exceeds 0.5, the assumption that the flexural compressive strength in bending equals the axial strength becomes extremely conservative, as can be seen by examining figures 8.4 and 8.6. A similar trend can also be observed for specimen 8-6 in figure 8.30, which shows tests of 4-2-4-in block-block cavity walls. Strength in this range could be more accurately estimated by determining the real value of af'_m in flexure for this type of masonry.

Axial compressive strength was computed on the basis of prism strength of the block and underestimates actual wall strength by approximately 10 percent. Observation of actual failures indicates that

above 150 kip specimens failed by block compression near the end. This behavior indicates that, at failure, load was controlled by the block as predicted, but in some cases end fixity probably exceeded the assumed partial fixity.

Figure 8.34 shows typical load-deflection curves for these walls. The relationships between vertical load and stiffness are qualitatively similar to the relationship observed for concrete block cavity walls. However, the brick and block cavity walls developed greater initial stiffness.

8.4.4.4. 8-in Composite Brick and Hollow Concrete Block Walls

The composite brick and hollow concrete block walls studied in this investigation consisted of two separate components: a 4-in thick brick wythe and a 4-in thick concrete block wythe. In order to act as a monolithic section, shear forces acting in the plane of the wall between these two components of the wall must be effectively resisted. In the test specimens, resistance to shear forces was provided by header courses of brick in every seventh brick course and by the mortar in the collar joint. Analysis of the test results indicates that the walls did act as monolithic sections.

The modulus of elasticity of the brick used in the experimental specimens was between 3×10^6 to 4×10^6 psi, and the modulus of elasticity of the concrete block, based on gross section, was approximately 900,000 psi. Thus the simplifying assumption has been made that, under equal strain, the brick component of the wall will carry four times the load of the block component. On the basis of this assumption, a transformed section was developed for analytical purposes. This idealized transformed section is illustrated in figure 8.35(a).

For the sake of simplicity, it has been assumed that the block area is concentrated in the center-line of the two face shells, since stresses must be transmitted through the mortar bed under the face shells. The interaction diagram of vertical force and moment developed in figure 8.35 is based on the transformed section shown in figure 8.35(a) and has been developed in accordance with eq (7.23) through (7.26). It should be noted that in this case the transformed section is not a symmetrical section. Two interaction diagrams, therefore, have to be used, depending on the direction in which the moment is applied. In figure 8.35, the interaction diagram shown by the solid curve to the right of the origin is developed for moments which tend to impose compressive stresses on the brick side of the wall. These moments are defined herein as brick compressive moments. They are the moments which are induced by the transverse loads. The interaction diagram shown by the solid curve to the left of the origin is for moments which tend to impose compressive stresses in the block components of the wall. These latter moments are defined herein as block compressive moments. Note that in this case interaction diagrams are developed for moments with respect to the section centroid, rather than the geometric centerline of the section. When section capacity is evaluated with the aid of these interaction diagrams, all moments must be computed with respect to the section centroid.

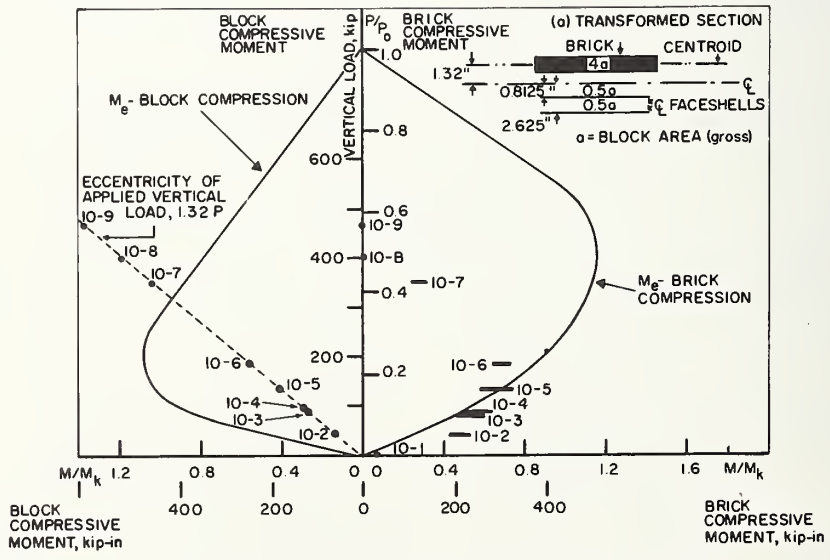

FIGURE 8.35. *8-in brick and concrete block composite walls, correlation with prism strength.*

Figure 8.35(a) shows the centroid of the transformed section which is located within the brick component of the wall at a distance of 1.32-in from the geometric center between the brick wythe and the block wythe. A vertical force acting through this geometric center will therefore impose a block compressive moment on the wall. The magnitude of this moment equals $1.32P$ kip-in. Figure 8.36 illustrates schematically the experimental loading conditions. It should be noted that under conditions of end fixity transverse loads may induce block compressive moments in excess of the initial moment Pe shown in figure 8.36. However, since the base fixity of the test panels was only partial it is assumed that the maximum moment at the base of the specimens did not exceed Pe.

FIGURE 8.36. *End moments acting on 8-in composite brick and block walls.*

A dual scale is used in figure 8.35 to show the total magnitude of loads and moments actually developed in a scale which is superimposed on the nondimensional scale. The dashed radial line drawn from the origin in the direction of the left-hand interaction diagram is the locus of the block compressive moments ($1.32P$) exerted by the axial loads which are applied through the geometric center between the brick wall and the block wall. The theoretical maximum axial load acting at that location which can be supported by this wall system can be determined from figure 8.35. It will occur at the intersection of the radial line with the block compressive interaction diagram. This intersection indicates that the magnitude of the maximum load applied at the geometric center is limited by the block compressive moment capacity and equals $0.39P_0$. If a load had been applied at the elastic centroid of the wall, presumably the wall could have supported an ultimate load of P_0. However, under test conditions the vertical load was applied at the geometric center.

Specimen tests are plotted in figure 8.35 and can be compared with the theoretical interaction curves which were developed on the basis of axial prism strength. To account for brick compressive and block compressive moments, each specimen test has been plotted in figure 8.35 on both interaction diagrams. The right side diagram shows net brick compressive moments acting on the specimens which equal the total moment due to transverse load less a moment of $1.32P$ to account for vertical load eccentricity. The points at the left side diagram show block compressive moments acting on the specimens, which are greatest near the end supports where they equal $1.32P$. Added moments caused by deflections ($P\Delta$) which magnify the brick compressive moments, are shown by solid horizontal lines on the right side diagram.

For instance, specimen 10-5, which was subjected to a vertical load of 130 kip, is plotted on the radial line in the left side diagram at a block compressive moment of $130 \times 1.32 = 172$ kip-in. This value represents the maximum block compressive moment acting on this wall. However, reference to the left-hand interaction curve will indicate that at this vertical load level the wall was capable of resisting a block-compressive moment of about 440 kip-in. This specimen therefore did not fail by block compression. The brick compressive moment due to lateral load, acting on this specimen will be the left end of the solid horizontal line plotted on the right-hand side of the diagram. The length of the solid horizontal line represents the added brick compressive moment acting on this specimen, which equals the product of the vertical force and the maximum deflection. Thus the right end of the horizontal line labeled 10-5 represents the total brick compressive moment acting on this specimen at failure. It can be seen that this moment slightly exceeded the maximum moment capacity predicted by the interaction curve for brick compressive moment. Thus this specimen, in accordance with theoretical prediction, should have failed by brick compression. This is borne out by observation, which indicates a flexural failure at mid-height in the direction of brick compressive moments, as described in section 6.2.

Observation of the mode of failure of the specimens indicates that specimens 10-1 through 10-5 failed by flexure at mid-height (i.e. brick compres-

sive moment). Specimen 10-6 did not fail since the capacity of the transverse loading system was exceeded. Specimens 10-7 through 10-9 failed by block compression near the supports. This observation is confirmed by the plot of the test results in figure 8.35, which shows that specimen 10-1 through 10-5 exceeded the computed section capacity for brick compressive moment. Specimen 10-6 could have developed additional capacity, and specimens 10-7 through 10-9 exceeded the computed section capacity for block compressive moment while not developing the section capacity for brick compressive moment.

Specimens 10-8 and 10-9 failed by axial load alone. These specimen tests have been plotted on the diagram at their proper eccentricity. Inspection of these plots indicates that the compressive strength developed by the wall system exceeds the predicted compressive strength of $0.39P_0$ by a considerable margin, probably because of greater flexural compressive strength (af'_m) than predicted for the 4-in block by axial prism tests. The plot of specimen 10-7 clearly indicates that this specimen failed by block compressive moment, a fact that is confirmed by the observed mode of failure.

The plot of specimen 10-1 indicates that the moment capacity developed at zero vertical load produced a tensile stress of 30 psi at the block face. This value compares with a 31 psi average tensile strength of the prism specimens.

It was noted at the beginning of this section that, for monolithic action, shear forces between the brick component and the block component of the wall must be effectively resisted. Observation of figure 6.18, which illustrates the failure of wall 10-5, indicates that horizontal shear did play a role in the failure of this specimen. However, the records indicate an observed flexural failure at mid-height, and the plot of the test results shows that maximum flexural capacity was developed and that the assumption of a monolithic section is justified.

Typical load-deflection curves for the wall system are shown in figure 8.37. Note the large block compressive moment that was imposed on the specimen tested under 350 kip vertical load. (The curve starts to the left of the origin.)

8.4.4.5. Conclusions

(1) The strength of slender cavity walls was approximately predicted by assuming that the ties between the two wythes are capable of transmitting

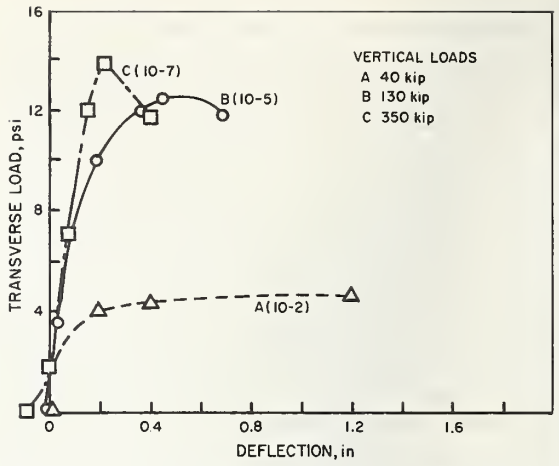

FIGURE 8.37. *Load-deflection curves for 8-in composite brick and block walls.*

transverse loads from wythe to wythe, but are not stiff enough to transmit shear forces parallel to the plane of the wall. Theoretical section capacity was computed on the basis of axial prism strength, and slenderness effects were predicted by the moment magnifier method. The general trend of observed relationships between vertical loads and moments and observed slenderness effects was correctly predicted by theory. The actual strength of the walls was closely predicted for axial loads up to $P_0/3$. For higher axial loads the theoretical prediction based on the assumption that the axial compressive strength of the masonry equals the flexural compressive strength was very conservative.

(2) The capacity of composite brick and concrete block walls was approximately predicted by assuming that the two wythes of this wall system acted as a monolithic section. The theoretical section capacity was evaluated by assuming that the ratio of the stiffnesses of the brick and block components approximately equals the ratio of the flexural compressive strengths of these components. It was demonstrated that end moments, as well as mid-height moments, must be considered when the strength of this wall system is evaluated and that the location of the line of action of the vertical load with respect to the elastic centroid of the monolithic section must be taken into consideration. The general trend of the relationship between vertical loads and moments as well as the actual strengths of the walls were reasonably closely predicted on the basis of these theoretical assumptions and of observed prism strengths of the brick and the block component of the wall system, as determined separately for each of the two components.

(3) All of the walls tested at zero vertical compressive load developed tensile strength which equaled or exceeded 50 percent of the tensile strength predicted on the basis of flexural tests on prisms.

9. Recommendations and Discussion of Present Design Practice

9.1. Determination of Transverse Strength of Masonry Walls

Two wall properties must be evaluated in order to determine the transverse strength of masonry walls:

1. The capacity of the wall cross section to resist combined bending and axial loads.
2. The effect of wall slenderness on load capacity.

It has been shown in section 7.2 that the moment capacity of a wall cross section is not only a function of the tensile and compressive strength of the masonry but also of the vertical load acting on the cross section. Thus an interaction curve can be developed which shows the maximum moment capacity as a function of vertical load. Such an interaction curve can be developed if flexural tensile and compressive strengths and the stress-strain properties of the masonry are known.

It has been shown that cross-sectional capacity can be conservatively determined by assuming a flexural compressive strength equal to the compressive strength of prisms under axial loading, a linear stress-strain relationship for masonry, and a flexural tensile strength equal to 50 percent of the modulus of rupture as determined by prism tests. This procedure is conservative since it appears that most specimens developed flexural compressive strengths in excess of the strength of axially loaded prisms, and that the assumption of a linear stress-strain relationship will underestimate the moment that the cross section is actually capable of developing.

In this study, the capacity of wall cross sections has been evaluated directly by testing eccentrically loaded prism specimens and indirectly by adding the moment exerted by the axial load on the deflected wall to the moment exerted by transverse loads.

Slenderness effects are caused by the additional moments which the vertical loads impose on the deflected wall. Not only will the vertical load impose added moments on the walls, which will equal the product of the vertical load and transverse deflections relative to the line of action of the vertical load, but the vertical load will also act to increase the magnitude of transverse deflections. These slenderness effects, which will magnify the moments acting on the walls, can be approximately predicted by the moment magnifier method, provided that EI, the stiffness of the wall, is correctly estimated.

Slenderness effects have been successfully and conservatively predicted for slender brick walls by using the moment magnifier equation with an equivalent stiffness which may be predicted either by eq (7.29) or by (7.30). Equation (7.29) is somewhat simpler, while eq (7.30) shows better agreement with test results for the entire range of vertical loads that the wall can support. No extensive data are available on slender concrete block walls. Transverse strength can be reasonably well predicted, however, by using eq (7.29) or (7.30) to predict slenderness effects for solid block walls, and by conservatively assuming for hollow block that the cracking line represents ultimate strength.

The moment magnifier equation [eq (7.28)] uses a coefficient C_m, which accounts for the shape of the deflection curve and a coefficient k, which accounts for end fixity. In the special case where moments are caused by transverse loads, the coefficient C_m is taken as 1. However, in the case where transverse moments are caused by eccentric vertical loads, a case which was not covered by this investigation, the moment magnifier equation is also applicable, with a factor C_m which will depend on the relationship between vertical load eccentricities at the wall supports. Thus the moment magnifier method could be applied to determine transverse strength under all practical loading conditions.

The practical procedure in an actual design problem would be to determine cross-sectional capacity on the basis of flexural compressive and tensile strengths, cross-sectional geometry, and the vertical load at which transverse strength is to be determined, and then to reduce this capacity to account for slenderness, on the basis of wall length, end-support conditions, and wall stiffness "EI" at the design vertical load.

The following equations may be used to predict ultimate and cracking strength. The ultimate transverse moment imposed on the wall in the direction of transverse loads, M_0', can be taken as:

$$M_0' = M_e \left(1 - \frac{P}{P_{cr}}\right)$$

The maximum end moment opposite to the direction of transverse loads, M_{end}, will be: $M_{end} = M'_e$

where:

M_e = maximum moment capacity of the wall in the direction of transverse loads,
M'_e = maximum moment capacity of the wall opposite to the direction of transverse load,
P = applied axial load,
P_{cr} = critical load for stability-induced compressive failure, computed on the basis of a modified EI, accounting for section cracking and reduced stiffness at maximum stress, where:

$$EI = E_i I_n \cdot \left(0.2 + \frac{P}{P_0}\right) \leq 0.7\, E_i I_n \qquad \text{or} \qquad EI = \frac{E_i I_n}{3}$$

E_i = initial tangent modulus of elasticity of masonry,
I_n = moment of inertia based on uncracked net section,
P_0 = short-wall axial load capacity (section 7.2.2.1).

The transverse cracking strength of a wall, M_c, can be determined by the following equation:

$$M_c = (M_t + Pe_k)\left(1 - \frac{P}{0.7P_{cro}}\right)$$

where:

M_c = moment at which cracking occurs (section 7.2.2.1),
M_t = maximum moment considering tensile strength with zero vertical load (section 7.2.2.1),
e_k = distance from centroid to edge of kern,
P_{cro} = critical load for stability-induced compression failure computed on the basis of E_i and I_n (section 7.3); 0.7 P_{cro} is recommended as critical load for uncracked walls.

In view of the loss of moment of inertia after cracking of hollow block walls, it is recommended that the ultimate strength of slender hollow concrete block walls equal the cracking strength.

9.2. Discussion of Present Design Practice

Present masonry design is based entirely on working stresses. Even though design provisions were developed with specific margins of safety relative t ultimate strength in mind, comparison of hypothet cal ultimate strength computed on the basis design practice standards with ultimate strength a tually achieved is not necessarily the only criterio by which these should be judged.

Three different design standards will be co sidered:

(1) The ANSI Standard Building Code Requir ments for Masonry [5]
(2) Building Code Requirements for Engineere Brick Masonry developed by SCPI [9]
(3) Design Specifications for Load-Bearin Concrete Masonry developed by NCM [10] and proposed recommendatio developed by ACI Committee 531 [1]

9.2.1. ANSI Standard Building Code Requirements

The ANSI building code requirements (A41. 1953) limit allowable slenderness as follows:

Type of masonry	h/t Ratio (based on nominal dimensions)
Hollow unit walls	18
Solid unit walls	20
Cavity walls	18 [13]

These limits may be compared with a nominal h/t o 24 for the brick walls, and a nominal h/t of 12 for th block walls as well as the cavity walls tested in thi program. Consequently, these design requirement permit the construction of walls that will be subjec to considerable slenderness effects, particularly i the case of cavity walls. On the other hand, this stan dard does not contain any provisions for stres reduction to account for these slenderness effects To assure a safe design, permitted allowabl stresses are extremely low, compensating for poten tial slenderness effects. Such a procedure, whic does not account for such an important variable requires a very high margin of safety which penal izes short walls and therefore leads to uneconomica design.

For composite walls, this standard limits the al lowable stress to that permitted for the weakest o the combinations of units and mortars of which th member is composed. There are no provisions fo considering the location of the vertical load wit respect to the weakest wall materials.

[13] t in cavity walls is the sum of both wythe thicknesses.

9.2.2. SCPI Standard for Engineered Brick Masonry

In the present SCPI Standard (1969), the following equation is used for the computation of allowable vertical loads on nonreinforced brick walls:

$$P = C_e C_s (0.20 f'_m) A_g$$

where C_e and C_s are determined from the following equations:

For $e \leq \frac{t}{20}$, $C_e = 1.0$

For $\frac{t}{20} < e \leq \frac{t}{6}$, $C_e = \frac{1.3}{1+\frac{6e}{t}} + \frac{1}{2}\left(\frac{e}{t} - \frac{1}{20}\right)\left(1 - \frac{e_1}{e_2}\right)$

For $\frac{t}{6} < e \leq \frac{t}{3}$, $C_e = 1.95\left(\frac{1}{2} - \frac{e}{t}\right) + \frac{1}{2}\left(\frac{e}{t} - \frac{1}{20}\right)\left(1 - \frac{e_1}{e_2}\right)$

where: e = maximum eccentricity,
e_1 = smaller eccentricity at lateral supports,
e_2 = larger eccentricity at lateral supports,
t = wall thickness.

Value of e_1/e_2 is positive for walls bent in single curvature and negative for walls bent in double or reverse curvature. For members subjected to transverse loads greater than 10 psf, e_1/e_2 is assumed as +1.0 in the computation of C_e.

$$C_s = 1.20 - \frac{\frac{h}{t}}{300}\left[5.75 + \left(1.5 + \frac{e_1}{e_2}\right)^2\right] \leq 1.0$$

Loads and moments at eccentricities in excess of $t/3$ are limited by allowable flexural tensile stresses.

Test results on Brick A walls with 1:1:4 mortar are compared in figure 9.1 with hypothetical ultimate strength curves based on the 1969 SCPI Standard. These curves were developed on the assumption that the ultimate loads are equal to $C_e C_s f'_m A_g$.

The dashed curve applicable to eccentric vertical loads was based on $e_1/e_2 = -0.4$ (assuming partial fixity at one end and a pinned condition at the other end). The axial load capacity predicted by this curve is in fair agreement with the test results obtained in this investigation and the capacity predicted by eq (7.30). However for smaller values of vertical load, there is considerable difference in the moment capacities. The reasons for these differences are discussed in the following paragraphs.

Figure 9.2 shows a comparison between the loading condition on the tested wall panels and the loading conditions which were used in SCPI tests. As shown, brick walls were subjected to eccentric vertical loads in the SCPI tests. If the moment magnifier method is applied to these two cases of loading, the following coefficients would be used:

Lateral loading: $C_m = 1, k = 0.8$
Vertical loading: $C_m = 0.5, k = 0.8$

The resulting predicted slenderness effects would be quite different for the two cases.

Figure 9.3 compares the SCPI curve with transverse strength predicted by the moment magnifier

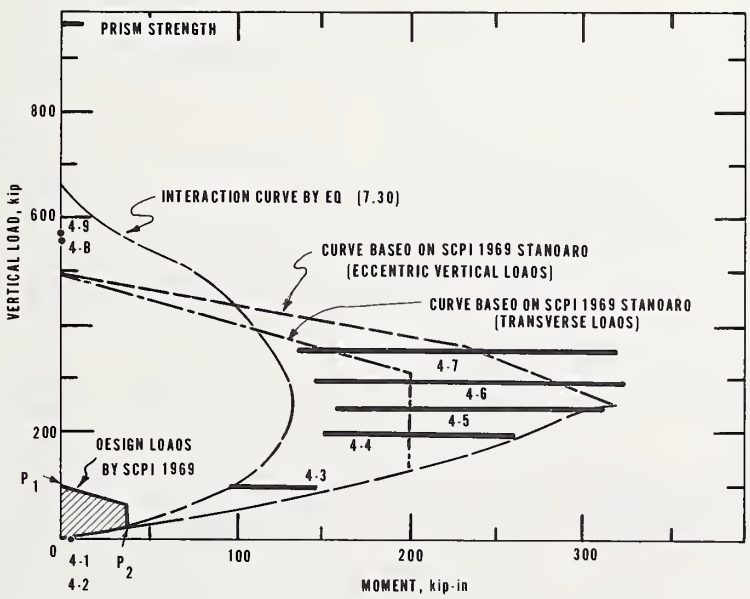

FIGURE 9.1. *Comparison of design recommendations for brick walls with test results on Brick A walls with 1:1:4 mortar.*

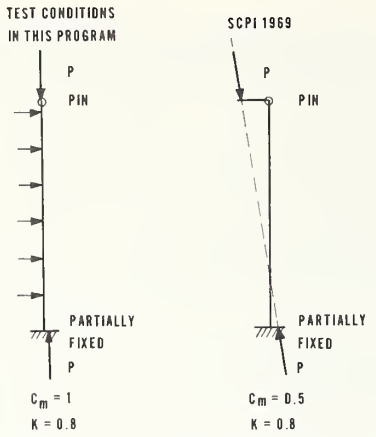

FIGURE 9.2. *Comporison of loading and end conditions.*

method using the coefficients $C_m = 0.5$ and $k = 0.8$. The predicted interaction curve for lateral loading is also shown for the sake of comparison. It can be seen that the moment magnifier curve for vertical load eccentricity approximately agrees with the SCPI curve.

It should be recognized that the SCPI test curve was developed on the basis of tests with eccentric vertical loads only. When slenderness effects are analyzed by considering added moments caused by deflections, it can be demonstrated that the case of lateral loading is not correctly simulated by eccentric vertical loads. However, this difference is generally not recognized in present design practice. Thus the moment magnifier method provides a more flexible approach for the prediction of slenderness effects under all loading conditions.

In the 1969 SCPI Standard, the case of transverse loading has been recognized as a result of the investigation presented in this report. This loading condition corresponds to the dashed-dotted curve in figure 9.1 and is in reasonable agreement with the results obtained in this investigation.

The shaded area in figure 9.1 shows the allowable loads and moments in accordance with the case of transverse loading specified in the SCPI 1969 standard. These values are safe, however the margin of safety seems to decrease with increasing e/t. It is obvious that these recommendations provide a margin of safety by "scaling down" a hypothetical ultimate strength curve. This scaling down is along constant e/t lines. At the eccentricity of $e/t = 1/3$ the interaction curve is scaled down radially, which provides a rather slim margin of safety at that eccentricity. For loads larger than P_2 (fig. 9.1), the margin of safety for transverse moments gradually increases. At load P_1 no moment is permitted, while actually a wall would be capable of supporting a much greater moment at that load than at load P_2, where the maximum transverse moment is permitted. The philosophy behind the method of scaling down the ultimate interaction curve is questionable and should be reexamined, considering all possible combinations of vertical loads and moments at ultimate loads, as well as at service loads.

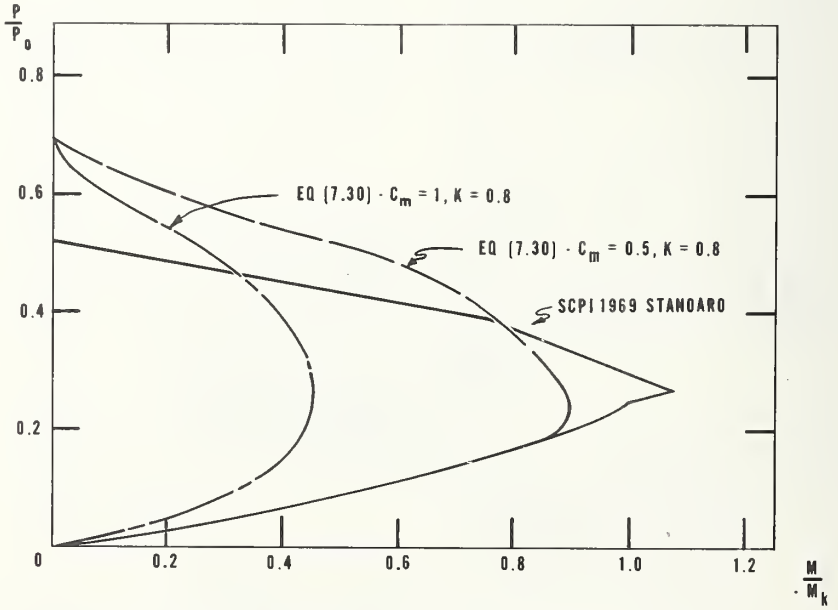

FIGURE 9.3. *Prediction of SCPI 1969 conditions by eq 7.30.*

9.2.3. NCMA and ACI Recommendations

These recommendations account for slenderness effects, but do not account for end or loading conditions. The following equations are recommended by NCMA and ACI for nonreinforced walls:

Axial load:

$$P = 0.20 f'_m \left[1 - \left(\frac{h}{40t}\right)^3\right] A_n$$

where: A_n = net cross-sectional area of the masonry.

Eccentric loads:

$$\frac{f_a}{F_a} + \frac{f_m}{F_m} \text{ shall not exceed 1.}$$

where: f_a = computed axial compressive stress,

$F_a = \frac{P}{A_n}$ = allowable axial compressive stress,

f_m = computed flexural compressive stress,

$F_m = 0.3 f'_m$ = allowable flexural compressive stress.

Up to an eccentricity of $e/t = 1/3$, a cracked section may be assumed to compute bending strength in solid unit walls, neglecting the flexural tensile strength. In hollow unit walls, eccentricity is limited to a value which would produce tension.

In figure 9.4 allowable axial load (P_{all}) computed by the NCMA standard is compared with critical axial load computed for the 8-in solid concrete block walls used in this program, where critical axial loads were assumed to equal 0.7 P_{cro}, (eq 7.30). Critical loads were computed for different h/t ratios for the pin ended case and for partial fixity as assumed in the interpretation of test results. It appears that the pin ended case is fairly close to the NCMA equation.

The slenderness reduction equation used by NCMA and ACI, which is also termed "empirical equation," considers only the geometry of the wall gross section. Variables which influence slenderness effects and which are not considered by the equation are: f'_m/E, cross-sectional geometry, end fixity, and loading conditions. The justification for not considering some of these variables may be in part attributed to the fact that there is a linear relationship between f'_m and E within a certain range of masonry strength, and that end conditions are similar for most conventional masonry structures. It is questionable whether, with the increasing use of high strength masonry and of high rise masonry construction, it is

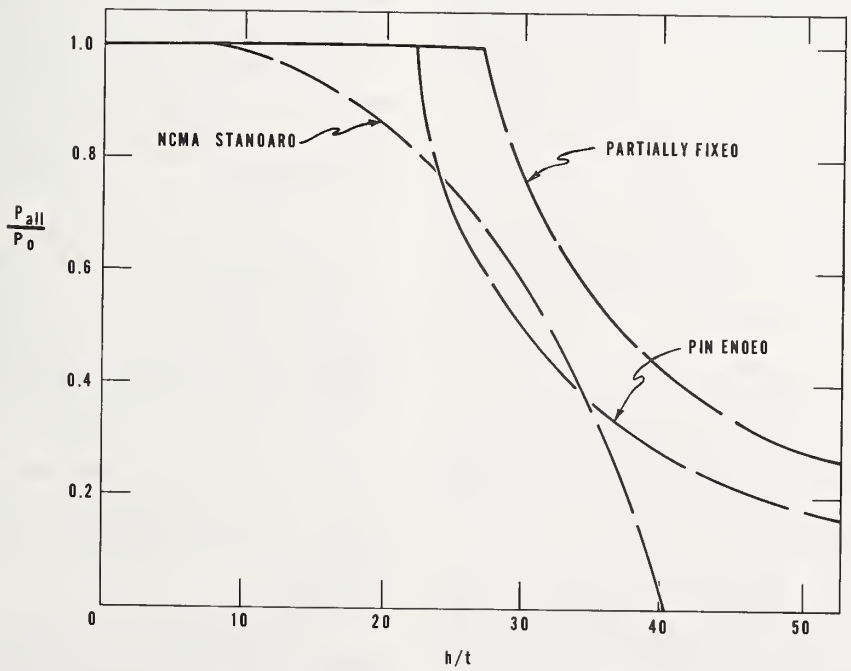

FIGURE 9.4. *NCMA expression for slenderness effects.*

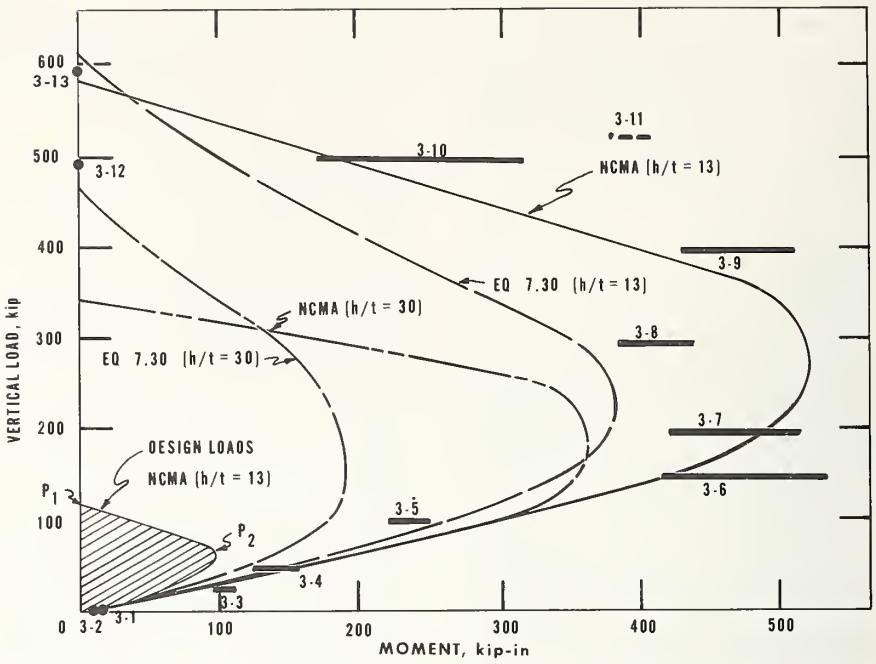

FIGURE 9.5. *Comparison of NCMA recommendations with test results on solid 8-in concrete block walls.*

still possible to disregard these variables without the use of unduly high margins of safety.

Interaction curves for ultimate and allowable loads are compared in figure 9.5 with test results and with interaction curves constructed in accordance with the analysis in section 8. It should be noted that the NCMA allowable flexural stress is $0.3f'_m$ and the allowable compressive stress only $0.2f'_m$. These stresses when multiplied by 5, which may be considered the axial load margin of safety and assumed constant throughout the e/t range, will result in a short-wall interaction curve. This curve assumes an "a" value greater than 1 for large e/t values, with a peak at P_0 and a distortion which will result in greater ultimate moments at higher e/t ratios. This short-wall interaction curve is modified for slenderness by reducing the part of the total stress due to axial load (P/A), without at the same time reducing the stress caused by moments (Mc/I).

For the slenderness of the walls tested, the modification of the interaction curves is relatively minor. Curves were therefore constructed for an h/t ratio of 30, to provide a better comparison between eq (7.30) and the NCMA equation.

For the small slenderness ratio the moments predicted by the NCMA equation are greater, accounting for an "a" value which is greater than 1. These increased moments are less conservative than the moments predicted by the interaction curve at $a =$ 1, and seem to show fairly good agreement wit some of the tested panels, while overestimating th strength of other specimens.

Comparison of the two theoretical curves for $h/$ = 30 shows that the NCMA curve predicts a smalle axial load, but greater moments. While no slende concrete masonry walls were tested, it appears o the basis of the agreement between predicted an observed strength of the more slender brick wall that the NCMA curve probably overestimates th transverse strength of transversely loaded slende walls, even though the curve plotted by eq (7.30) which assumes $a = 1$, is very conservative. However the NCMA equation is probably conservative for th case of eccentric vertical loads.

Allowable moments by the NCMA equation for ar h/t ratio of 13 are shown in the shaded area in figure 9.5. As in the case of the SCPI equation, the philosophy of scaling down predicted ultimate interaction curves should be reexamined.

9.3. Recommended Research

Based on this program the following research is recommended to supplement and expand this investigation.

(1) *Investigation of stress-strain properties of masonry and short-wall section capacity.* The objective of this investigation would be to develop an in-

teraction curve for short-wall section capacity on the basis of short specimen tests. This study should include a thorough investigation of the relationship between compressive strength in one-dimensional compression and in flexure and investigation of the stress distribution corresponding to linear strain gradients.

(2) *Investigation of slenderness effects on transverse strength with particular emphasis on concrete masonry.* The purpose of this investigation would be to study the strength of slender walls with the slenderness ratio as a variable.

(3) *A mathematical study of the effects of section cracking and the change in* E *with increasing stress.* The purpose of this investigation would be to mathematically determine the relationship between stiffness *EI* and the level of vertical loading at failure for different wall systems.

(4) *Investigation of walls resisting transverse loads as two-way slabs, by studying walls supported along three and four edges.*

(5) *Investigation of walls subjected to a combination of transverse and eccentric vertical loads.* The purpose of this investigation would be to evaluate the difference between slenderness effects on walls loaded by eccentric vertical loads, by combined axial vertical and transverse loads and by combinations of these two modes of loading. The feasibility of using the moment magnifier method to predict wall strength under all these modes of loading would also be investigated.

10. Summary

The following conclusions can be drawn from this investigation:

10.1. Conclusions from Test Results

(1) Transverse strength of masonry walls is reasonably predicted by evaluating the cross-sectional capacity and reducing that capacity to account for the added moment caused by wall deflection. The general trend of the test results is in good agreement with theory, and the magnitude of individual test results is conservatively predicted.

(2) Cross-sectional moment capacity of wall panels was conservatively predicted by a theoretical interaction curve which was based on compressive prism strength and linear strain gradients.

(3) Slenderness effects, computed by the moment magnifier method as modified to account for section cracking, predicted closely the slenderness effects observed in the 4-in thick brick walls, and reasonably predicted these effects for concrete masonry walls, concrete block cavity walls, and brick and block cavity walls.

(4) The qualitative observation was made that at large eccentricities, the flexural compressive strength of masonry exceeds the compressive strength developed in pure one-dimensional compression by a significant margin, and that flexural compressive strength increases with increasing strain gradients.

(5) The transverse strength of cavity walls was conservatively predicted by assuming that each wythe carries its proportional share of vertical loads and moments, and that transverse loads, but not shear forces parallel to the plane of the wall, are transmitted by the ties.

(6) The transverse strength of composite brick and block walls was approximately predicted by assuming that the walls act monolithically.

(7) Whenever walls did not fail by stability-induced compression failure, their axial compressive strength was reasonably predicted by prism tests. In the case of concrete masonry with high-bond mortar, compressive tests with prisms capped with high strength plaster overestimated wall strength, while prisms set on fiberboard showed good correlation with wall strength.

(8) Flexural tensile strength of all the wall panels tested equaled or exceeded 1/2 of the flexural strength as determined by prism tests.

10.2. Comparison of Test Results with Existing Design Practice

(1) The ANSI American Standard Building Code Requirements for Masonry do not take into account slenderness and end-conditions and compensate for variability in wall strengths by high margins of safety.

(2) The design equations in the 1969 SCPI Standard account for end conditions as well as slenderness. The equations were developed on the basis of eccentric vertical load tests but also provide for the case of transverse loading.

(3) The NCMA and ACI recommendations consider slenderness but not end conditions. The NCMA equations probably overestimate wall strength under transverse loading conditions.

(4) The interaction diagrams for ultimate transverse strength as a function of lateral loads,

developed by SCPI and NCMA were scaled down radially to determine allowable working load. This scaling down in some cases results in extremely low factors of safety in bending, while the factor of safety under vertical loads is very high.

(5) Neither the NCMA nor the SCPI standard provide for the design of composite (brick and block) walls. This type of construction is widely used.

(6) While existing design standards are primarily intended for the case of eccentric vertical loads, and in most cases do not account for end conditions, the moment magnifier method, if used for the prediction of transverse wall strength, could cover both the case of eccentric vertical loading and the case of transverse loading and could also account for end conditions.

11. Acknowledgment

The contribution of the following persons is acknowledged:

Louis E. Cattaneo, Research Engineer, was in charge of the laboratory testing program.

Dallas G. Grenley, Research Associate from The Dow Chemical Company, at the National Bureau of Standards, 1966-67, was in charge of construction and testing of the high bond mortar specimens.

Frank A. Rankin, was the Mason Contractor in charge of construction of the specimens.

Timothy Miles, Jr. and Harvey M. Shirley, Laboratory Technicians, assisted in the preparation of specimens for testing.

James W. Raines, was the Electronic Technician in charge of instrumentation.

Edward O. Pfrang, Chief of the Structures Section, participated in the analysis of test results and made many contributions to this report.

John E. Breen, Professor of Civil Engineering, at the University of Texas, critically reviewed this report and contributed to the analysis of test results.

12. References

[1] Standard Methods of Sampling and Testing of Brick, ASTM Designation C67-66 (1966).

[2] Tentative Methods of Sampling and Testing Concrete Masonry Units, ASTM Designation C140-65 (1965).

[3] Standard Specifications for Mortar for Unit Masonry, ASTM Designation C270-68 (1968).

[4] Tentative Specifications for Aggregate for Masonry Mortar, ASTM Designation C144-66T (1966).

[5] American National Standards Institute, American Standard Building Code Requirements for Masonry (National Bureau of Standards, 1953).

[6] Standard Method of Test for Bond Strength of Mortar to Masonry Units, ASTM Designation E149-66 (1966).

[7] McGregor, J. G., Breen, J. E., Pfrang, E. O., Design of Slender Concrete Columns, Journal of the American Concrete Institute, **V. 67,** No. 1, pp. 6–28 (January 1970).

[8] Column Research Council, Guide to Design Criteria for Metal Compression Members (John Wiley and Sons, Inc., New York, 1966).

[9] Structural Clay Products Institute, Building Code Requirements for Engineered Brick Masonry (August 1969).

[10] National Concrete Masonry Association, Specification for the Design and Construction of Load-Bearing Concrete Masonry (1968).

[11] American Concrete Institute, Committee 531, Concrete Masonry Structures—Design and Construction, Journal of the American Concrete Institute, **V. 67,** No. 5, pp. 380-403, (May 1970), and V. 67, No. 6, pp. 442–460, (June 1970).

Latest developments in the subject area of this publication, as well as in other areas where the National Bureau of Standards is active, are reported in the NBS Technical News Bulletin. See following page.

U. S. GOVERNMENT PRINTING OFFICE : 1971 OL - 410-021

HOW TO KEEP ABREAST OF NBS ACTIVITIES

Your purchase of this publication indicates an interest in the research, development, technology, or service activities of the National Bureau of Standards.

The best source of current awareness in your specific area, as well as in other NBS programs of possible interest, is the TECHNICAL NEWS BULLETIN, a monthly magazine designed for engineers, chemists, physicists, research and product development managers, librarians, and company executives.

If you do not now receive the TECHNICAL NEWS BULLETIN and would like to subscribe, and/or to review some recent issues, please fill out and return the form below.

Mail to: Office of Technical Information and Publications
National Bureau of Standards
Washington, D. C. 20234

Name _____

Affiliation _____

Address _____

City _____ State _____ Zip _____

☐ Please send complimentary past issues of the Technical News Bulletin.

☐ Please enter my 1–yr subscription. Enclosed is my check or money order for $3.00 (additional $1.00 for foreign mailing).
Check is made payable to: SUPERINTENDENT OF DOCUMENTS

BSS 34

(cut here)

(cut here)

Announcement of New Publications in Building Science Series

Superintendent of Documents,
Government Printing Office,
Washington, D. C. 20402

Dear Sir:

Please add my name to the announcement list of new publications to be issued in the series: National Bureau of Standards Building Science Series.

Name _____

Company _____

Address _____

City _____ State _____ Zip Code _____

(Notification key N–339)

NBS TECHNICAL PUBLICATIONS

PERIODICALS

JOURNAL OF RESEARCH reports National Bureau of Standards research and development in physics, mathematics, chemistry, and engineering. Comprehensive scientific papers give complete details of the work, including laboratory data, experimental procedures, and theoretical and mathematical analyses. Illustrated with photographs, drawings, and charts.

Published in three sections, available separately:

• Physics and Chemistry

Papers of interest primarily to scientists working in these fields. This section covers a broad range of physical and chemical research, with major emphasis on standards of physical measurement, fundamental constants, and properties of matter. Issued six times a year. Annual subscription: Domestic, $9.50; foreign, $11.75*.

• Mathematical Sciences

Studies and compilations designed mainly for the mathematician and theoretical physicist. Topics in mathematical statistics, theory of experiment design, numerical analysis, theoretical physics and chemistry, logical design and programming of computers and computer systems. Short numerical tables. Issued quarterly. Annual subscription: Domestic, $5.00; foreign, $6.25*.

• Engineering and Instrumentation

Reporting results of interest chiefly to the engineer and the applied scientist. This section includes many of the new developments in instrumentation resulting from the Bureau's work in physical measurement, data processing, and development of test methods. It will also cover some of the work in acoustics, applied mechanics, building research, and cryogenic engineering. Issued quarterly. Annual subscription: Domestic, $5.00; foreign, $6.25*.

TECHNICAL NEWS BULLETIN

The best single source of information concerning the Bureau's research, developmental, cooperative and publication activities, this monthly publication is designed for the industry-oriented individual whose daily work involves intimate contact with science and technology—*for engineers, chemists, physicists, research managers, product-development managers, and company executives.* Annual subscription: Domestic, $3.00; foreign, $4.00*.

* Difference in price is due to extra cost of foreign mailing.

NONPERIODICALS

Applied Mathematics Series. Mathematical tables, manuals, and studies.

Building Science Series. Research results, test methods, and performance criteria of building materials, components, systems, and structures.

Handbooks. Recommended codes of engineering and industrial practice (including safety codes) developed in cooperation with interested industries, professional organizations, and regulatory bodies.

Special Publications. Proceedings of NBS conferences, bibliographies, annual reports, wall charts, pamphlets, etc.

Monographs. Major contributions to the technical literature on various subjects related to the Bureau's scientific and technical activities.

National Standard Reference Data Series. NSRDS provides quantitative data on the physical and chemical properties of materials, compiled from the world's literature and critically evaluated.

Product Standards. Provide requirements for sizes, types, quality and methods for testing various industrial products. These standards are developed cooperatively with interested Government and industry groups and provide the basis for common understanding of product characteristics for both buyers and sellers. Their use is voluntary.

Technical Notes. This series consists of communications and reports (covering both other agency and NBS-sponsored work) of limited or transitory interest.

Federal Information Processing Standards Publications. This series is the official publication within the Federal Government for information on standards adopted and promulgated under the Public Law 89–306, and Bureau of the Budget Circular A–86 entitled, Standardization of Data Elements and Codes in Data Systems.

Order NBS publications from:

Superintendent of Documents
Government Printing Office
Washington, D.C. 20402

U.S. DEPARTMENT OF COMMERCE
Washington, D.C. 20230

OFFICIAL BUSINESS

Penalty for Private Use, $300

POSTAGE AND FEES PAI
U.S. DEPARTMENT OF COMMERC